AFOSR-TR-97

0221

REPORT DOCUMENTATION PAGE

1. AGENCY USE ONLY (Leave blank)	2. REPORT DATE	3. REPORT TYPE AND DATES COVERED
		FINAL REPORT 01 Jul 93 - 31 Dec 96

4. TITLE AND SUBTITLE
(AASERT-92) Graduate Student Support for Research in 3-D Optical Disks

5. FUNDING NUMBERS
61103D
3484/TS

6. AUTHOR(S)
Professor Psaltis

7. PERFORMING ORGANIZATION NAME(S) AND ADDRESS(ES)
Department of Electrical Engineering
California Institute of Technology
Pasadena, CA 91125

8. PERFORMING ORGANIZATION REPORT NUMBER

9. SPONSORING/MONITORING AGENCY NAME(S) AND ADDRESS(ES)
AFOSR/NE
110 Duncan Avenue Suite B115
Bolling AFB DC 20332-8050

10. SPONSORING/MONITORING AGENCY REPORT NUMBER
F49620-93-1-0340

11. SUPPLEMENTARY NOTES

12a. DISTRIBUTION/AVAILABILITY STATEMENT
APPROVED FOR PUBLIC RELEASE: DISTRIBUTION UNLIMITED

12b. DISTRIBUTION CODE

13. ABSTRACT *(Maximum 200 words)*

In this final report, results from several different high density holographic data storage experiments are presented to demonstrate that information can be stored more densely using holography. We start with a preliminary experiment to show that the DuPont photopolymer could indeed be used to record high density holograms with sufficient SNR and end with an experiment where a surface density of 100 bits/um^2 was achieved. For one of the high density experiments, we constructed a functional holographic 3-D disk record/read station. A new multiplexing method called 'shift' multiplexing was used to write overlapping holograms in a spiral track on the disk, just like the compact disc format. The capacity of a 120 mm disk with a surface density of 100 bits/um^2 would be around 100 Gbytes, roughly 100 times more than the current compact disc. We end the final technical report with some suggestions for future experiments in the area of holographic 3-D disks.

14. SUBJECT TERMS

15. NUMBER OF PAGES

16. PRICE CODE

17. SECURITY CLASSIFICATION OF REPORT	18. SECURITY CLASSIFICATION OF THIS PAGE	19. SECURITY CLASSIFICATION OF ABSTRACT	20. LIMITATION OF ABSTRACT
UNCLASSIFIED	UNCLASSIFIED	UNCLASSIFIED	

Abstract

In this final technical report, results from several different high density holographic data storage experiments are presented to demonstrate that information can be stored more densely using holography. We start with a preliminary experiment to show that the DuPont photopolymer could indeed be used to record high density holograms with sufficient SNR and end with an experiment where a surface density of 100 bits/μm^2 was achieved. For one of the high density experiments, we constructed a functional holographic 3-D disk record/read station. A new multiplexing method called 'shift' multiplexing was used to write overlapping holograms in a spiral track on the disk, just like the compact disc format. The capacity of a 120 mm disk with a surface density of 100 bits/μm^2 would be around 100 Gbytes, roughly 100 times more than the current compact disc. We end the final technical report with some suggestions for future experiments in the area of holographic 3-D disks.

1.1 Introduction

Holographic data storage offers several advantages when compared to conventional storage devices. The data stored and retrieved is organized as a two-dimensional page, consisting of a large number of pixels (bits). The read-out rate can be very high since an entire page of data is presented when a hologram is reconstructed. For example, accessing a page of data consisting of 1,000 × 1,000 pixels within 1 ms would give a data transfer rate of 1 gigabits per second. Furthermore, holographic data storage allows many pages of data to be stored at the same location with little cross-talk by using multiplexing techniques such as angle [1, 2], wavelength [3, 4], phase-code [5, 6], fractal [7, 8], peristrophic [9], and shift [10]. To a first-order approximation, the density achievable with holography is simply :

$$D_{3D} = M \times D_{2D} \tag{3.1}$$

where M is the number of holograms multiplexed at one location, D_{2D} is the density per page of hologram, and D_{3D} is the holographic density. For thin recording materials such as the photopolymer, it is convenient to think of the 3-dimensional holographic density as a surface density. This allows easy comparison with conventional data storage devices.

The surface density of current compact disc memories is approximately 1 bit μm^2 and is limited primarily by the size of the illuminating spot. The next generation of optical compact discs that are scheduled to appear in the near future will have a surface density of ~6 bits/μm^2 [11]. Dual-layer and double-sided systems are expected to have an equivalent surface density in excess of 20 bits/μm^2. For holographic memories to be competitive, the surface density of holographic 3-D disks must be higher than the projected density of conventional media by a comfortable margin. This concern makes surface density the primary goal in the design of a holographic 3-D disk system. The storage density of holographic disks was analyzed in great detail by Li and Psaltis [12]. For the system they had in mind, it was determined that for an optimal recording medium thickness of 1.6 cm, a storage density of 110 bits/μm^2 is obtainable by angle multiplexing alone. This gives nearly an order of magnitude of margin over the projected surface density of the next compact disc technology.

Much in the thinking of holographic data storage system design has changed since Li and Psaltis' paper. New multiplexing methods such as peristrophic and shift have increased the storage density possible while using thinner recording materials. The old thinking of more holograms stored at a given location equals higher storage density has been proven to be only partially true. In an previous experiment where 1,000 image plane holograms were stored in the 100 micron thick DuPont photopolymer was discussed. The size of each data pixel was 100 $\mu m \times 100 \mu m$, giving a storage density of only ~.1 bit/μm^2 (1,000 holograms / (100 $\mu m \times 100 \mu m$)). This is about an order of magnitude lower than the surface density of compact discs despite being the largest number of holograms ever stored in a 100 micron thick recording material. In Chapter 1.2 we will show an

experiment where a surface density of 10 bits μm^2 was achieved in the same 100 micron thick photopolymer by recording only 32 high bandwidth holograms.

The 10 bits/μm^2 experiment was to demonstrate that high density holograms could indeed be recorded in DuPont's photopolymer films with sufficient signal-to-noise ratio (SNR). In Chapter 1.3, we make our first attempt at constructing a functional holographic 3-D disk system using the DuPont photopolymer. The same 10 bits/μm^2 experiment was repeated except that the recording material was in the shape of a disk and shift multiplexing was used. Shift multiplexing is especially well suited for the holographic 3-D disk application. It allows holograms to be stored sequentially on the disk, in a spiral track much like the compact disc. The holograms partially overlap in the track and adjacent tracks also overlap to further increase the surface density. All this is done with a simple spherical reference beam and the disk motion provides the means of multiplexing. A very nice feature of using a spherical reference beam is the ability to diminish the effect of photopolymer shrinkage on the stored holograms. This is discussed in detail in Chapter 1.3.3.3.

A surface density of 10 bits/μm^2 is not enough to make holographic 3-D disks more attractive than conventional compact discs. To be truly impressive, a demonstrated surface density of 100 bits/μm^2 would be nice. However, this requires a thicker recording medium than the 100 micron thick photopolymer. Chapter 1.4 shows an experiment where a surface density of 100 bits/μm^2 was demonstrated with a 1 mm thick $LiNbO_3$, using nearly the same setup as in Chapter 1.3. This experiment shows that it is possible to achieve a holographic surface density that is much higher than conventional data storage devices.

A lot of kinks remain to be ironed out before holographic 3-D disks can become a commercial product. Chapter 1.5 discusses some of the technical problems and possible solutions.

1.2 10 bits/μm^2 High Density Experiment Using Peristrophic and Angle Multiplexing

1.2.1 Introduction

Eq. 1.1 shows that the holographic storage density is equal to the number of holograms multiplexed at a given location times the page density of a single hologram. The same storage density can be achieved with many low page density holograms or a few high page density holograms. Given the desired storage density, the choice between many low density holograms or a few high density holograms is a complex issue. It depends on the system components available, the desired page size (number of pixels or area), the thickness and dynamic range of the recording material.

System components such as lenses and spatial-light modulators usually define the page density while the number of holograms is limited by the thickness and the dynamic range of the recording material. Since the maximum storage density is fixed for a given volume, there is also some cross relationship between page density and the number of holograms storable at a single location. The number of pixels in each hologram is usually picked to optimize the performance of the system. Depending on the application, it might be desirable to have the memory space divided into large or small pages. For example, the Intel 8088 processors organized its 1 megabyte memory space into 64 kilobyte pages for

easy access. This caused many headaches for programmers but was most efficient for the processor.

For the high density experiments in this chapter, we maximized the page density first and then tried to store as many holograms as possible in the recording material. This method uses the dynamic range of the recording material most efficiently since diffraction efficiency is inversely proportional to the number of holograms squared ($\eta \propto 1/M^2$). The pixel size was picked to ease data readout and the number of pixels in each hologram was defined by the lens aperture. Using our high density setup, we were able to achieve a surface density that is many times higher than any conventional data storage devices.

1.2.2 Experimental Setup

Figure 1.1 shows a schematic diagram of the high density setup using peristrophic and angle multiplexing. A photographic glass plate of a random binary bit pattern was used as the input SLM. The center-to-center spacing of the pixels was 45 microns (in both directions), and the fill factor was 100%. A pair of Nikon *f*/1.4, 3.9-cm-aperture camera lenses were used in a 4-*f* geometry to image the SLM to the detector array. The glass data mask plate was pressed up against the Nikon lens to ensure that all the pixels within the lens aperture were captured and imaged to the detector plane. A total of 590,000 pixels fit in the apertures of the two Nikon lenses and a sharp image of the entire field was obtained at the detector plane. The holograms were recorded by a planewave reference beam with the recording material placed slightly past the Fourier transform plane. At that position, the diameter of the signal beam on the photopolymer was 1.5 mm and its spatial uniformity was much better than at the exact Fourier plane. The aperture of

the reference planewave on the recording material was controlled by an iris. To avoid diffraction effects, the iris was imaged to the photopolymer by a 4-f system with the iris at the first image plane and the photopolymer at the other image plane. The intensity of the reference planewave was 250 $\mu W/cm^2$ and the intensity of the signal planewave before the data mask was 1.8 $\mu W/cm^2$. The photopolymer was tilted by 5° out of the x-y plane to reduce back reflections. Peristrophic multiplexing was achieved by rotating the photopolymer around its own surface normal. Angle multiplexing was combined with peristrophic multiplexing to increase the number of pages stored at a single location. For simplicity, angle multiplexing was achieved by rotating the recording material around the x-axis with a second rotational stage. The signal and reference beams made an angle of 25° and 35° (respectively, measured from outside the photopolymer) with respect to the surface normal of the photopolymer initially. The rotation of the recording material around the x-axis during angle multiplexing changes these angles but the angle between the signal and reference beams remains constant at 60°. At the detector plane, a simple video rate CCD camera was used. Its output was linked to a computer via a framegrabber board.

Figure 1.2 shows a picture of the high density setup using peristrophic and angle multiplexing. The dimensions of the setup, measured from the front of the data mask to the end of the CCD was approximately 28 cm with a width of 12 cm. A photographically produced data mask was used in the setup instead of a liquid-crystal type SLM for several reasons. (1) The 100% fill factor of the photographically produced data mask eliminated the repetitive higher orders. This simplified the setup since no filtering was required. (2) To ensure that the highest possible density is achieved in a page of hologram, the entire

aperture of the Nikon lens must be filled with data. The liquid-crystal SLMs we had in the labs were too small to cover the entire 3.9 cm Nikon lens aperture. Therefore, a large but fixed data mask was used in the setup. Since this is a first-order experiment to demonstrate the high storage density capability of holographic devices, we feel that the inability to change the data pixels from page to page is but a small kink in the experiment.

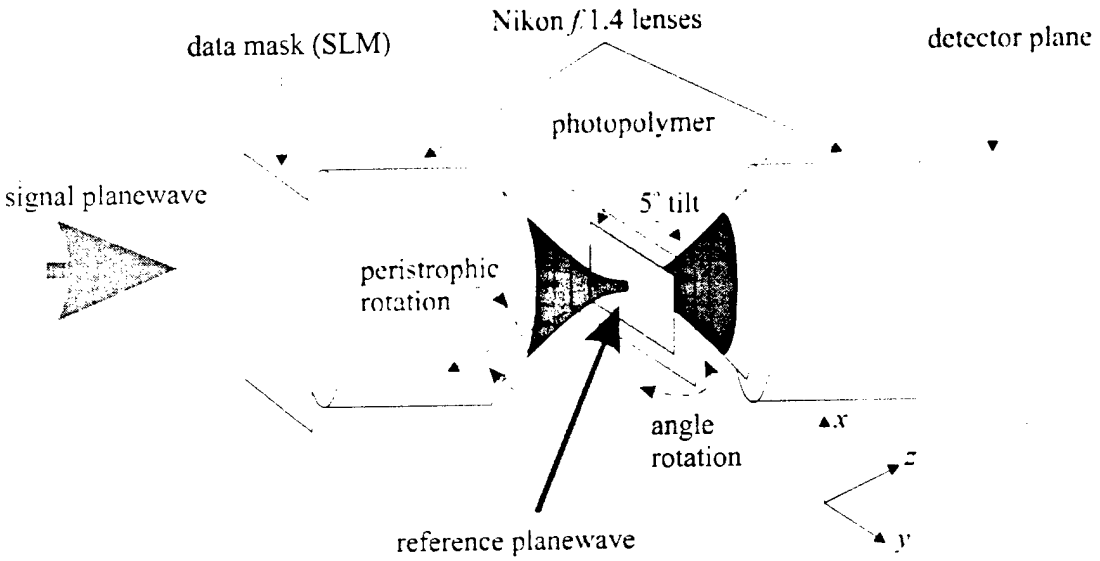

Figure 1.1 : Schematic diagram of the high density setup using peristrophic and angle multiplexing.

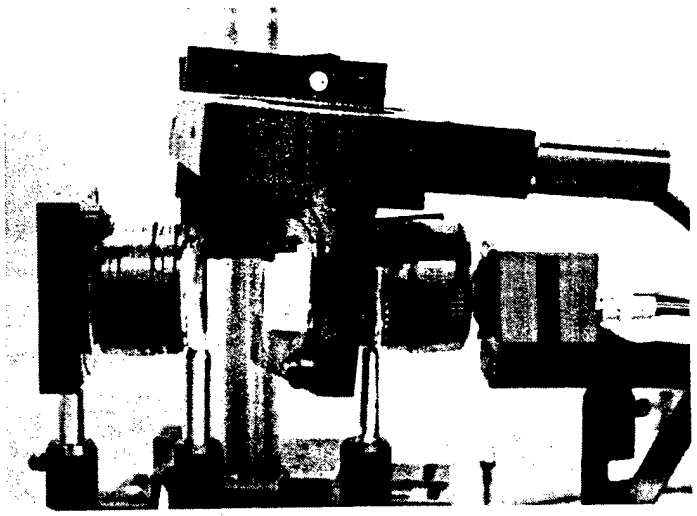

Figure 1.2 : A picture of the high density setup using peristrophic and angle multiplexing.

Nikon camera lenses were used in the setup because they are relatively inexpensive for a multi-element lens and they are very well corrected across the entire aperture. For imaging applications where a low *f*/# system is required, significant image distortion usually results at the edges of the lenses. Camera lenses are designed to faithfully reproduce the input scenes on films without much distortion. This is achieved by using multiple lens elements in a single package. For example, the Nikon *f*/1.4 lens (Product Number 1904) has 7 elements in 6 different groups to correct for distortions. Camera lenses are produced for the mass market, therefore they are relatively inexpensive (~$400 for a Nikon *f*/1.4 lens) when compared to custom designed lenses with the same specification (~$30,000 for the design and production of the first lens). No significant image distortion was encountered anywhere within the apertures of the Nikon lenses. .

Notice in Figure 1.1, the 4-*f* system constructed with the two Nikon *f*/1.4 camera lenses is actually backwards. To construct a true 4-*f* system in the way these lenses were designed, the side of the lens that normally faces the photographic film should face the data mask and the CCD array. There is a separate ring that allows two Nikon camera lenses to be screwed together to form a perfect 4-*f* system. The ring screws the sides of the lenses that normally face the scene together. The problem with that setup is then the Fourier plane becomes inaccessible since the focal plane of the side that normally faces the scene is only a few millimeters from the lens casing. On the other hand, the focal plane of the side that faces the photographic film is about 4 cm from the lens casing. By building the 4-*f* system backwards, we can get almost 8 cm of working space between the lenses, enough room to place the recording material and the rotational stages near the Fourier

plane. This backward 4-*f* system undoubtedly has some aberrations. However, it was not noticeable with the large 45 μm × 45 μm pixels in our data mask.

We chose near Fourier plane recording instead of the image plane because it is easier to achieve high page density holograms in the Fourier plane. Figure 1.3 shows a typical image plane setup using two 4-*f* imaging systems. The data to be stored is first imaged to the photopolymer by the first 4-*f* system. The interference pattern created between the image of the data mask and a planewave reference beam is stored as a hologram. During readout, the reconstructed hologram is imaged to the detector array with the second 4-*f* system.

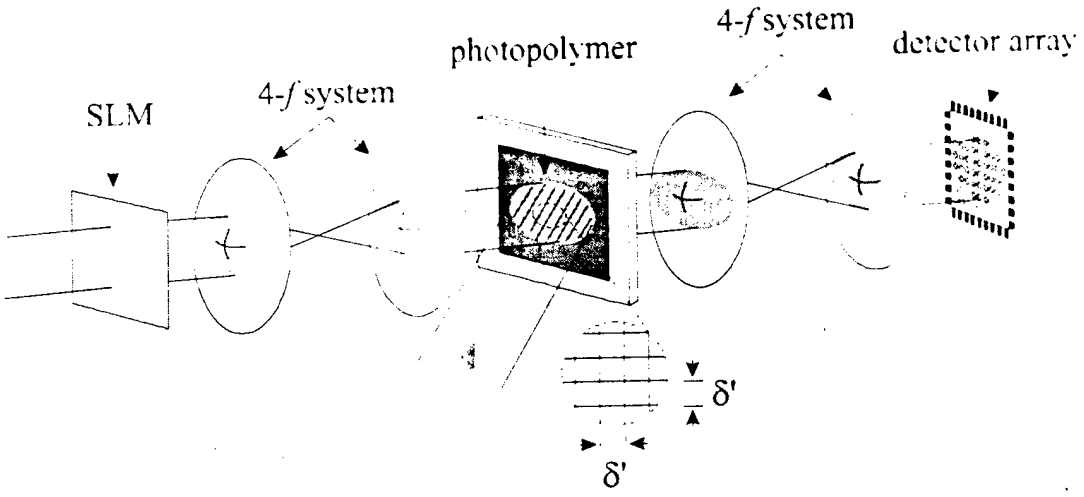

Figure 1.3 : Typical image plane recording setup.

In the image plane, the density per page is given by the inverse of the pixel area (density $\simeq 1/\delta'^2$). Therefore, in order to achieve high density per page, the pixel size must be very small. However, the pixel width of most SLMs and detector arrays are usually from slightly less than 10 μm to tens of microns. This gives a very low density value unless the first 4-*f* system reduces the pixel size and the second 4-*f* system re-expands the pixels. Lens systems that can reduce input pixels to the micron range are very expensive.

Some lithographic reduction lenses manufactured for the VLSI industry can be applied to this application. For example, the Nikon Ultra-Micro-Nikkor 28 mm *f*/1.7g ultra high resolution lens was designed for printing minute image patterns on plates coated with photo-resist under g-line monochromatic lighting (435.8 nm wavelength). Its standard reduction is 1/10 and this lens guarantees a resolving power of more than 800 lines per mm over the 8 mm image diameter (minimum pixel width of 1.25 μm). Using two of these lenses to image the data from the input SLM to the detector array would give a maximum page density of .64 bits μm^2 at the reduced image plane between the two lenses. This density value is very good considering that the same resolution is maintained over a large field (unlike compact discs where the objective lens only needs to produce a single spot at the optical axis of the lens). However, these lenses are very specialized, expensive, and sometimes even unobtainable. Newer lens systems that can resolve sub-micron pixels are currently exposing the next generation VLSI chips with feature sizes less than .2 microns. However, these lithographic systems are sold with million dollar price tags and the lenses cannot be brought separately.

Another draw back of these high resolution reduction lens systems is that their overall working distance is large. For the Nikon Ultra-Micro-Nikkor 28 mm *f*/1.7g lens, the distance from the input image to the reduced image is 31.5 cm. Using two of these lenses to reduce and re-expand the input image would require a system with a length of at least 63 cm. Furthermore the distance from the lens casing to the reduced image plane is only 1.1 cm. This gives a distance of only 2.2 cm between the two lenses to place the rotational stages and the recording material.

For Fourier plane recording, the criteria for high density holograms is completely different. Figure 1.4 shows a simple Fourier plane holography setup using one 4-f system. At the Fourier plane of the 4-f system, the width of the signal beam is given by $2\lambda f/\delta$, where λ is the wavelength, f is the focal length of the lens, and δ is the pixel size of the SLM. For large pixels, the spot at the Fourier plane will be small and vice versa. The density per page at the Fourier plane is equal to the number of pixels captured by the apertures of the 4-f system over the spot size of the hologram. For a square SLM with N_p by N_p number of pixels that fit within the lens aperture, the page density is given by :

$$\text{page density at the Fourier plane} = \frac{N_p^2\delta^2}{(2\lambda f)^2} \tag{1.2}$$

where $N_p\delta$, the number of pixels per dimension times the pixel size, can be thought of as the maximum aperture of the lens system. Then $N_p\delta/f$ is like the inverse f/# of the lens system. By plugging f/# = $f/N_p\delta$ into Eq. 1.2 and multiply the whole thing by a circular lens aperture correction factor, we get :

$$\text{page density at the Fourier plane} = \frac{1}{(2\lambda f/\#)^2}\frac{\pi}{4} \tag{1.3}$$

where f/# is the f-number of the 4-f system. Notice in Eq. 1.3, the page density at the Fourier plane is independent of the SLM pixel size. This means that larger pixels can be used and still get the maximum possible page density given the f/# of the 4-f system. Hence the pixel size can be picked to match conveniently with the pixel size of the detector array without expansion or reduction. Furthermore, when compared with the image plane setup, the Fourier plane system is much more compact and fewer lenses are required.

The only requirement on the lens system for the Fourier plane setup is that the lenses be well corrected for distortion. If the pixels at the edges of the lenses get warped or distorted in some way, then the actual f/# of the 4-f system is higher because those pixels cannot be used. This decreases the density possible per page. Luckily, camera lenses are very well corrected across the entire field of view and some have low f/#'s. For the Nikon f/1.4 camera lenses used in this experiment, the maximum possible density per page at the Fourier plane, using a wavelength of 532 nm would be .35 bits μm^2. Even higher density can be achieved with lower f/# camera lenses. We also tried to use Nikon f/1.2 camera lenses (Product Number 1435). However for these lenses, the focal plane of the side that faces the scene is inside the lens casing. This means that when used as a 4-f system, the image plane is inaccessible. So far we have not found any other lower f/# camera lenses with both focal planes outside the lens casing.

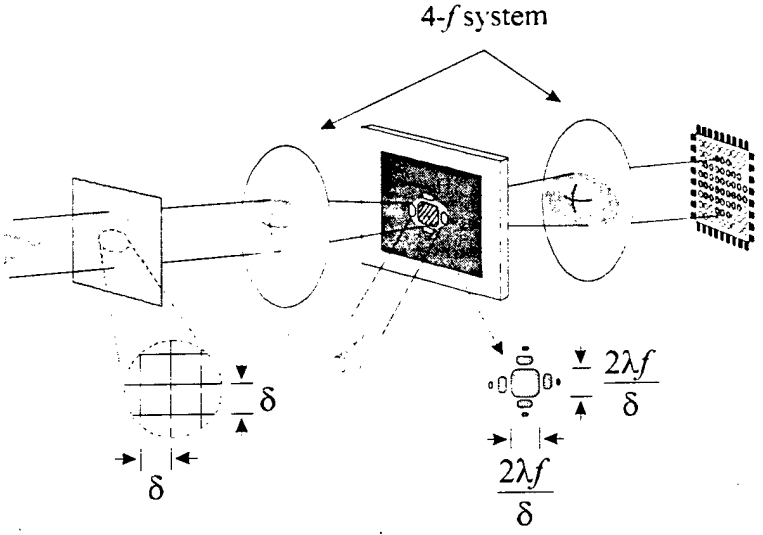

Figure 1.4 : A simple Fourier plane holography setup.

The ability to pick convenient pixel sizes (and still maintain the same page density) and readily available camera lenses that can be used to construct a well corrected 4-f

system are the two major reasons why the Fourier plane geometry is so attractive. In the limit of the resolvable spot size given the $f/\#$ of the lens system ($\delta = 2\lambda f/\#$), the density achievable in the image plane is the same as in the Fourier plane. However, Fourier plane holography offers better immunity to dusts, scratches, and surface defects since the energy of each pixel is spread out over a larger area.

On the other hand, there is a big problem with recording holograms at the exact Fourier plane. At the Fourier plane, the signal beam has a very strong DC component. The DC spike at the Fourier plane is from the non-spatially varying part of the input image. If a hologram was recorded at the exact Fourier plane, the strong DC quickly exhausts the dynamic range of the photopolymer at the DC spot. This causes subsequent holograms that are recorded at the same location to become edge enhance, since only the higher frequency components are stored. One method to get around this problem is to use a random phase diffuser [13-15]. A phase diffuser placed right before or after the SLM modulates the phase of the input image. The non-spatially varying part of the input image gets modulated by a random phase, which causes the DC to broaden in area. If the resolution of the random phase diffuser is better than the SLM, then the Fourier transform spot would get bigger since the effective δ has gotten smaller. This is undesirable since the density per page would decrease due to the increased hologram area. However, by making the random phase diffuser pixel matched with the SLM pixel, the same page density can be obtained with a more uniform Fourier transform.

In practice, it is often difficult or costly to obtain a good random phase diffuser. We tried to make binary (0, π) random phase diffusers in-house for the high density experiments. However, we were unable to achieve the desired effects due to poor etch

uniformity and rough pixel alignments. For the experiments in this chapter, instead of using a phase diffuser, we move the recording material slightly past the exact Fourier plane so that the DC component could defocus and become more uniform. Figure 1.5 shows a simple graphical representation of how the rays converge at the Fourier plane.

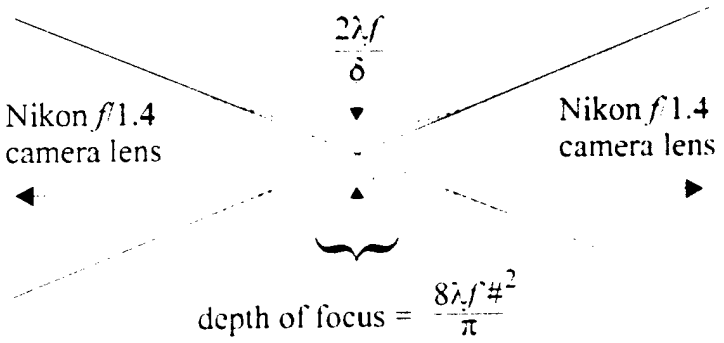

Figure 1.5 : Graphical representation of how the rays converge at the Fourier Plane.

The Nikon f/1.4 camera lenses produce a cone of rays nearly 40° in spread. The DC component focuses down to a waist size of a few microns while the higher frequency components produce a zeroth order waist of $2\lambda f/\delta$. Approximately 90% of the energy is in the zeroth order with the remaining 10% in higher orders. The depth of focus of the DC spot (when the waist becomes $\sqrt{2}$ times larger) is given by the expression shown in Figure 1.5. For the small f/# Nikon lenses used, the DC spot defocuses very quickly and catches up with the higher frequency components with only a small displacement off of the Fourier plane. At the exact Fourier plane, the waist size of the zeroth order is 1.3 mm (λ = 532 nm, f = 5.5 cm, and δ = 45 μm). For the high density experiments, we slightly displaced the recording material past the exact Fourier plane and the diameter of the signal spot on the photopolymer was 1.5 mm when sufficient DC spreading was achieved. In measuring this spot size, the very weak higher frequency components in the signal were excluded. These low intensity components do not record well due to their poor modulation index.

Therefore, they could be filtered during recording or just not illuminated during readout to keep the effective area of the hologram small. This low-pass filtering process causes the edges of the reconstructed pixels to be not quite as sharp as the original data mask. However, the smaller signal spot size does increase the page density. The density per page at the slightly past Fourier plane position is 590,000 pixels / (0.75 × 0.75 mm^2 × π) = 0.33 bits/μm^2. Not as good as the maximum possible density of 0.35 bits/μm^2 at the exact Fourier plane but pretty close.

1.2.3 Experimental Results

The goal of this experiment is to achieve an equivalent surface density of 10 bits/μm^2 in DuPont's HRF-150-100 (100 microns thick) photopolymer using angle and peristrophic multiplexing. With a page density of .33 bits/μm^2, a minimum of 30 holograms must be multiplexed in the same area to get a surface density of 10 bits μm^2. This might sound like a simple proposition since 1,000 holograms were stored in the same recording material, using the same multiplexing methods in a previous experiment. However, to store 30 holograms in this experiment will prove more difficult due to the much higher bandwidth of the signal beam.

For the 1,000 hologram experiment done previously, 100 peristrophic holograms were multiplexed at each of the 10 angle multiplexing positions (position here refers to the angular position of the rotational stage, all the holograms were stored at one location). The photopolymer was rotated in-plane by 1.8° for peristrophic multiplexing and angular positions were separated by 1.5°. For our high density experiment, the aperture of the Nikon *f*/1.4 camera lens is 3.9 cm and the focal length is approximately 5.5 cm. The signal

and reference beams made an angle of 25° and 35° (respectively, measured from outside the photopolymer) with respect to the surface normal of the photopolymer. The theoretical Fourier plane peristrophic selectivity (where $N_p\delta = 3.9$ cm) is a minimum of 41 degrees in rotation to shift the reconstruction completely out of the aperture of the Nikon lens. Experimentally, we found that a 45° in rotation was sufficient to completely Bragg mismatch and shift the undesired hologram off of the Nikon lens aperture. Therefore, up to four peristrophic holograms can be multiplexed from 0 to π with this configuration. The small difference between theory and experiment is probably due to the slight displacement of the recording material off of the exact Fourier plane.

Due to the much higher bandwidth signal beam in the high density experiment, instead of being able to store 100 peristrophic holograms from 0 to π (as in the 1,000 hologram experiment), only four can be stored without cross-talk. The reconstructed hologram in the high density setup is much harder to get rid of since it is so large (3.9 cm in diameter) and the focal length of the Nikon camera lenses are so short (5.5 cm). We could have used longer focal length lenses to decrease the amount of rotation required to shift away the undesired hologram. However, the density per page would decrease if the aperture of the new camera lens was not bigger to capture more pixels (since the area of the hologram would increase with the longer focal length). On the other hand, by increasing the aperture of the new lenses, the undesired hologram would again become harder to get rid of. We can derive the surface density achievable with peristrophic multiplexing based on the *f*/# of the imaging system.

Fourier plane peristrophic selectivity can be rewritten as :

$$d\psi = \frac{1}{f/\#(\sin\theta_r + \sin\theta_s)} \tag{1.4}$$

by replacing $f/N_p\delta$ by the $f/\#$ of the imaging system. The number of holograms that can be peristrophically multiplexed from 0 to π in rotation is given by :

$$\text{number of peristrophic holograms} = \pi f/\#(\sin\theta_r + \sin\theta_s) \tag{1.5}$$

Eq. 1.5 can be combined with Eq. 1.3 to get the surface density achievable with peristrophic multiplexing.

$$\text{surface density with peristrophic multiplexing} = \frac{\pi^2}{4}\frac{\sin\theta_r + \sin\theta_s}{(2\lambda)^2 f/\#} \tag{1.6}$$

From Eq. 1.5 we can see that if a lot of peristrophic holograms is what we want, then a large $f/\#$ lens system should be used. However, the surface density achievable at the Fourier plane is inversely proportional to the square of the $f/\#$. Therefore, in order to get high surface density, the lowest $f/\#$ imaging system should be used (Eq. 1.6). This reduces the number of peristrophic holograms but increases the overall surface density.

The maximum number of holograms that can be angularly multiplexed at each location is given by :

$$\text{number of angle holograms} = \frac{\Theta}{\Delta\theta'} = \frac{\Theta L \sin(\theta_r' + \theta_s')}{\lambda' \cos\theta_s'} \tag{1.7}$$

where Θ is the range of angle that can be used to store angle multiplexed holograms. $\Delta\theta'$ is the angular selectivity inside the recording material (first null), L is the thickness of the hologram, λ' is the wavelength of the laser inside the recording material, θ_r' (θ_s') is the angle between the reference (signal) beam and the photopolymer's surface normal measured from inside the material. For our experimental setup, L = 100 μm, the index of

refraction of the photopolymer = 1.525, λ' = 349 nm, θ_r' = 22°, and θ_s' = 16°, which gives $\Delta\theta'$ a value of 0.31° to the first null of the sinc function inside the material. However, Eq. 1.7 is valid only for planewave holograms. The signal beam spread inside the recording material was nearly 25° because of the large numerical aperture of the *f*/1.4 Nikon lenses. The actual angular selectivity curve from one hologram stored using the high density setup is shown in Figure 1.6.

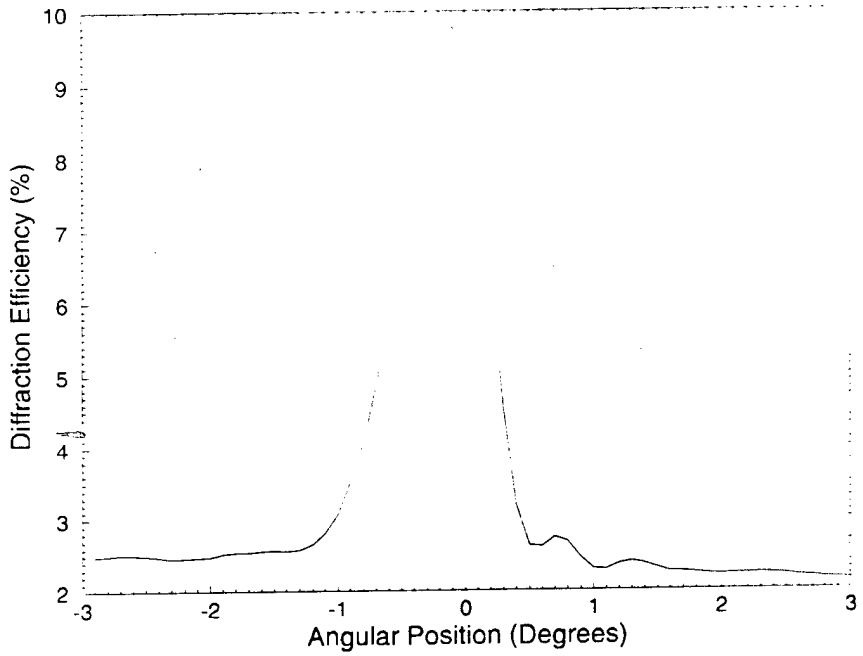

Figure 1.6 : The angular selectivity of one hologram recorded with θ_r' = 22° and θ_s' = 16°.

The diffraction efficiency of the hologram was measured by placing a lens with sufficient aperture to cover the entire reconstruction at the image plane of the hologram. The lens collected the entire hologram and a silicon detector was placed near the focal plane of the lens to measure the diffracted power as the recording material was rotated to different angular positions. The hologram was stored with θ_r' = 22° and θ_s' = 16° and the

'0' angular position in Figure 1.6 represents the angle of the rotational stage at which the hologram was stored.

Notice that the selectivity curve in Figure 1.6 is asymmetric and doesn't have the maximum diffraction efficiency at '0' angular position. This behavior does not match the simple angular selectivity theory of a sinc() function with regular null spacing. As stated previously, DuPont's photopolymer shrinks slightly when exposed to light. This shrinkage is part of the chemical process that creates the index grating and causes the Bragg condition of the stored hologram(s) to change slightly. The shrinkage effect is most apparent for high bandwidth holograms recorded in an asymmetric geometry. Figure 1.7 shows the κ-sphere representation of a high bandwidth hologram in an asymmetric geometry.

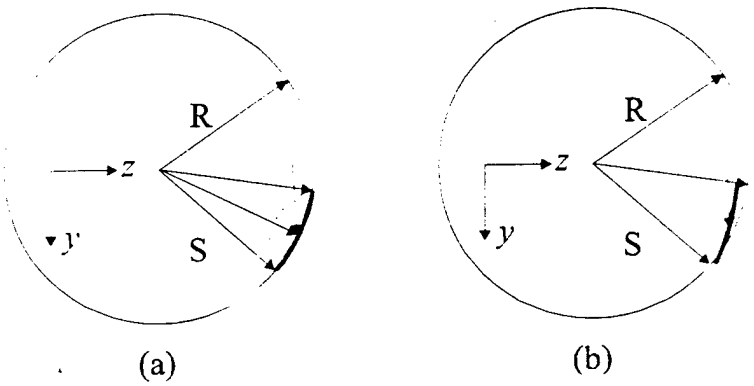

Figure 1.7 : κ-sphere representation of a high bandwidth hologram in asymmetric geometry. (a) The grating cone before shrinkage. (b) The grating cone after shrinkage.

Figure 1.7 (a) represents the κ-sphere diagram of a high bandwidth hologram before shrinkage has occurred. The planewave reference beam is represented as a single vector while the high bandwidth signal beam is represented as a spectrum of vectors. There exists a grating vector from the tip of the reference beam vector to every signal beam vector in the signal cone. One such grating vector is drawn in Figure 1.7 for

illustration and the grating cone on the κ-sphere in the y-z plane is highlighted with a thick, curved line. Shrinkage of the photopolymer occurs mostly in the z direction since the material is anchored on a glass substrate in the x-y plane. Photopolymer shrinkage compresses the grating cone in the z direction and lifts it off of the κ-sphere as shown in Figure 1.7 (b). The only part of the grating cone that remains on the κ-sphere is where the signal beam has the same angle as the reference beam, with respect to the surface normal of the photopolymer. For that special case, the grating vector has no z-components and therefore shrinkage has no effect on its Bragg condition.

We can re-Bragg-match portions of the grating cone by changing the reference beam angle slightly or by rotating the photopolymer around the x-axis. Figure 1.8 shows how this is done in the κ-sphere. In Figure 1.8 (a), by rotating the photopolymer counter-clockwise around the x-axis, the reference beam angle would appear smaller and this pushes the grating cone away from the κ-sphere. With sufficient counter-clockwise rotation, the upper portion of the grating cone will get pushed back on the κ-sphere. In Figure 1.8 (b), by rotating the photopolymer clockwise around the x-axis, the reference beam angle would appear larger, and this pulls the lower portion of the grating cone back on the κ-sphere. Notice in either case, the portion of the hologram that is Bragg-matched diffract at a slightly different angle than the original image. Furthermore, only a portion of the hologram can be Bragg-matched at a time using this method. For the asymmetric recording geometry shown in Figure 1.8, the upper portion of the grating cone requires a larger rotation to Bragg-match than the lower portion. This causes the diffracted power to dissipate slower when rotated in the counter-clockwise direction. Also, since a larger portion of the grating cone requires a counter-clockwise rotation to Bragg-match, the

maximum diffracted power angular position changes from no rotation to favor a slight counter-clockwise rotation. These effects are depicted in the angular selectivity curve of Figure 1.6. Negative angular positions refer to counter-clockwise rotation while positive angular positions refer to clockwise rotation of the photopolymer around the x-axis.

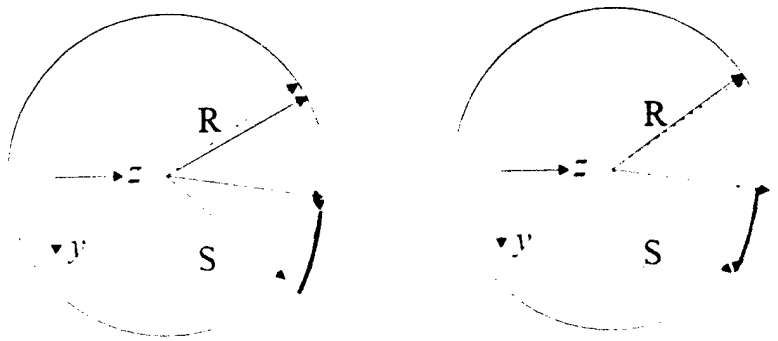

Figure 1.8 : κ-sphere representation of the Bragg-match condition. (a) To Bragg-match the upper portion of the grating cone. (b) To Bragg-match the lower portion of the grating cone.

We can figure out how much the photopolymer has shrunk by using the amount of rotation required to re-Bragg-match the different portions. Experimentally for our setup, the lower portion required almost no rotation to re-Bragg-match while the middle and the upper portions required a counter-clockwise rotation of 0.3 and 0.7 degrees, respectively. Assuming the modification to the reference beam angle is small when the photopolymer is rotated to re-Bragg-match different portions and the total index of refraction change is negligible, we can compute the shrinkage factor, γ, as :

$$\gamma = 1 - \frac{\cos\theta_s' - \cos\theta_r'}{\cos\theta_s' - \cos\left(\theta_r' + \Delta\theta'\right)} \tag{1.8}$$

where θ_r' is the reference beam angle, θ_s' is the signal beam angle for that portion of the hologram, $\Delta\theta'$ is the change in the reference beam angle due to the rotation (all angles

measured from inside the recording material). By plugging in the numbers corresponding to the upper portion of the hologram ($\theta_r' = 22^\circ$, $\theta_s' = 3.3^\circ$, $\Delta\theta' = 0.4^\circ$) we get a shrinkage factor of $\gamma = 0.04$. This means that the photopolymer shrunk by about 4% for that hologram.

It is hard to tell the null spacing from the angular selectivity curve of Figure 1.6 since the spacing is different for clockwise and counter-clockwise rotations. A better indication of where the next angle hologram can be multiplexed is the amount of noise introduced by adjacent angle holograms. This can be obtained by storing three angle multiplexed holograms and then measure the amount of noise experienced by the middle hologram. The SNR measured from three angularly multiplexed holograms with an angular separation of 5° was 4 (a rotation of 5° around the x-axis). The quality of the reconstructions were good and no bit errors were observed. By decreasing the angular separation to 2°, the SNR of the middle hologram dropped to 3.2 and the distinction between the 'on' and 'off' pixels were not as clear. No bit-errors were observed in the reconstruction of the middle hologram but errors were likely if the angular separation was decreased further. For comparison, the SNR measured for a single hologram (no multiplexing) was 4.5. Figure 1.9 shows the center portion of the reconstructed hologram for the three cases.

Figure 1.9 shows that visually, the quality of the hologram decreased as the angular separation was decreased from 5° to 2°. In order to avoid bit-errors with this setup, the angular separation must be greater than 2°. On the other hand, we would also like to store as many angle holograms as possible to boost the overall surface density. As stated before, with a page density of .33 bits/μm^2, we need at least 30 holograms to

achieve a surface density of 10 bits/μm^2. We have already determined that up to 4 peristrophic holograms can be stored from 0 to π without cross-talk. In order to get at least 30 holograms, we would need to store 8 angle holograms at each of the 4 peristrophic positions. Our setup has a geometrically limited Θ (Eq. 1.7) of slightly less than 20°. Therefore we picked an angular separation of 2.5° per hologram and hoped the SNR would be good enough to avoid bit-errors.

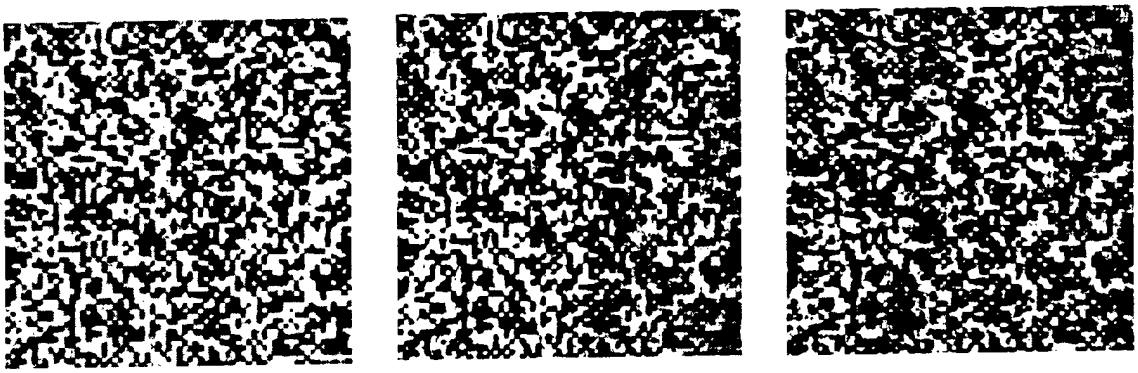

(a) (b) (c)

Figure 1.9 : The center portion of the middle hologram for three different cases. (a) One hologram. (b) Three angle multiplexed holograms separated by 5° each. (b) Three angle multiplexed holograms separated by 2° each.

The method in which we determine the amount of noise in a hologram is shown in Figure 1.10. The reconstructed hologram is viewed by a CCD detector array placed at the image plane. The active area of our CCD array (.65 mm × .48 mm) is much smaller than the aperture of the reconstructed hologram. Therefore, in order to get a fair representation of the quality of a hologram, the CCD array was physically moved to capture an image from the left, center, and right sides of the reconstructed hologram. The reported SNR of a hologram is usually the average SNR of the three images. From the approximately 140 × 100 data mask pixels captured within the CCD array aperture, a smaller image of 300 × 300 CCD pixels (about 65 × 65 data mask pixels) is sent to a

computer program for analysis. Because the pixel pitch of the data mask is 45 μm and the pixel pitch of the CCD array is approximately 10 μm, each data mask pixel is over-sampled during readout. In order to get the true intensity values of the data mask pixels, a grid with the correct spacing is overlaid on the image and the intensity values of the CCD pixels within each grid box is integrated to produce the data mask pixel value. The computer program first expands the image by 2X to generate an image with 600 × 600 CCD pixels so that a grid can be more easily placed. This also allows the user to specify a margin in which the edges of the grid box will not be integrated. In the un-expanded image, each data mask pixel is sampled by 20.5 CCD pixels on the average, and the program produces an estimate for the intensity of an data mask pixel by integrating only 9.5 CCD pixel values (on the average, at the center of the grid). Therefore, on the average, 11 CCD pixels are discarded as edge pixels. The computer program has *a priori* knowledge of which data pixels are supposed to be 'on' and 'off'. This allows the program to compute the SNR, generate a histogram of the data mask pixels, and determine the bit-error-rate (BER) given a threshold value. The program can also 'auto-jiggle' the overlaid grid by a few CCD pixels to obtain the best SNR value possible.

After determining the necessary angular separation, sets of eight angularly multiplexed holograms (2.5° separation) were recorded at each of the four peristrophic positions (45° in rotation), for a total of 32 holograms stored. The overall surface density was 32 holograms × 0.33 bits/μm^2 or 10.6 bits/μm^2. The exposure time per hologram varied from 2 to 4 seconds and the exposure schedule was obtained iteratively through trail-and-error. We did not use the method discussed in a previous experiment to compute the exposure schedule since only 32 holograms were required in this experiment. Figure

1.11 shows the diffracted powers of the 32 holograms. The average diffraction efficiency of the stored holograms was approximately 3.5×10^{-3}.

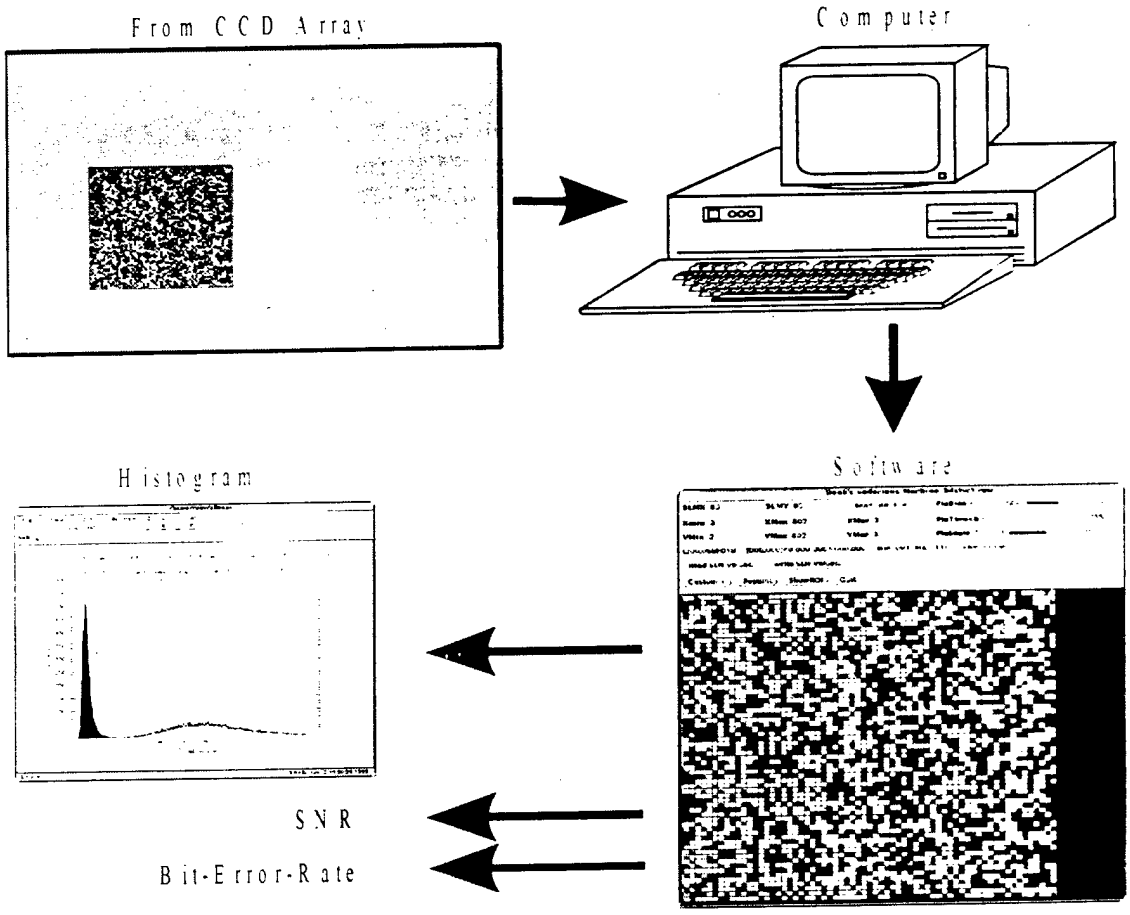

Figure 1.10 : Block diagram of how the stored data is read out and analyzed.

The left, center, and right sides of the data mask imaged through the system without any holograms can be compared with the reconstructions of some of the stored holograms in Figure 1.12. Visually, the quality of the stored holograms were fairly good and no bit-errors were found in the sampled holograms.

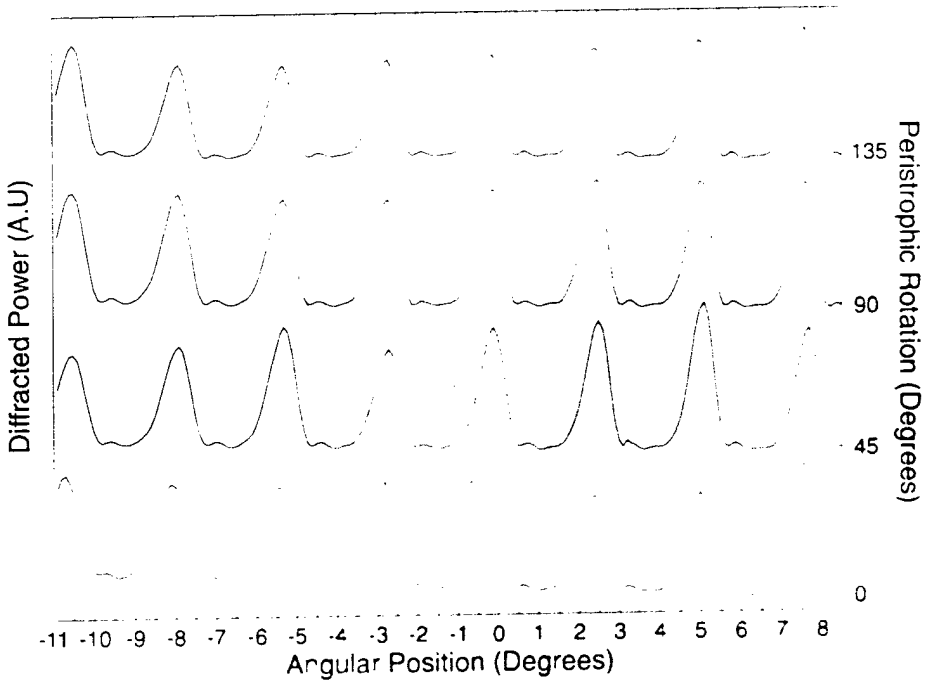

Figure 1.11 : Diffracted powers of the 8 angle multiplexed holograms at each of the 4 peristrophic positions.

The most challenging aspect of the high-density experiment proved to be the suppression of noise in the system in order to achieve acceptable levels of SNR and probability of error. The results shown in Figure 1.11 and 1.12 were achieved only after many iterations of fine tuning the setup. The way we achieved high density was by increasing the angular bandwidth of the signal and reference arms. The noise level goes up as the angular bandwidth increases for the majority of noise sources, while the signal level does not. Consequently, the SNR starts to decrease as we attempt to achieve higher surface density and it becomes necessary to track carefully each of the noise sources and to optimize the system in order to minimize their effect. Through this process we were able to demonstrate a surface density of 10 bits/μm^2 without any errors detected among the bits that were tested.

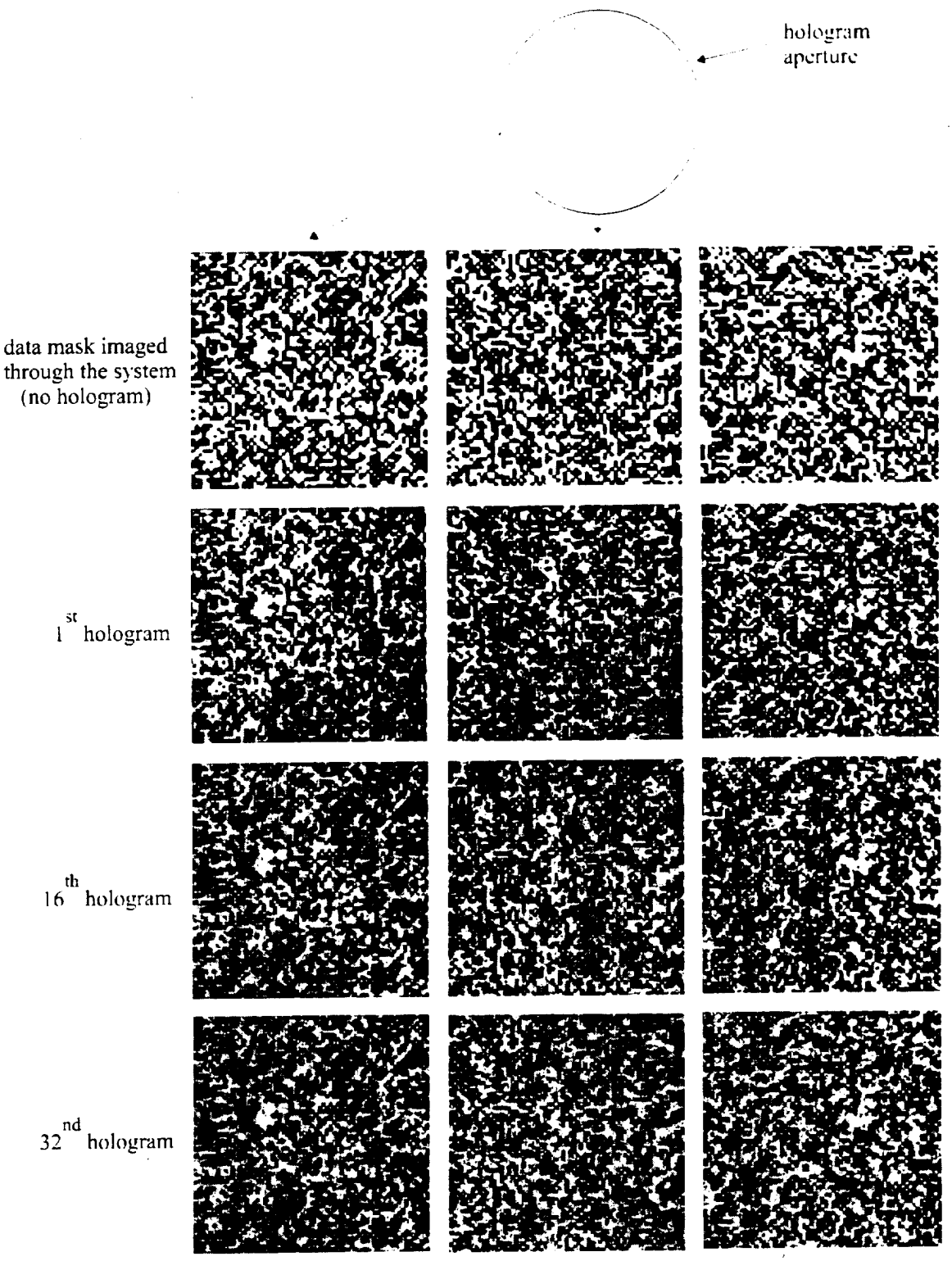

Figure 1.12 : The left, center, and right sides of the data mask and the reconstructions from some of the 32 stored holograms.

We can divide the noise sources into two categories: system noise and hologram noise. Lens aberrations, data mask imperfections, detector noise, scattering, and multiple reflections from lenses and other optical components, laser non-uniformity and fluctuations, and data mask-to-CCD pixel misalignment are examples of system noise. The rest of the noise arises from the hologram itself. Specifically, the hologram can introduce inter-page cross-talk, inter-pixel cross-talk, scattering from the recording material, multiple reflections in the medium, non-uniform diffraction efficiency in the recorded holograms, distortions that are due to surface imperfections, blurring that is due to limited spatial resolution of the material, and material shrinkage. We can separately determine the system noise level by simply imaging a page of data onto the CCD array without any recording material and measure the SNR of the detected image. After minimizing the system noise, we then followed a step-by-step procedure to identify the various sources of hologram noise.

The SNR obtained from various experimental conditions are plotted in Figure 1.13. The first measurement is SNR = 10, which is due to system noise only. We obtained this by transmitting the signal beam through the system without any recording material. The histograms of the 'on' and 'off' pixels were well separated and no errors were observed. Next, a glass substrate on which the photopolymer is usually laminated was placed at the recording plane of the system. The SNR dropped to 9 because of the parallel plate interference effect and the slight aberrations caused by the substrate. When we introduced a piece of UV-cured photopolymer laminated on a glass substrate at the place where the holograms are normally located, the SNR dropped from the upper limit of 9 to approximately 7. The major cause of this drop in SNR is most likely due to internal

reflections within the film and the glass substrate (parallel plate interference effect) and possibly scattering. The interference fringes could perhaps be eliminated with antireflection coatings applied to both the glass and the photopolymer.

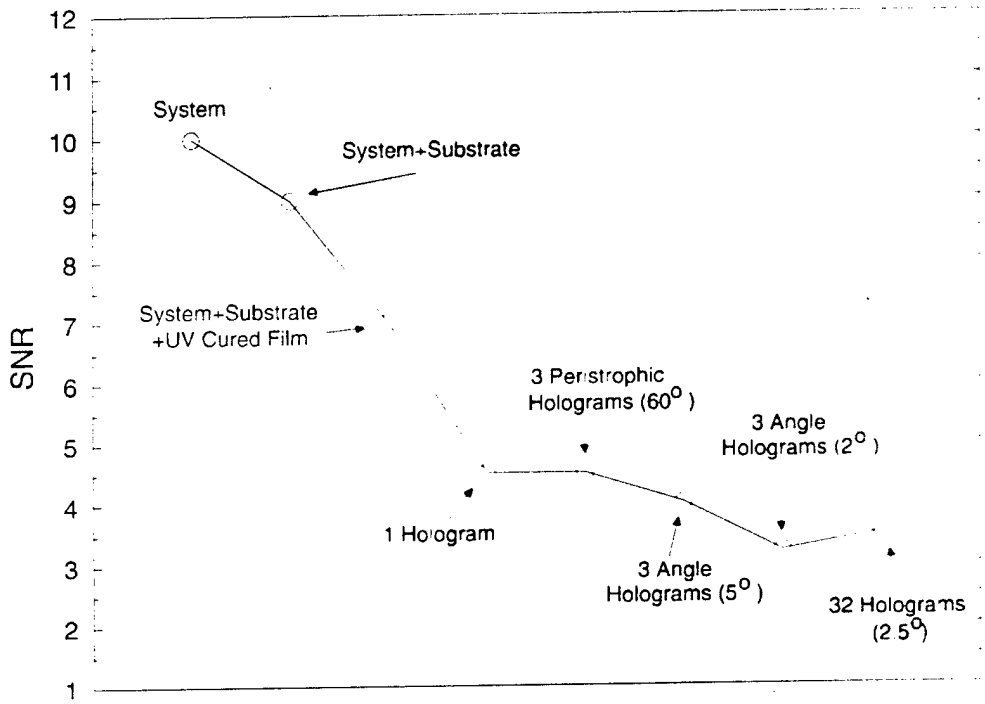

Figure 1.13 : SNR characterization for the high density setup.

A SNR of approximately 4.5 was obtained when a single hologram was recorded and its reconstruction evaluated. The histogram of the 'on' and 'off' pixels were still clearly separated and no errors were observed. This shows that the resolution of the photopolymer is sufficient to record high density holograms with clarity. The reason the SNR dropped from 7 to 4.5 for one hologram is strongly connected to the internal reflections from the boundaries. As stated above, the signal beam creates an interference pattern (fringes) when it passes through the film and the glass substrate. This is also true for the reference beam when it is brought in to record a hologram. Furthermore, when the reference beam is used to reconstruct the stored holograms, it also creates an interference

pattern that can be seen with the naked eye on the film. Therefore, the reconstruction suffers from the fringes that are in the reference beam twice. Other effects such as the fidelity of the recording material also plays a role in degrading the SNR.

When compared to the SNR of a single hologram, the average SNR of three peristrophically multiplexed holograms (60° separation) remained at ~4.5. This indicates two things: peristrophic multiplexing does not introduce cross talk (as expected), and the superposition of three holograms does not significantly deteriorate the quality of each hologram. The average SNR of three angle-multiplexed holograms (5° separation) dropped to ~4. This is a clear indication of cross-talk noise in the angle holograms. The SNR dropped further to ~3.2 for angle holograms separated by 2°. With a SNR of only 3.2, the histograms of the 'on' and 'off' pixels almost overlapped, but no errors were observed. The final SNR for the 10 bits/μm^2 experiment is 3.5 with an angular separation of 2.5° between angle holograms.

In the course of the experiment, we discovered that the strength of the holograms is strongly related to the SNR. If the initial holograms are very strong, then the later holograms will suffer from the index modulation of the previously stored holograms. This effect can be observed by imaging the data mask though the spot where strong holograms have been stored. The image of the data mask gets blurred and the 'off' pixels get filled with some of the 'on' pixels' energy. This means that any subsequent holograms recorded at that spot would have poor SNR. On the other hand, the holograms cannot be recorded too weakly neither. For the high density setup, the hologram area is about 1.77 mm^2 and the final reconstruction at the detector plane has an area of about 12 cm^2. There is nearly a 700X increase in area from the hologram to the detector plane. This means the intensity

of the reconstructed hologram would decrease by the same amount at the detector plane. In order to have good SNR, a sufficient number of photons must strike the detector array. For the 10 bits/μm^2 experiment where 32 holograms were stored, the diffraction efficiency of each hologram was approximately $\eta = 3.5\times10^{-3}$. This hologram strength was chosen through trail-and-error to avoid excessive index modulation of later holograms and to have sufficient diffracted power to achieve a good SNR. With the experimentally measure *M*/# of 6.5 for the HRF-150-100 photopolymer, the diffraction efficiency per hologram should have been around 4×10^{-2} for each of the 32 holograms. However, we did not use the entire dynamic range of the photopolymer for this experiment since that would have caused index modulation problems. Instead, we used only approximately 30% of the dynamic range of the material, which effectively reduced the *M*/# to 1/3rd of its original value.

For the high density experiment, we also determined that with a proper setup, photopolymer scattering is not a big factor in hologram SNR. A proper setup means: (1) the aperture of the reference beam is closed down to the minimum size required so the energy from material scattering does not over-power the reconstruction. (2) The reference beam angle is large enough so the scattering cone have very little energy in the signal beam direction. In the high density setup, we used a 4-*f* system plus an iris in the reference arm to control the aperture of the reference beam. This allowed us to illuminate only the area of the photopolymer that had holograms stored. To reduce the amount of scattered energy that gets collected by the signal beam lenses, the reference beam angle was made bigger than the signal beam angle by 10° in our setup. The diffraction efficiency of each hologram was approximately 3.5×10^{-3} whereas the equivalent

diffraction efficiency of the light scattered from the photopolymer when it is illuminated by the reference beam is only 3×10^{-5}. Therefore, scattering is a negligible contributor to the overall noise level for the 10 bits/μm^2 experiment.

Even with all the noise sources discussed above, the nine sampled reconstructions from the 32 holograms stored (Figure 1.12) had no detectable errors. The combined histogram from the nine different sampled windows is shown in Figure 1.14. We obtained an estimate for the probability of error by fitting a first-order χ^2 distribution to the histogram of Figure 1.14. The estimated probability of error from this model is approximately 10^{-4}, in the same range as compact discs (10^{-4} to 10^{-6}).

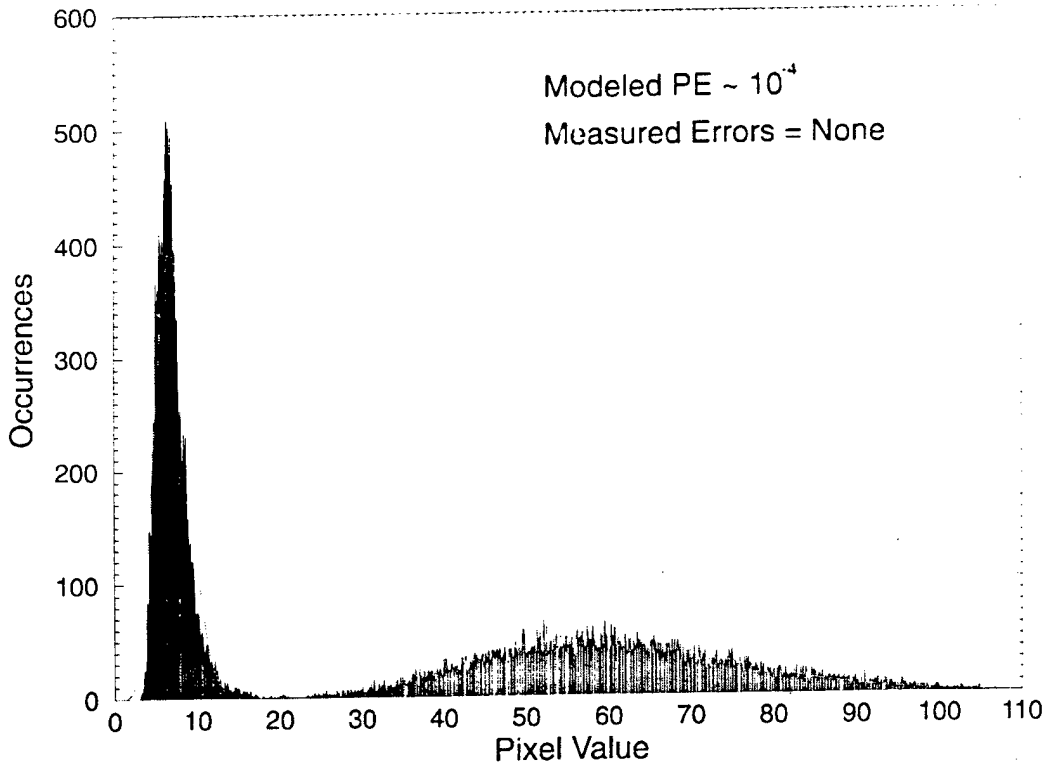

Figure 1.14 : Combined histogram obtained from nine different sampled windows for the 10 bits/μm^2 experiment using angle and peristrophic multiplexing.

1.3 Holographic 3-D Disks Using Shift Multiplexing

1.3.1 Introduction

In the previous experiment (Chapter 1.2), we demonstrated a storage density of 10 bits/μm^2 using the 100 micron thick DuPont photopolymer. This was achieved by utilizing a combination of peristrophic and angle multiplexing to store 32 overlapping holograms in one area. Each hologram contained approximately 590,000 pixels (bits) for a total of 2.25 MBytes stored in an area of 1.77 mm^2. The raw estimated bit-error-rate (BER) of the system, determined from reconstructed holograms, was around 10^{-4}.

The above experiment is important for several reasons. First, it shows that a storage density of approximately ten times higher than the compact disc can be achieved holographically, using a recording material that is only 100 micron thick. The projected storage density of that system, using a 1 mm thick recording material, is around 100 bits/μm^2. Second, it shows that high resolution holograms can be recorded in the DuPont photopolymer with sufficient signal-to-noise ratio for commercial applications. With two-dimensional error correction codes, the BER can be reduced to the industry standard, with overheads similar to CDs.

In this section, we discuss a new 10 bits/μm^2 experiment that builds upon the previous experiment. A novel multiplexing method called shift multiplexing, is used to record holograms in a holographic 3-D disk. The disk architecture is interesting to us because most of today's randomly accessed mass storage devices are based on the disk architecture. The compact disc alone has revolutionized the way information is stored and distributed. Its low cost per megabyte, high storage capacity, and removability makes it ideal for mass distribution. In this section, we will show a holographic 3-D disk system

that is very similar to the compact disc in most respects. However, our holographic system offers higher storage density and potentially greater data transfer rate than conventional disk based storage devices.

1.3.2 Holographic 3-D disks

There are several formats in which holograms can be stored on a disk. Stacks of holograms can be stored in non-overlapping areas on the disk as shown in Figure 1.15. In each stack, a number of holograms are multiplexed by using angle, peristrophic, wavelength, and other multiplexing methods to increase the surface density. To increase the storage capacity of the disk, stacks of holograms are then spatially multiplexed on non-overlapping areas on the disk. This is the most natural method of storing holograms on a disk using conventional multiplexing techniques. During readout, the disk is first rotated to the correct stack and then a reference beam of the proper angle or wavelength is introduced to reconstructed the desired hologram. To accomplish this, a complicated reference beam delivery system or a wavelength tunable laser is required.

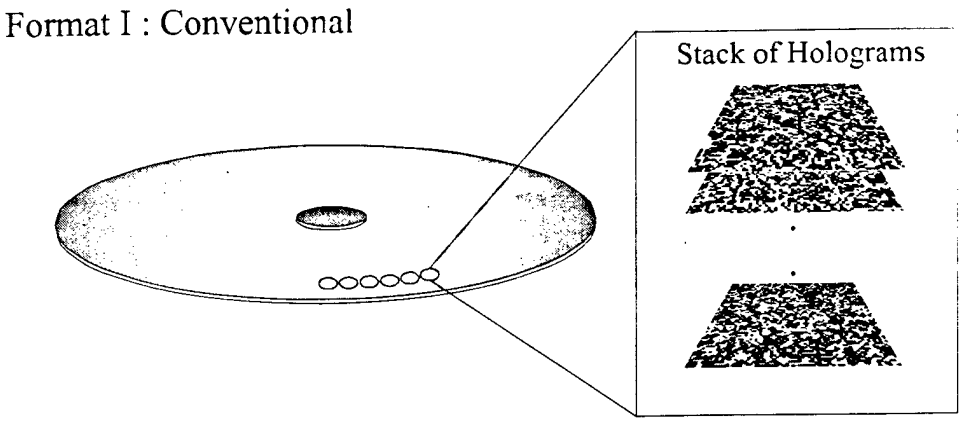

Figure 1.15 : Format in which holograms can be stored in a holographic 3-D disk using conventional multiplexing methods.

For example, Figure 1.16 shows the schematic diagram of a disk system using angle and peristrophic multiplexing. The signal beam is on axis and the reference beam is off axis (with respect to the disk's surface normal). The angle of the reference beam is changed to achieve angle multiplexing while the rotation of the reference beam around the signal beam gives peristrophic multiplexing. The disk motion provides access to different spatial locations for storage and the entire signal and reference beam assembly can be moved radially to access more locations. Using this setup, we can pretty much repeat the same high density experiment of Chapter 1.2 at many locations on the disk. The only problem is how to deliver the reference beam in the angles shown in Figure 1.16.

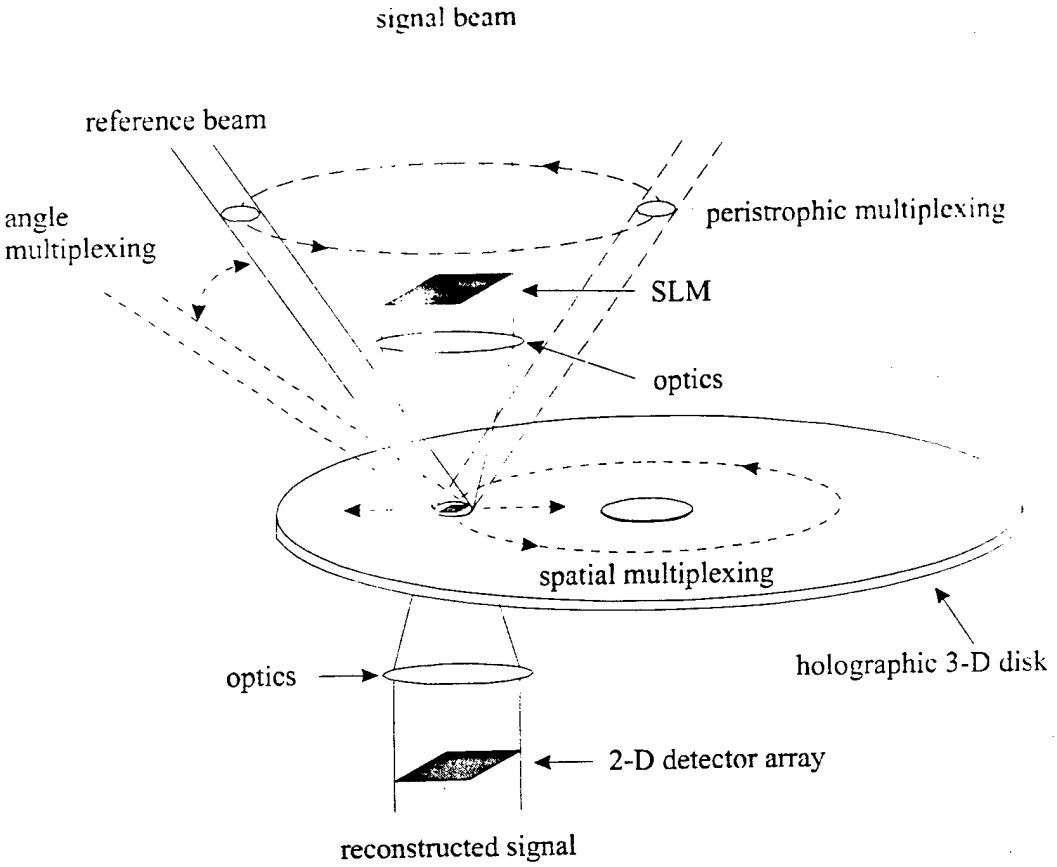

Figure 1.16 : Schematic diagram of a holographic 3-D disk system using peristrophic and angle multiplexing.

Furthermore, holograms stored in this stack format is unnatural when compared to the compact disc. It is highly desirable in the disk architecture, to store holograms sequentially in a spiral fashion, from the inner radius to the outer. Likewise, the reference beam system should be as simple and practical as possible. To accomplish these two goals, we use a new multiplexing method called shift multiplexing in our holographic 3-D disk system. Shift multiplexing allows holograms to be stored sequentially in partially overlapping areas as shown in Figure 1.17. The spiral tracks can also be overlapped to further increase the surface density. With shift multiplexing, holograms are recorded with a multiple planewaves reference beam or a spherical reference beam. When a hologram recorded with a multiple planewaves reference beam is shifted, reconstructions from the multiple planewaves will add destructively and constructively in a periodic cycle. Overlapping holograms can be stored at the nulls of the periodic function. When a hologram recorded with a spherical reference beam is shifted slightly, the wavefront the hologram experiences becomes different from the wavefront used to record it. Therefore, the hologram will simply Bragg mis-match (if shifted parallel to the plane of interaction) or the reconstruction will deflect at a different angle and miss the detector (if shifted perpendicular to the plane of interaction). Hence, instead of using several different reference beam angles or wavelengths to multiplex holograms in a stack, a single fixed reference beam can be used to record partially overlapping holograms in a spiral track. During readout, the disk is spun and sequential holograms will become Bragg matched and be readout by the fixed reference beam, much like the pits on the compact disc. However, with our holographic system, instead of reading out one bit at a time as the disk rotates, an entire page of a hologram can be read out at a much higher data transfer rate.

Furthermore, since holograms overlap in area, the surface density is increased. The theory behind shift multiplexing is discussed in the next section.

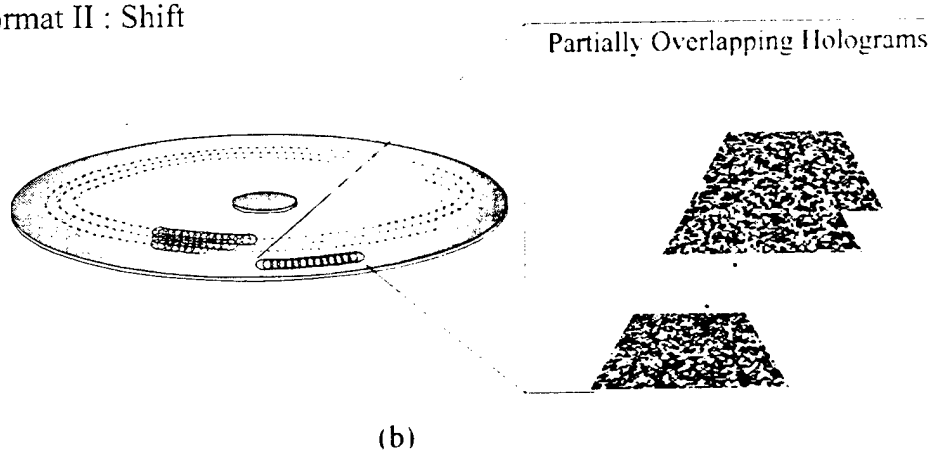

Figure 1.17 : Format in which holograms can be stored in a holographic 3-D disk using shift multiplexing.

1.3.3 Shift Multiplexing

1.3.3.1 Multiple Planewaves Reference Beam

In all the experiments shown previously in this thesis, the holograms were recorded by interfering the signal with a planewave reference beam. By changing the angle of the reference beam (either angularly or peristrophically), more holograms can be multiplexed at the same location. For the holographic 3-D disk, we would like to store holograms sequentially by slightly shifting the recording material between holograms: This slight displacement must somehow get rid of the reconstructions from the previously stored holograms, so that another hologram could be stored without too much cross-talk. For a hologram recorded with a single planewave reference beam, shifting the recording material during reconstruction slowly decreases the hologram's diffracted power. This is because part of the hologram's area moves out of the reference beam's illumination (Figure 1.18).

The amount of shift required for the hologram's diffracted power to reach zero is the width of the hologram, x. This means that in order to store another hologram, we would have to shift to a new location on the recording material. Therefore, when using a single planewave reference beam, no more than one hologram can be stored at a location by shifting the recording material.

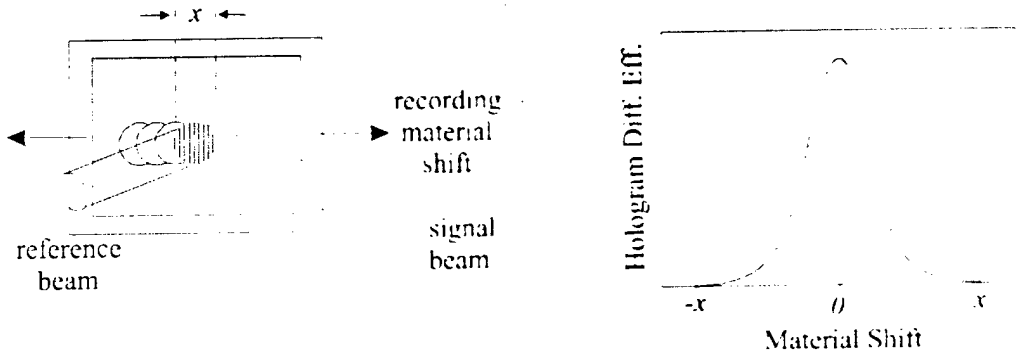

Figure 1.18 : Shift multiplexing using a single planewave reference beam.

What if instead of recording with only one planewave reference beam, a hologram was recorded by interfering the signal with multiple planewaves simultaneously? In that case, each planewave will form a separate hologram with the signal beam. Initially, all the reconstructions from the separate holograms will be in phase and add constructively. However, if the recording material is shifted during reconstruction, the phases of the holograms will start to differ and with sufficient shift, the holograms will completely destructively interfere and a null in diffracted power appears (Figure 1.19). The reconstruction's diffracted power is periodic because at some point in shift, the holograms will again add constructively. However, the diffracted power will not be as strong as at the zero shift position because some of the hologram's area is outside the reference beam's illumination.

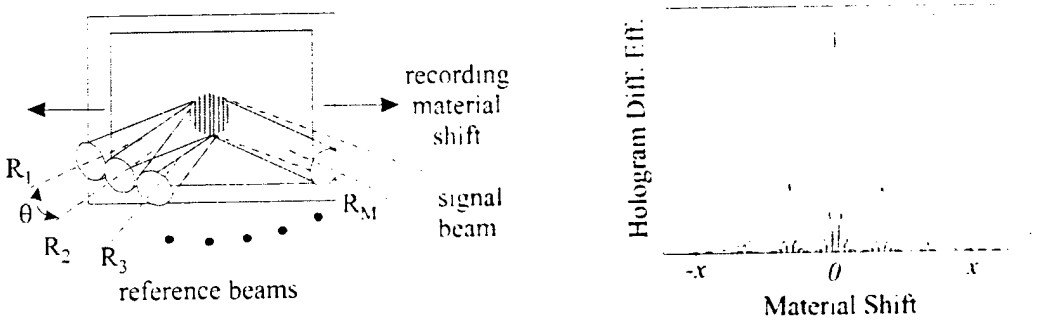

Figure 1.19 : Shift multiplexing using multiple planewaves.

The theory behind shift multiplexing using multiple planewaves is very simple. Figure 1.20 (a) shows a diagram of multiple planewaves recording a hologram with the signal beam. The angular separation between the reference planewaves is θ and they all have the same intensity. Each planewave records a separate hologram with the signal beam and all the holograms are in-phase when the recording material is not shifted. For the reference beam that makes an angle of $\theta/2$ with respect to the surface normal of the recording material (Figure 1.20 (b)), shifting the recording material during reconstruction introduces a phase difference of :

$$\frac{2\pi}{\lambda}\delta \sin(\frac{\theta}{2}) = \frac{2\pi}{\lambda}\zeta \qquad (1.9)$$

where δ is the shift distance, ζ is the phase introduced, and λ is the wavelength of the laser. Since the reference planewaves are symmetric with respect to the surface normal of the recording material, the sum of the phases for all the shifted holograms can be written as :

$$\text{sum of the phases} = \sum_{\theta_m} e^{i\frac{2\pi}{\lambda}\delta \sin(\theta_m)} \qquad (1.10)$$

where $\theta_m = \left(m - \frac{M-1}{2}\right)\theta$, for m = 0,..., M - 1, and M is the total number of planewaves in the reference arm. Eq. 1.10 can be simplified further to show the intensity of the reconstructed signal as a function of recording material shift δ:

$$I(\delta) = \left(\sum_{\theta_m} 2\cos\left(\frac{2\pi}{\lambda}\delta \sin(\theta_m)\right) \right)^2 \qquad (1.11)$$

Assuming the angle between the reference planewaves is small ($\theta \simeq \sin\theta$), the period of Eq. 1.11 is :

$$\delta_p = \frac{\lambda}{\theta} \qquad (1.12)$$

and the zeros of Eq. 1.11 within a single period are at :

$$\delta_l = \frac{\lambda}{M\theta} l, \qquad l = 1, \ldots, M\text{-}1 \qquad (1.13)$$

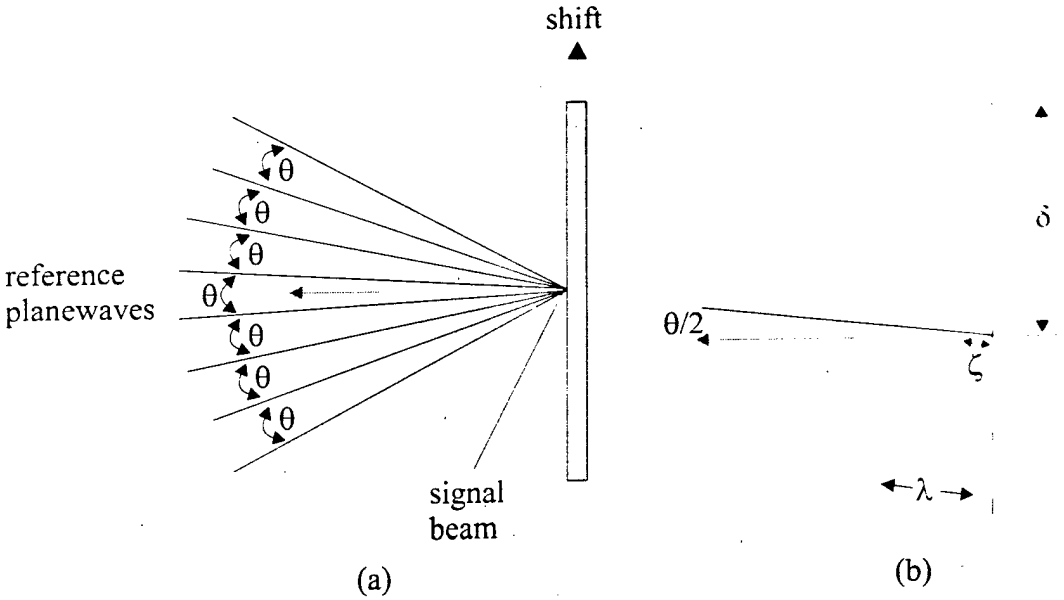

Figure 1.20 : Multiple planewaves shift multiplexing setup. (a) The delivery of multiple planewaves. (b) Phase introduced when shifted, for one planewave.

According to Eq. 1.13, it is theoretically possible to record M partially overlapping holograms within the period defined by Eq. 1.12, each separated by $\delta = \lambda / M\theta$. After recording the first hologram, there are M-1 nulls before the first hologram becomes bright again. At each of the nulls, one additional hologram can be written, bring the total number of holograms stored to M. To store more holograms, the material must be shifted until the first hologram is completely out of the illumination of the reference beam, eliminating the periodicity of the first hologram.

M, the number of planewaves in the reference arm determines how many overlapping holograms could be stored in one period and θ, the angle between the reference planewaves determines the period of the stored hologram. A large M allows many holograms to be stored in a given area and a small θ increases the period width. So far, the thickness of the recording material, the signal beam angle with respect to the recording material's surface normal, and the signal bandwidth have nothing to do with the number of holograms that can be stored in a given volume. However, they must be accounted for somehow or else we could break the V/λ^3 density maximum by using a large number of planewaves in the reference arm to store many high bandwidth holograms in a very thin recording material. Figure 1.21 shows the κ-sphere representation of a two planewaves reference beam recording a hologram with a planewave signal beam. Each planewave reference records a separate grating with the signal beam as shown in Figure 1.21 (a). Since the grating vectors can be read by either reference beams, the κ-sphere diagram during reconstruction looks like Figure 1.21 (b). Figure 1.21 (b) shows that two 'ghost' signals get reconstructed along with the desired signal beam. If the angle between the two planewaves reference is θ, then the angles the 'ghost' signals make with the desired

signal is $\pm\theta$. The strength of the 'ghost' signals depends on the Bragg selectivity since the grating vectors for them are off the κ-sphere. There are two ways to get rid of these 'ghost' images. One is to select the correct angle between the reference planewaves so the 'ghost' reconstructions are at the nulls of the Bragg selectivity. This can be achieved by picking a minimum $\theta \simeq \lambda/L\tan\theta_s$, where λ is the wavelength, L is the thickness of the recording material, and θ_s is the angle of the signal beam with respect to the surface normal of the recording material. The second method is to filter the 'ghost' reconstructions with a spatial filter placed somewhere before the detector. In this case, the minimum angular separation between the reference planewaves for thin recording materials is the bandwidth of the signal beam. Both methods restrict the minimum angular separation between the reference planewaves. This limits the number of reference planewaves that can be in the reference arm and therefore the number of shift holograms that could be stored in a setup.

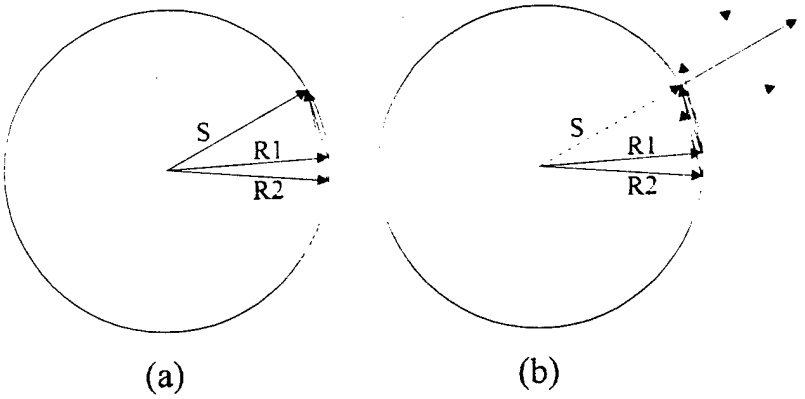

Figure 1.21 : κ-sphere representation of a hologram recorded with a two planewaves reference beam. (a) Double grating formation during recording. (b) Reconstruction showing 'ghost' images.

To experimentally demonstrate shifting multiplexing with a multiple planewaves reference, we constructed the setup shown in Figure 1.22. A multiple planewaves

reference was generated by recording 20 regularly spaced planewave holograms in a piece of HRF-150-38 photopolymer. The reference planewave* was fixed while the angle of the signal planewave* was changed by 0.25° between holograms with a rotational stage and a 4-*f* lens system. The diffraction efficiency of the 20 planewave holograms were equalized by using a recording schedule generated with the iterative method shown in a previous experiment. Once the holograms have been stored and the photopolymer properly cured, illumination with the fixed reference planewave* reconstructs all 20 planewave holograms simultaneously. The second 4-*f* system re-images the fan of 20 planewaves onto another piece of HRF-150-38 photopolymer as the multiple planewaves reference beam. The second photopolymer was mounted on a linear translation stage so the diffracted power from the stored holograms could be measured as a function of material displacement. Another signal planewave was bought in to record a hologram in the photopolymer with the multiple planewaves reference. For this experiment, the angular separation of 0.25° was much smaller than the Bragg selectivity of the 38 micron thick photopolymer. Therefore, a spatial filter was placed at the Fourier plane of the third 4-*f* system to block the 'ghost' images. A power detector was placed at the image plane of the third 4-*f* system to measure the diffracted power of the reconstructed hologram.

Figure 1.23 shows the diffracted power of a planewave hologram recorded using the setup shown in Figure 1.22 as the photopolymer was shifted. The diffracted power as a function of material shift is a periodic function modulated by the width of the hologram. Shifting the hologram moves some of the hologram's area out of illumination and therefore, the intensity of the periodic function falls off as the material is shifted further away from the center. The blow-up of the center portion of Figure 1.23 is shown in

Figure 1.24, along with the theoretical prediction according to Eq. 1.11. The experimentally obtained period of 115 μm and a null spacing of 5.75 μm match closely with the theoretical prediction of δ_P = 112 μm and δ_Z = 5.6 μm. The slight discrepancy is caused by the $\theta \simeq \sin\theta$ approximation used in the theoretical prediction.

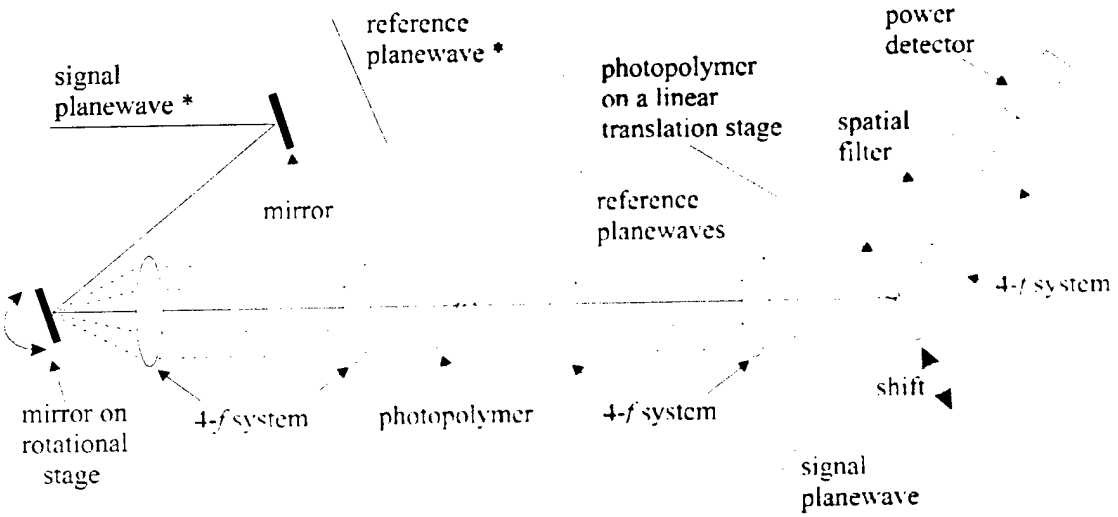

Figure 1.22 : The setup used to experimentally demonstrate shift multiplexing using a multiple planewaves reference beam.

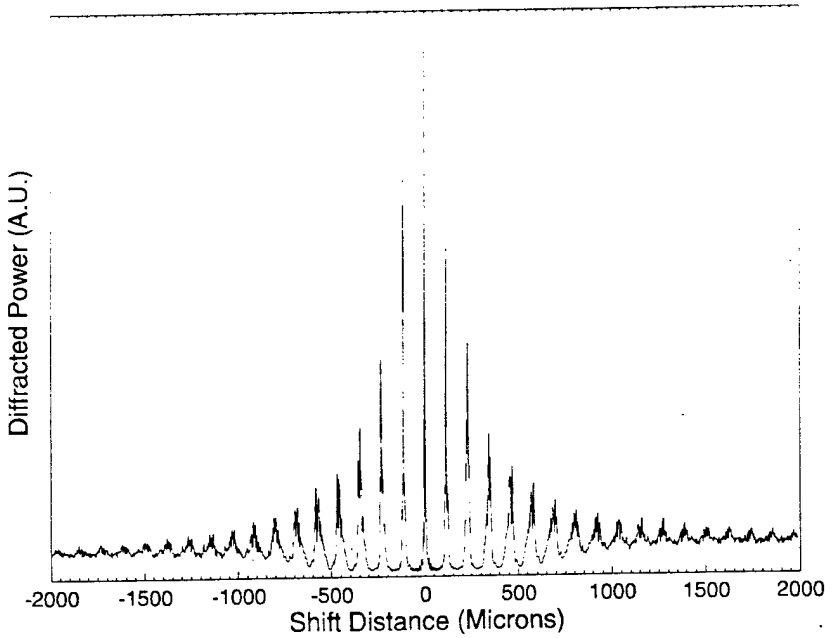

Figure 1.23 : The diffracted power as a function of material shift for a planewave hologram recorded with a 20 planewaves reference arm.

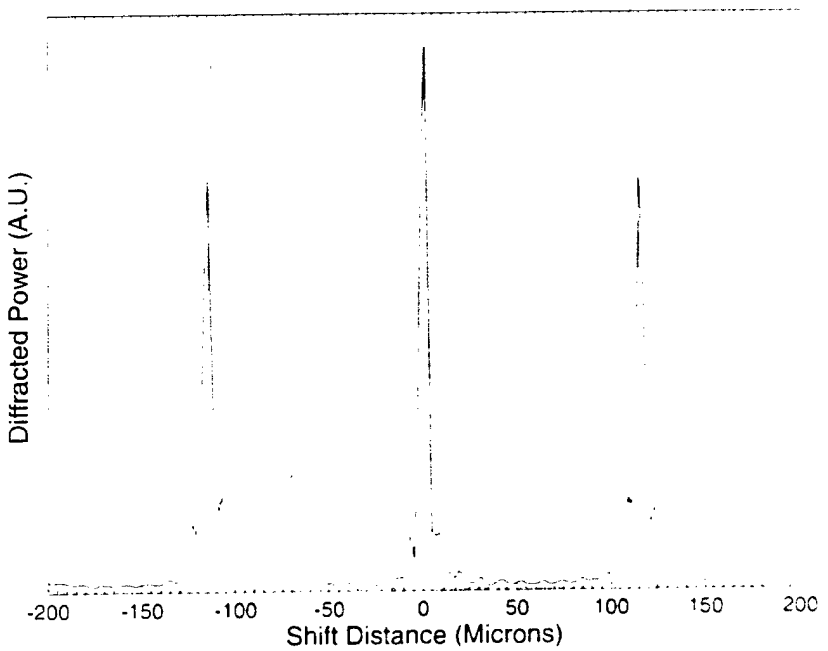

Figure 1.24 : Blow-up of the center portion of Figure 1.23 and the theoretical intensity curve according to Eq. 1.11.

Figure 1.25 shows the diffracted power a 100 × 100 random bit pattern image plane hologram recorded and measured with the same setup. The period and the null spacing remained the same but the nulls are less distinguishable due to the increased signal beam bandwidth. As with angle multiplexing, the nulls rarely have zero diffracted power in an actual experiment. In order to reduce cross-talk noise, angle multiplexed holograms are usually stored several nulls away from one another. Figure 1.26 shows three holograms shift multiplexed within one period. Holograms #2 and #3 were multiplexed within a single period of Hologram #1, with comfortable separations. Each hologram have its own array function which decays with material displacement. The quality of the reconstructed holograms were very good with no noticeable cross-talk noise. However from Figure 1.26 it is clear that even though we used 20 planewaves in the reference arm, fewer than 20 holograms could be stored within the same period with acceptable SNR.

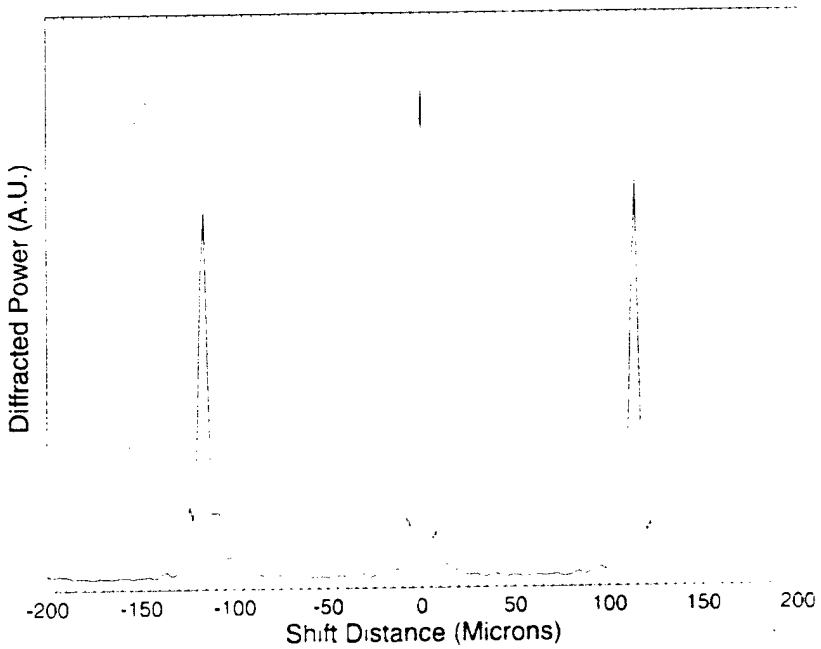

Figure 1.25 : The diffracted power as a function of material shift for a 100 × 100 random bit pattern image plane hologram recorded with a 20 planewaves reference arm.

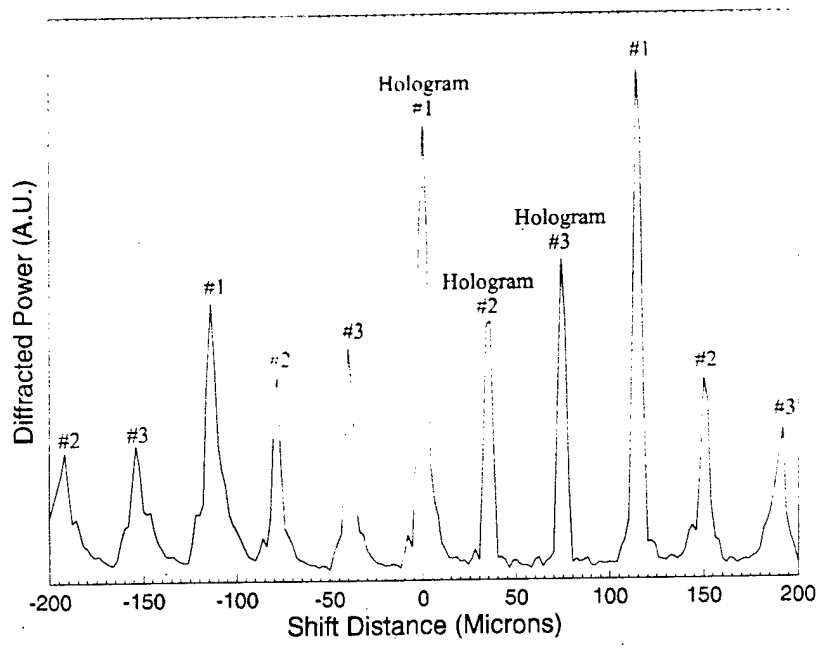

Figure 1.26 : The diffracted power of three random bit pattern image plane holograms recorded with a 20 planewaves reference beam as a function of material shift.

According to Eq. 1.12 and 1.13, by decreasing θ and increasing M, it is theoretically possible to store holograms that are very sharp (null spacing is very small)

and have no periodicity (the period is larger than the width of the hologram). To demonstrate this effect, we replaced the photopolymer that generated the multiple planewaves with an etched glass plate. The glass plate was patterned with random on and off lines with a pitch of 5 μm and then etched to roughly $\lambda/2$ in depth. When illuminated on axis, the etched glass plate produced a continuous fan of planewaves in the direction that is perpendicular to the etched lines. The second 4-*f* system in the setup shown in Figure 1.22 re-images the continuous fan of planewaves onto the recording material as the multiple planewaves reference beam. Figure 1.27 shows the diffracted power as a function of material shift for a planewave hologram recorded with a continuous fan of planewaves. The null spacing became much closer together and the periodicity of the hologram was destroyed. However, since the angular separation between the reference planewaves was very small, there was no way to filter all the 'ghost' reconstructions with the spatial filter at the Fourier plane of the third 4-*f* system. Therefore the noise floor is much higher. This means that even though the holograms can be multiplexed closer together using the continuous fan of planewaves, the increase in noise will limit the maximum number of holograms that could be stored in one area.

So far we have only talked about generating a fan of planewaves in one-dimension to store shift multiplexed hologram. The direction of shift is the same as the spread of the planewaves. We could also generate a 2-D fan of planewaves to store shift multiplexed holograms in two orthogonal directions. This further increases the number of holograms that could be stored in one area, which translates into an increase in surface density and storage capacity.

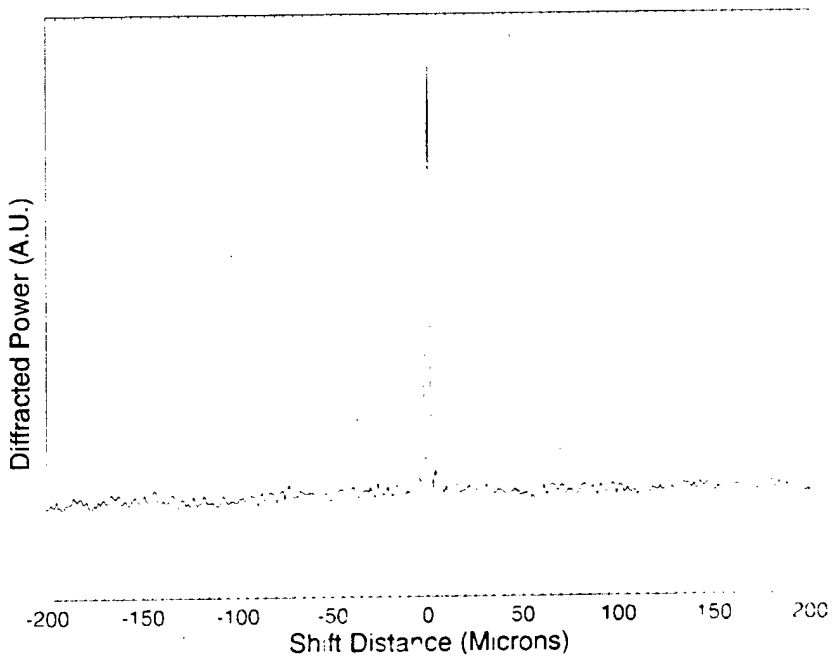

Figure 1.27 : The diffracted power as a function of material shift for a hologram recorded with a continuous fan of planewaves.

1.3.3.2 Spherical Reference Beam

In the previous section, when the angular separation between the planewaves was decreased and the number of planewaves was increased (in the reference arm), the one-dimensional multiple planewaves reference beam looked a lot like a cylindrical beam. Perhaps we could use a cylindrical lens to generate a continuous fan of planewaves for shift multiplexing. However, a cylindrical lens when used as shown in Figure 1.28 does not actually produce a fan of planewaves, but a fan of rays. These rays are spatially separated and they converge to a line at the focal plane and then diverge again. When a hologram is recorded with the setup shown in Figure 1.28, the diffracted power still decreases rapidly as the recording material is shifted parallel to the fan of rays, but the mechanism is different when compared to holograms recorded with a fan of planewaves.

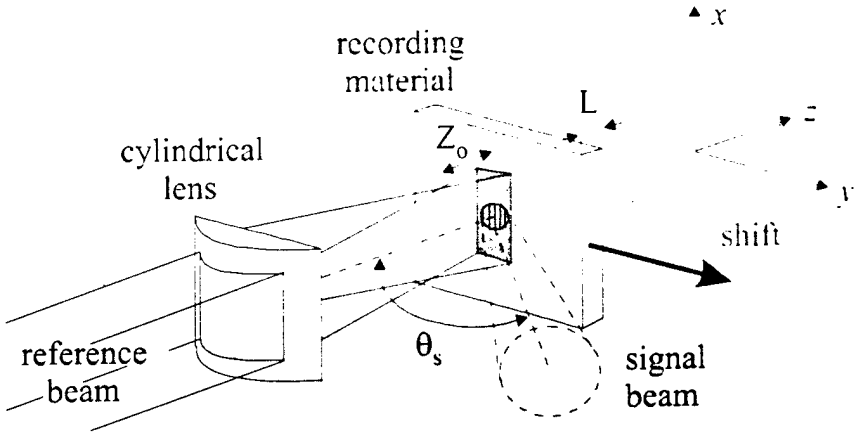

Figure 1.28 : Using a cylindrical lens to produce a fan of rays for shift multiplexing.

Figure 1.29 (a) shows a cylindrical reference beam recording a hologram with a planewave signal beam in the y-z plane of Figure 1.28. During grating formation, the hologram is formed with the rays in the reference beam as shown in Figure 1.29 (a). If the recording material is shifted during reconstruction (Figure 1.29 (b)), the angle of the rays the hologram now experiences is different from the rays used to record it. Therefore, the hologram will Bragg-mismatch very similar to the angle multiplexing effect.

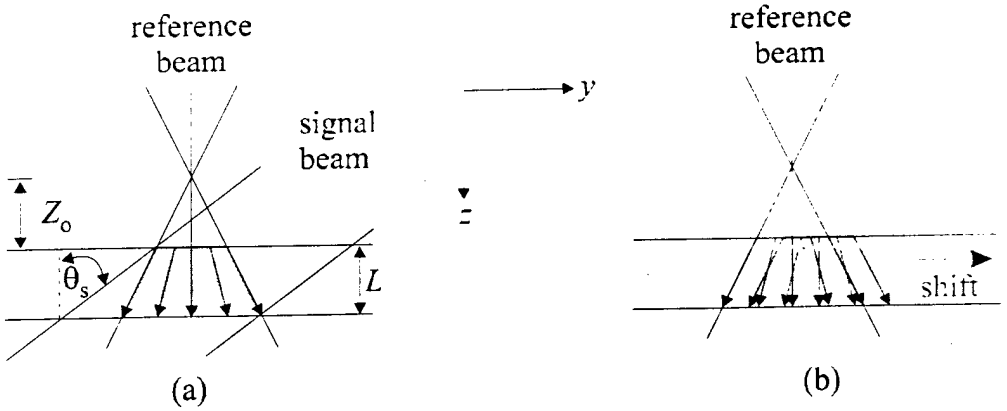

Figure 1.29 : Cylindrical reference beam shift multiplexing mechanism. (a) A cylindrical reference beam recording a hologram. (b) Shifting the recording material during reconstruction.

For thin recording materials such as DuPont's photopolymers, the amount of shift required to reach a null in the Bragg condition can be computed easily. For the setup

shown in Figure 1.29 (a), the center ray of the cylindrical reference beam is on-axis and the signal beam is off-axis by θ_s, both measured with respect to the surface normal of the recording material. The focal plane of the cylindrical beam is Z_o away from the recording material and the recording material has a thickness of L. For the hologram formed between the on-axis reference ray and the off-axis signal beam, the amount of angular change introduced by shifting the recording material a distance δ is $\Delta\theta \simeq Z_o\delta$. According to Bragg theory, the amount of angular change required to reach the first null is given by Eq. 1.7. For the case where $\theta_r = 0°$, Eq. 1.7 can be simplified to :

$$\Delta\theta = \frac{\lambda}{L\tan\theta_s} \tag{1.14}$$

By equating the angular change to the angular selectivity, a shift distance of $\delta_{Bragg} = \lambda Z_o/L\tan\theta_s$ is required to reach the first null. As a fudge factor to prevent δ from going to zero when the cylindrical reference beam is focused on the recording material ($Z_o = 0$), we need to model the finite numerical aperture (NA) of the cylindrical reference lens. The finite numerical aperture broadens the selectivity curve by an additional $\delta_{NA} \simeq \lambda/2(NA)$. For most setups, δ_{NA} is extremely small when compared to δ_{Bragg}. The final equation for the amount of shift required to reach the first null of the Bragg condition for a hologram recorded between the on-axis reference ray and a planewave signal with an angle of θ_s is :

$$\delta = \delta_{Bragg} + \delta_{NA} \cong \frac{\lambda Z_o}{L\tan\theta_s} + \frac{\lambda}{2\,NA} \tag{1.15}$$

Eq. 1.15 only predicts the null spacing of the grating recorded between the on-axis reference ray and a planewave signal with an angle of θ_s. In order to get the selectivity function for the entire hologram, it is necessary to compute the diffraction pattern for all

the gratings produced by the different rays in the reference beam and then sum them together. This is demonstrated later for a special recording geometry (Chapter 1.3.3.3). Nevertheless, Eq. 1.15 tells us how the shift selectivity function δ, depends on λ, Z_o, θ, and L. As with angle multiplexing, shorter wavelengths, thicker recording materials, and larger angles between the signal and reference beams improve the selectivity function. The extra parameter, Z_o, determines the rate of angular change as a function of material shift. A small Z_o causes the ray angle to change rapidly and therefore, improves the selectivity. The minimum Z_o that can be used in a setup depends on the spot size of the signal beam on the recording material and the NA of the cylindrical reference beam. The focal plane of the cylindrical reference beam must be placed far enough from the recording material so that the entire signal beam spot is covered by reference illumination during recording. There was no such restriction with the multiple planewaves reference beam setup shown in Chapter 1.3.3.1. The aperture of the multiple planewaves reference beam at the recording material is the same as the aperture of the diffractive element that generated the multiple planewaves. The minimization of Z_o becomes tougher for thicker recording materials because the signal beam defocus inside the material and causes the entrance spot size to be different from the exit spot size. For best quality holograms, Z_o should be chosen to be large enough to cover both the entrance and exit signal spots. So for thick recording materials, there is some cross relationship between Z_o and L. For the thin photopolymers, we can assume Z_o and L to be independent.

There are other differences between using a fan of planewaves and a fan of rays to record shift multiplexed holograms. For holograms recorded with a cylindrical reference beam, the holograms have no periodicity as the recording material is shifted and there are

no 'ghost' images. This is because each ray of the cylindrical reference beam illuminates a separate, infinitely small portion of the entire hologram. Each grating vector on the κ-sphere is illuminated by only one reference ray at a time. Therefore, there is no constructive and destructive periodicity and no 'ghost' images.

To further increase the number of holograms stored in a given area, we would also like to shift multiplex in directions other than just parallel to the fan of rays. For example, shift multiplex by moving the recording material in the direction that is orthogonal to the fan of rays. However for a cylindrical reference beam, the holograms experience no change in the ray angles when shifted orthogonally to the fan of rays. Therefore, the holograms would have to be shifted completely out of the reference illumination for the reconstruction to disappear. To introduce a fan of rays in the orthogonal direction, we could use another cylindrical lens to focus the rays in the x-direction but why stop there? Why not introduce a fan of rays in every direction so we could shift in any direction and get some selectivity. A fan of rays in all directions can be generated by using a single spherical lens. Figure 1.30 shows a shift multiplexing setup using a spherical reference lens. Later in Chapters 1.4 and 1.5, we will use a spherical reference beam to record many high density holograms in the same volume.

When the recording material is shifted parallel to the plane of interaction (y-z plane) for a hologram recorded with a spherical reference beam, the response of the stored holograms is exactly the same as the analysis we did for the cylindrical beam setup. How about when the recording material is shifted perpendicular to the plane of interaction? Figure 1.31 (a) shows a spherical reference beam recording a hologram with a planewave signal beam in the x-z plane of Figure 1.30. The solid lines inside the hologram volume

represent the grating and the dotted lines represent the signal planewave. The focal point of the spherical reference beam is Z_o away from the recording material. Figure 1.31 (b) shows the recording material shifted along the x-axis. When shifting orthogonal to the plane of interaction, the holograms are much harder to Bragg-mismatch compared to shifting parallel to the plane of interaction. Similar to peristrophic multiplexing, the initial tendency of the shifted hologram (along x) is to reconstruct at a different angle. Therefore, we call the orthogonal direction the Bragg degenerate direction.

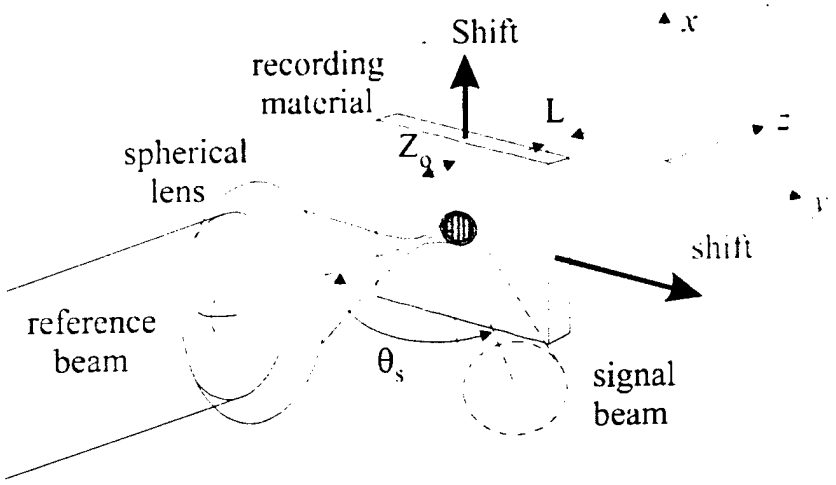

Figure 1.30 : Shift multiplexing setup using a spherical reference beam.

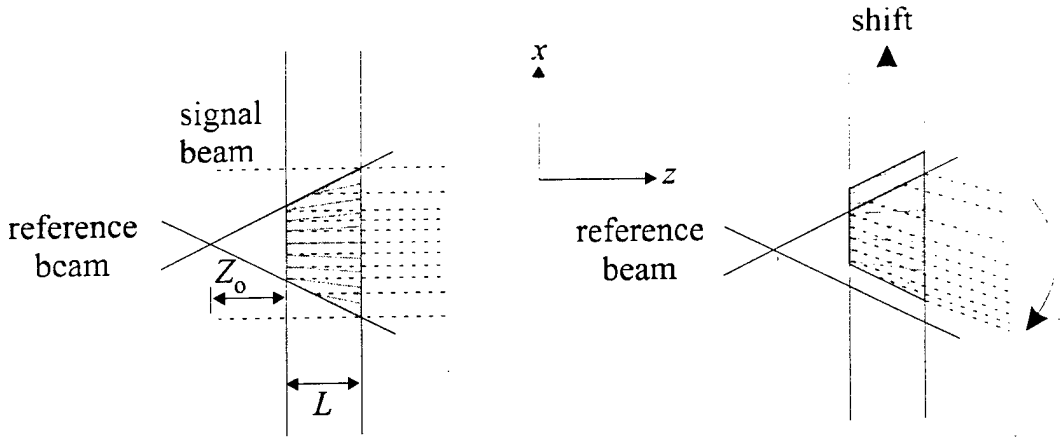

Figure 1.31 : Spherical reference beam shift multiplexing mechanism in the Bragg degenerate direction. (a) A spherical reference beam recording a hologram with a planewave signal beam. (b) Shifting the recording material in the degenerate direction during reconstruction.

Figure 1.32 shows the κ-sphere representation of shift multiplexing using a spherical reference beam. In Figure 1.32 (a), the 2-D fan of rays in the spherical reference beam is represented by a circular patch on the κ-sphere. Each ray on the patch records a separate grating with the planewave signal beam. One such grating is shown in Figure 1.32 for the on-axis reference ray. If the recording material is shifted orthogonal to the plane of interaction, all the recorded gratings move and some get illuminated by rays with different angles and some move out of the reference beam's illumination. However instead of shifting the gratings along the y-axis, which would have immediately caused some Bragg-mismatch (the tip of the grating vectors would either poke through or dive below the κ-sphere), the gratings are moved along the x-axis. For a wide-range of orthogonal shifts, the grating vectors that have no x-components remain relatively on the κ-sphere (for example, the grating vector shown in Figure 1.32). To see this, you have to imagine Figure 1.32 (b) as half of a sphere sticking out of the page and see the movement of the gratings on the sphere as they are shifted along the x-axis. For the grating vectors with some x-components, they reside below the apex of the sphere. Therefore, when shifted orthogonally, they either initially lift off or dive below the κ-sphere and Bragg-mismatch quickly. In experiments, what is usually seen at the detector plane as the recording material is shifted orthogonally is a strip of Bragg-matched gratings that moves up or down until the reconstruction is out of the field of view of the detector.

In order to store another hologram in the orthogonal direction, the existing hologram must be shifted enough so that either: (1) the grating vectors that have no x-components are shifted completely out of the illumination of the reference beam; (2) the change in the hologram's reconstruction angle is sufficient for filtering, like peristrophic

multiplexing; (3) the reconstructions from the grating vectors that have no x-components are shifted off of the detector array. For the first case, the amount of orthogonal shift required is usually half the hologram height, if the reference spot size is the same as the signal spot size on the recording material. For the second case, the amount of orthogonal shift required to move the entire reconstruction out of the detector array's aperture is $\delta \simeq 2Z_o\tan^{-1}(1/2f/\#)$, where Z_o is the distance from the focal point of the spherical reference beam to the recording material and $f/\#$ is the distance between the detector array and the recording material divided by the aperture of the detector array, if free space propagation. If lenses are used in the signal arm, then $f/\#$ is defined as the focal length of the imaging lens divided by the aperture of the detector array. For the last case, the amount of orthogonal shift required to shift just the reconstructions from the grating vectors that have no x-components off of the detector array is $\delta \simeq Z_o\tan^{-1}(1/2f/\#)$ (half the hologram height if the signal and reference beams have the same bandwidth and overlap exactly). The last case is the most common since we usually only need to shift the strip of Bragg match reconstructions off the detector array in order to store another hologram.

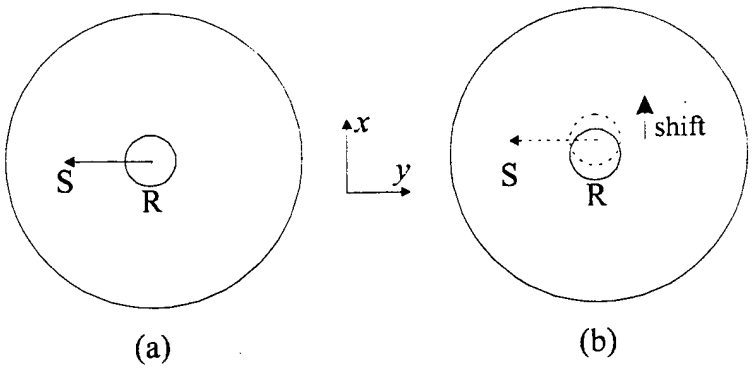

Figure 1.32 : κ-sphere representation of shift multiplexing using a spherical reference beam. (a) Recording a hologram between a planewave signal beam and a spherical reference beam. (b) Shifting in the degenerate direction during reconstruction.

In the high density experiment shown in Chapter 1.2, we were able to read only a portion of the reconstructed hologram at a time due to photopolymer shrinkage. Different portions of the hologram can be obtained by slightly de-tuning the angle of the reference beam. For a hologram recorded with a spherical reference beam, it is not clear how one would re-Bragg match a shrunken hologram. In the next chapter we discuss an off axis recording geometry, using a spherical reference beam, that eliminates the effect of photopolymer shrinkage on hologram reconstruction. We will continue our analysis of spherical reference beam shift multiplexing for this special geometry there.

1.3.3.3 Shrinkage Insensitive Recording Geometry

For the high density holograms recorded with a planewave reference beam shown in Chapter 1.2, portions of the recorded gratings would lift-off or dive below the κ-sphere due to shrinkage. These Bragg-mismatched portions can be brought back on the κ-sphere by changing the reference beam angle slightly during reconstruction. However, the reconstruction angle of the re-Bragg-matched portion is different when compared to the original signal direction and only a portion of the entire hologram can be Bragg-matched at a time. It might be possible to use a slightly cylindrical reference beam to re-Bragg-match the entire hologram at the same time. However, the reconstructed image would still be a little bit compressed.

For a high density hologram recorded with a spherical reference beam using the setup shown in Figure 1.30, to re-Bragg-match a portion of the shrunken hologram, we need to both shift the recording material and move the focus of the reference beam lens. Shifting the recording material brings some grating vectors back on the k-sphere.

However, this changes the distance between the grating vectors and the focal point of the spherical reference beam. In order to satisfy the imaging condition of the stored gratings, we need to move the focal point of the spherical reference until the Bragg-matched gratings have the correct displacement from the focal point. Just like before, only a portion of the entire hologram can be Bragg-matched at a time and the reconstructed portion deflects at a slightly different angle when compared to the original signal beam.

Instead of trying to re-Bragg-match the shrunken gratings during reconstruction, is there a way to prevent the gratings from shrinking in the first place? Specifically, can we use the ray nature of the spherical reference beam to record shrinkage insensitive hologram? In Chapter 1.2.3 we stated that for gratings recorded with symmetric rays (with respect to the recording material's surface normal), shrinkage has no effect on its Bragg condition. Figure 1.33 (a) shows a planewave reference beam interfering with a high bandwidth signal beam to produce a high density hologram (neglecting Snell's law). The angle of the reference beam is symmetric with the center ray of the signal beam. Therefore, that portion of the hologram will remain Bragg matched after shrinkage. This is shown in the *k*-sphere diagram of Figure 1.33 (b).

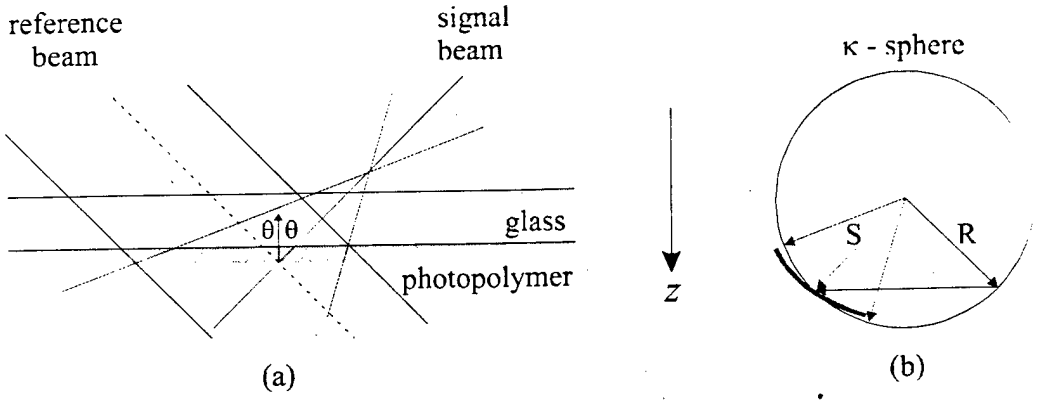

Figure 1.33 : A planewave reference beam recording a hologram with a high bandwidth signal beam. (a) The recording geometry. (b) The κ-sphere diagram after shrinkage.

However, the planewave reference beam has only one incident angle so it cannot record symmetric holograms with all the rays in the signal beam. This is where the spherical reference beam comes in. Figure 1.34 (a) shows a spherical reference beam recording a hologram with a high bandwidth signal beam. The focal point of the signal beam is in front of the recording material and the focal point of the spherical reference beam is behind. The lenses that produce the cone of rays for the signal and reference arms have the same *f*/#. When the rays are positioned properly as shown, the entire hologram is formed by symmetric rays. More specifically, a pair of symmetric signal and reference rays form a single grating at a localized area. This is repeated through out the entire hologram. Since the gratings have no *z*-components, photopolymer shrinkage has no effect on their Bragg conditions. This is shown in the κ-sphere diagram of Figure 1.34 (b) for three grating vectors.

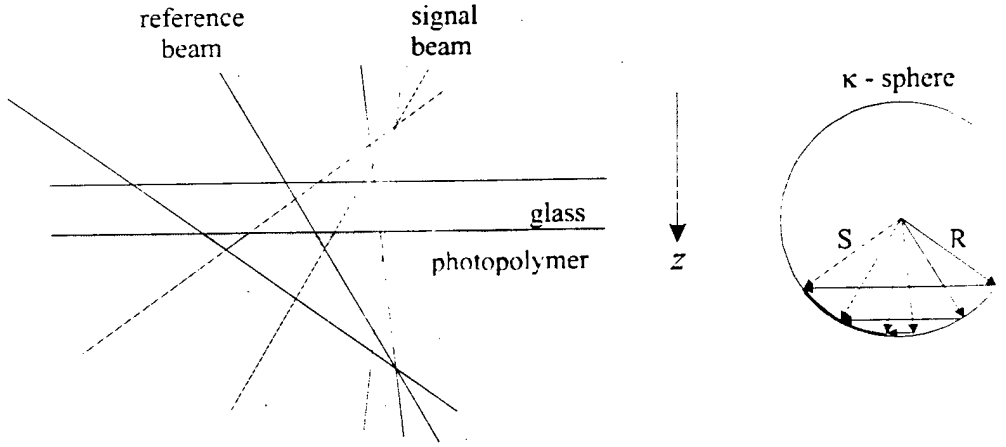

Figure 1.34 : A spherical reference beam recording a hologram with a high bandwidth signal beam in the shrinkage insensitive geometry. (a) The rays of the signal and reference beams in the setup. (b) The κ-sphere diagram after shrinkage.

To demonstrate that this shrinkage insensitive geometry actually works, we used basically the same high density setup as shown in Chapter 1.2. A piece of photopolymer is

placed slightly after the focal point of the signal beam. To show the Bragg-mismatch effect induced by photopolymer shrinkage, we first use a planewave to write a hologram with the high bandwidth signal beam (Figure 1.35 (a)). The center ray of the signal beam and the reference planewave have an incident angle of $\pm$ 30° (outside angle) with respect to the surface normal of the photopolymer. The reconstructed hologram is viewed by a CCD detector placed at the detector plane of the Nikon lenses. Figure 1.35 (b) shows the shrinkage insensitive recording geometry. Instead of using a planewave to record the hologram, a spherical reference beam is generated by a *f*/1.4 CCD camera lens. The rays are positioned so that the signal beam spot on the photopolymer is covered by the reference beam spot and the center ray of the signal and reference beams overlap symmetrically with respect to the photopolymer's surface normal (at $\pm$ 30°).

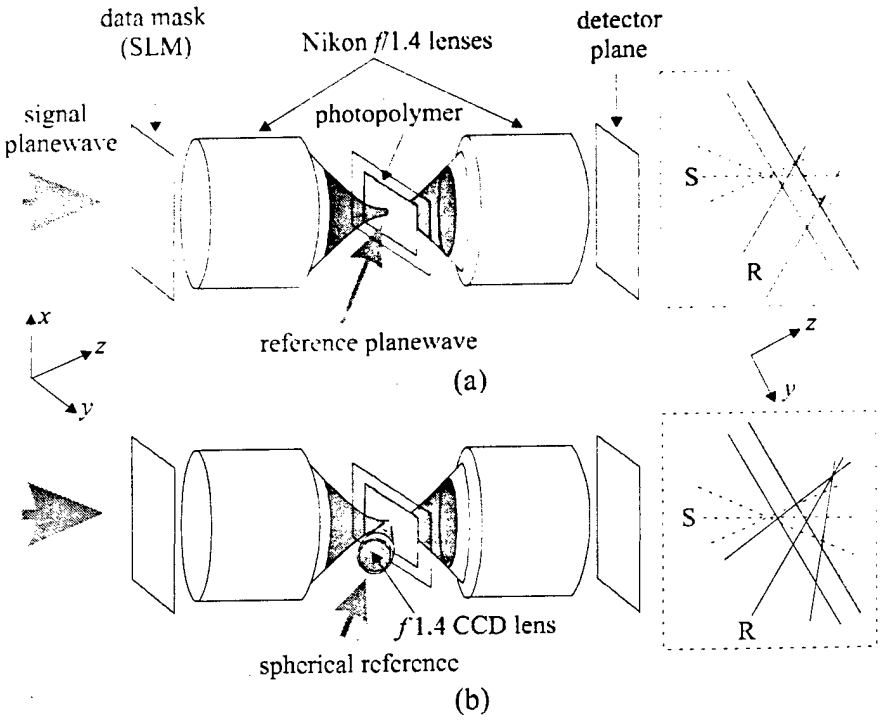

Figure 1.35 : Setups used to demonstrate the effects of photopolymer shrinkage. (a) High density setup using a planewave reference beam. (b) High density setup in the shrinkage insensitive geometry.

Figure 1.36 shows the resulting reconstructions and an image of the original data mask for comparison. Since the CCD array we used is much smaller than the entire aperture of the Nikon camera lens, we physically moved the detector array across the aperture to get the images shown in Figure 1.36. The 'original image' is the data mask imaged through the system without any recording material. The second image is the reconstruction of a hologram recorded with a planewave reference beam, using the setup shown in Figure 1.35 (a). Nearly half of the reconstruction is dark due to the shrinkage induced Bragg-mismatch problem. The dark half can be re-Bragg-matched by slightly changing the reference beam angle in the y-z plane, but then the other half would go dark. The last image shown in Figure 1.36 is the reconstruction of a hologram recorded with a spherical reference beam in the shrinkage insensitive geometry (Figure 1.35 (b)). The entire reconstruction is visible at the same time so there is no need for any re-Bragg-matching. Furthermore, the reconstructed image is not distorted or compressed in any direction since the gratings did not suffer any shrinkage effect. This shows that the shrinkage insensitive geometry works and we will apply it to record shift multiplexed holograms in the photopolymer based holographic 3-D disks later.

The shrinkage insensitive setup shown in Figure 1.35 (b) has the signal beam focused in front of the recording material and the reference beam focused behind. Of course the same principles would still work the other way around. We choose to focus the signal beam in front of the recording material because that usually yields the best signal beam uniformity. For the reference beam, we purposely put a one-sided Gaussian profile on the planewave before the reference lens to smooth its intensity on the photopolymer.

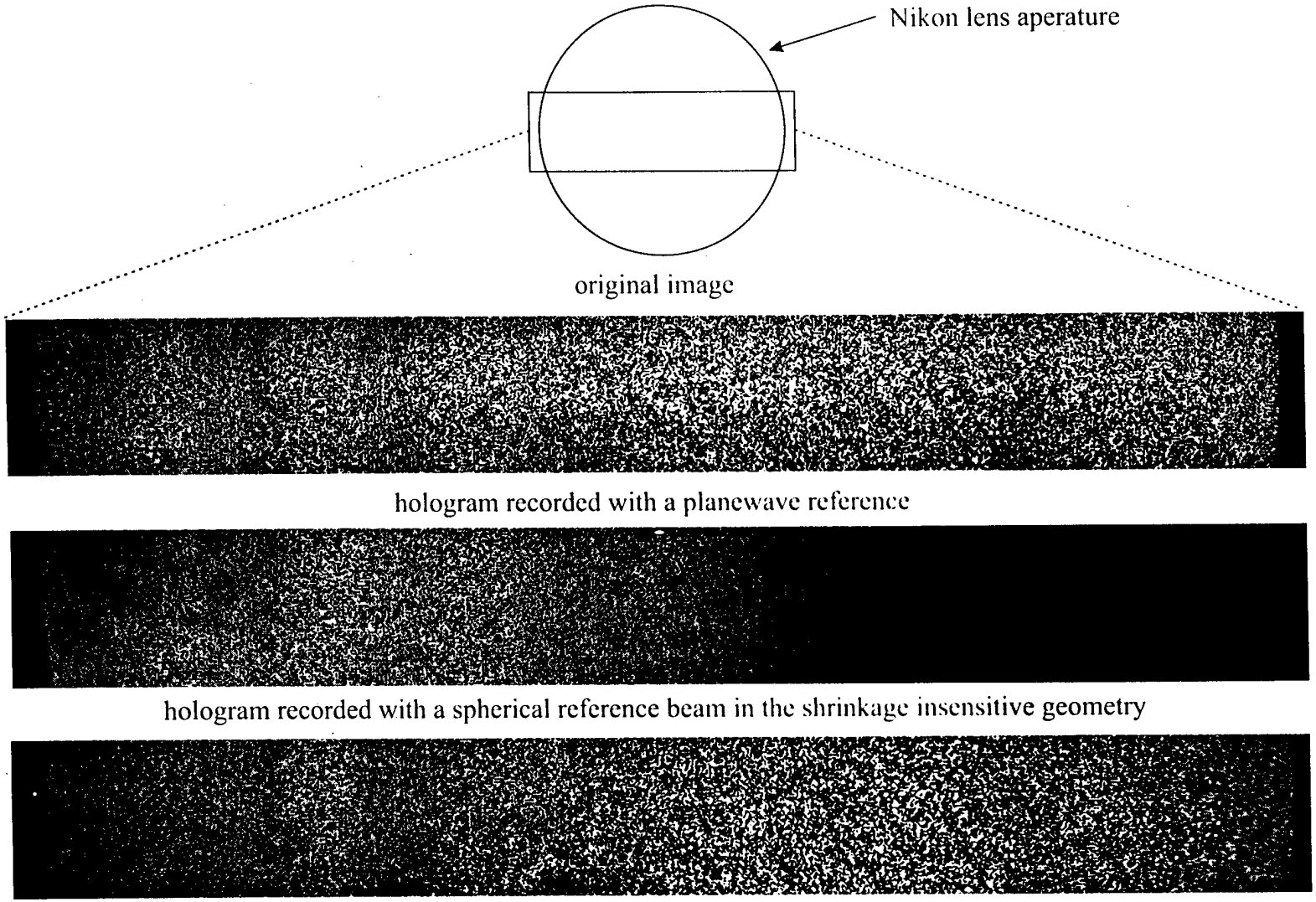

Figure 1.36 : The reconstruction from a hologram stored with a planewave reference beam and a hologram stored with a spherical reference beam in the shrinkage insenstive geometry for comparison with the original image.

We can compute the theoretical diffracted power as a function of hologram shift for the shrinkage insensitive geometry. For shifting parallel to the interaction plane, this is done by summing the diffracted power of each grating according to the angular selectivity function. The reconstruction intensity of a grating as a function of angular change in the reference ray is defined as:

$$I(\Delta\theta)=\left|\operatorname{sinc}\left(\frac{L}{\lambda}\frac{\sin(\theta_r+\theta_s)}{\cos\theta_r}\Delta\theta\right)\right|^2 \tag{1.16}$$

where $\operatorname{sinc}(x) = \sin(\pi x)/\pi x$, L is the thickness of the recording material, λ is the wavelength, θ_r (θ_s) is the angle of the reference ray (signal ray) with respect to the surface normal of the recording material, and $\Delta\theta$ is the angular change in the reference ray as the recording material is shifted. Since the signal and reference rays are symmetric, Eq. 1.16 cane be further simplified to:

$$I(\Delta\theta)=\left|\operatorname{sinc}\left(\frac{L}{\lambda}\frac{\sin(2\theta')}{\cos\theta'}\Delta\theta\right)\right|^2 \tag{1.17}$$

where θ' is the angle between either the signal or the reference ray and the surface normal of the recording material. Now we need to determine $\Delta\theta$, the angular change in the reference ray as a function of recording material shift. After recording a hologram using the shift insensitive geometry, the same reference beam is brought back to reconstruct the hologram as shown in Figure 1.37. Snell's refraction is not shown in Figure 1.37 to simplify the diagram (the three rays shown do not actually intersect at the same location if refraction is taken into account). In Figure 1.37, θ is the angle of the largest ray measured with respect to the surface normal of the recording material, ϕ is the angle of the smallest

ray measured with respect to the surface plane of the recording material, and y is the spot size of the spherical reference beam on the recording material.

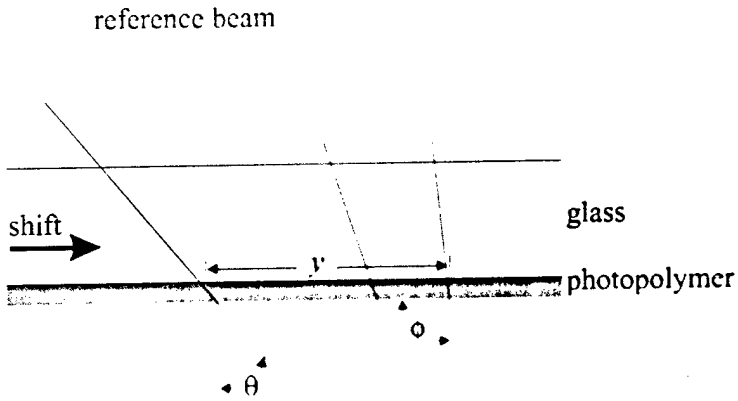

Figure 1.37 : The angular change in the reference ray experienced by the shifted gratings for a spherical reference beam incident as shown.

Using simple trigonometry, the angular change for the grating recorded by a reference ray with an angle θ' with respect to the surface normal of the recording material, as the recording material is shifted from left to right is:

$$\Delta\theta \cong \frac{\cos\theta'}{\sin\phi}\frac{\cos(\theta-\phi)}{\cos\theta}\frac{\Delta y}{y} \tag{1.18}$$

where Δy is the shift distance. Substituting Eq. 1.18 into Eq. 1.17, we get:

$$I(\Delta y)=\left(\operatorname{sinc}\left(\frac{L}{\lambda}\frac{\sin(2\theta')}{\sin\phi}\frac{\cos(\theta-\phi)}{\cos\theta}\frac{\Delta y}{y}\right)\right)^2 \tag{1.19}$$

Eq. 1.19 is the theoretical diffracted power as a function of recording material shift, for the grating recorded by the reference ray with an angle of θ' with respect to the

surface normal of the recording material. In order to get a complete picture of what is going on with the entire hologram as the recording material is shifted, we need to integrate the diffracted powers from all the gratings as a function of material shift. For computational purposes, this integration is usually broken down to a sum over a finite number of reference ray angles, such as

$$I(\Delta y) = \sum_{\theta'} \left(\operatorname{sinc}\left(\frac{L}{\lambda} \frac{\sin(2\theta')}{\sin\phi} \frac{\cos(\theta - \phi)}{\cos\theta} \frac{\Delta y}{y} \right) \right)^2 \qquad (1.20)$$

where θ' is in the range of $90°-\phi$ to θ.

Figure 1.38 shows the diffracted power as a function of hologram shift (in the Bragg direction) for a high density hologram recorded using the same setup as Figure 1.35 (b). For this experiment, the *f*/1.4 CCD camera lens was moved closer to the DuPont HRF-150-100 photopolymer to project a larger reference beam spot size than the signal beam. This was done to ensure the signal beam is completely covered by the reference beam during recording (it will become more important later for the holographic 3-D disks with tilts and wobbles). The diameter of the reference spot on the photopolymer was ~ 4 mm while the diameter of the signal spot was 1.5 mm. For comparison, the theoretical diffracted power as a function of hologram shift for a hologram recorded with a reference spot size of y = 1.5 mm, $\theta = 30.1°$ and $\phi = 96.5°$ (inside angles) is also plotted in Figure 1.38. By moving the reference beam lens closer to the photopolymer to get a bigger spot size, the focal point of the spherical reference beam becomes displaced further away from the recording material. This increases the amount of material shift required to obtain the

appropriate $\Delta\theta$ for Bragg-mismatching. Therefore, the experimental selectivity curve is much wider than the theoretical prediction.

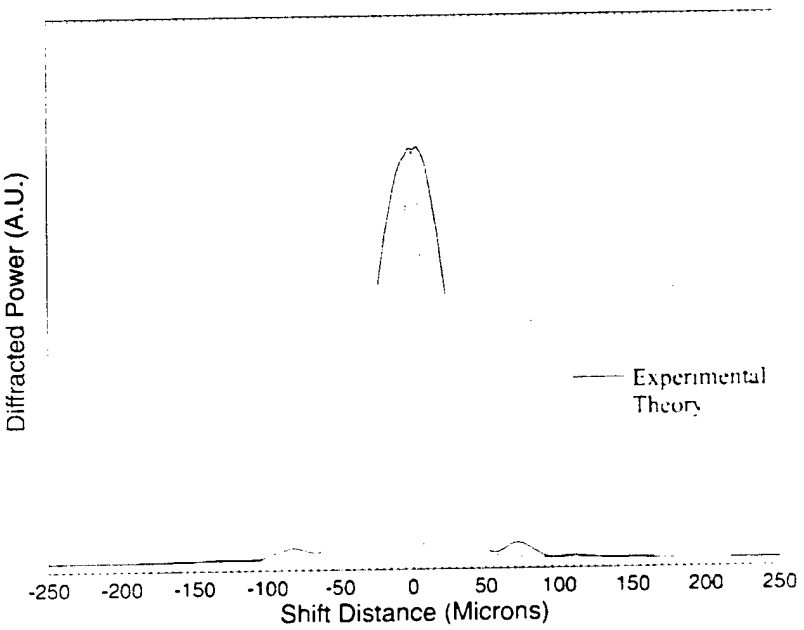

Figure 1.38 : Diffracted power as a function of shift distance for a high density hologram recorded with a *f*/1.4 reference beam lens.

Not only is the theoretical selectivity curve narrower than the experimental, it also doesn't have any side lobes. This is because the nulls of the sinc function for each grating does not occur at the same shift distance. Therefore, when the diffracted powers are summed together, the nulls get filled. Eq. 1.20 assumes each ray in the reference beam records similar strength holograms. In reality, since the reference beam is focused, the gratings near the center of the hologram are usually stronger. This in effect narrows the spectrum of reference rays that make real contributions to the diffracted power. When the strength of each grating was weighted by a Gaussian profile in Eq. 1.20, the theoretical diffracted power curve also had side lobes.

Notice the experimental selectivity curve of Figure 1.38 is asymmetric with respect to zero shift distance. The first null occurs at 57 μm for positive shift and -65 μm for

negative shift. This is because the hologram wasn't recorded in the shrinkage insensitive geometry. Since the *f*/1.4 CCD camera lens for the reference beam was moved closer to the recording material, the reference rays were no longer exactly symmetric with the signal rays. Therefore, most gratings have some *z*-components which shrunk during recording.

In order to maintain a larger reference spot size on the photopolymer than the signal beam and record in the shrinkage insensitive geometry, we need a lower *f*/# lens in the reference arm. Figure 1.39 shows that a lower *f*/# lens in the reference arm allows us to record holograms in the shrinkage insensitive geometry while illuminating a larger area of the photopolymer. We found a small (16.5 mm in length and 15.9 mm in diameter) projection lens from Universe Kogaku Inc. (Part Number TK-11) with a *f*/# of 1.1 that could be used in the reference arm to produce a spherical reference beam. Figure 1.40 shows the resulting selectivity curve for a hologram recorded with the *f*/1.1 projection lens.

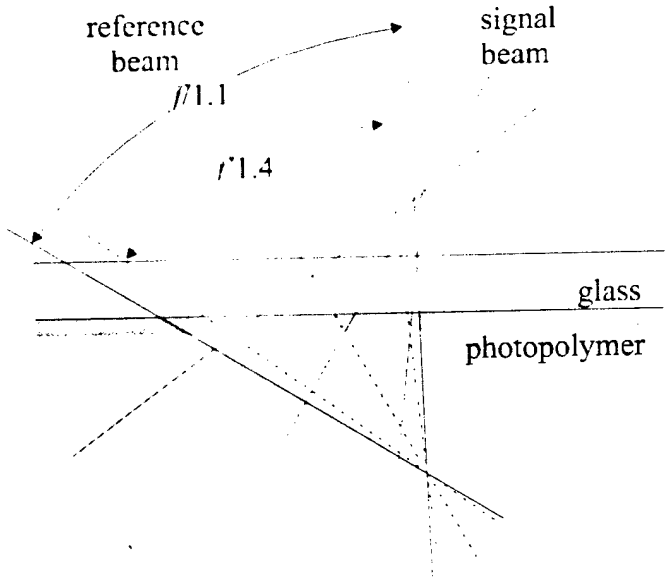

Figure 1.39 : Using a lower *f*/# lens in the reference arm (as compared to the signal arm) for shift multiplexing in the shrinkage insensitive geometry.

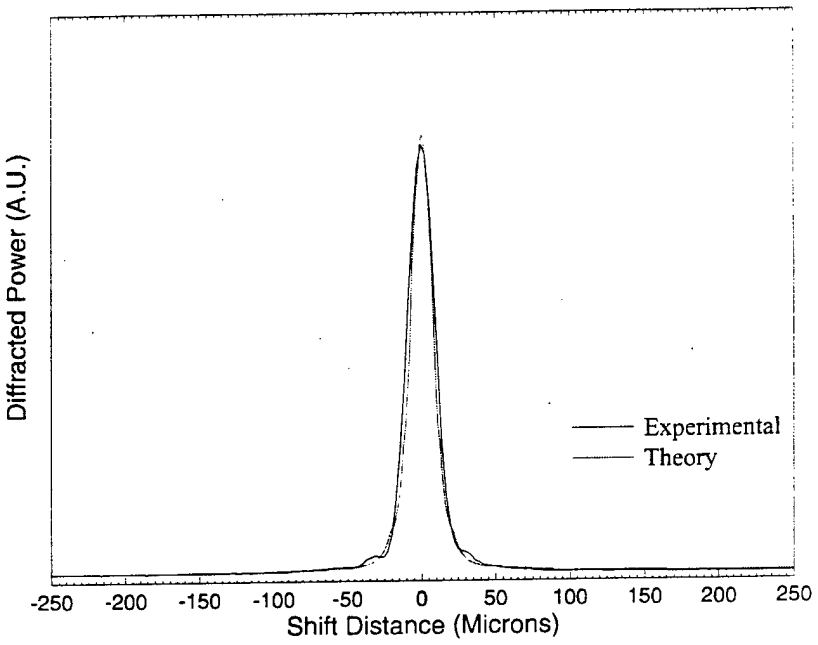

Figure 1.40 : Diffracted power as a function of shift distance for a high density hologram recorded with a *f*/1.1 reference beam lens.

Figure 1.40 shows that the experimental selectivity curve became much narrower and more symmetric with the *f*/1.1 projection lens in the reference arm. The reference beam diameter on the photopolymer was approximately 2 mm, just a little bit bigger than the theoretical diameter of 1.83 mm for the shrinkage insensitive geometry using a *f*/1.1 lens. Therefore, the theoretical selectivity curve is still slightly narrower than the experimental. According to the experimental selectivity curve in Figure 1.40, another hologram could be shift multiplexed, with little cross-talk noise, by shifting the recording material in the Bragg direction by 50 or more micron. This means that we could have a new hologram every 50 micron in shift, along the track of a holographic 3-D disk.

For the shrinkage insensitive geometry, the holograms are recorded with signal and reference beams of the same bandwidth. Therefore, the amount of shift required in the Bragg degenerate direction before another hologram could be stored is half the hologram

height, or .75 mm for this setup. Figure 1.41 (a) shows the κ-sphere diagram during recording with three representative grating vectors and Figure 1.41 (b) shows the κ-sphere diagram after shifting in the Bragg degenerate direction by half the hologram height. Grating vectors with some x-components quickly Bragg-mismatch when shifted in the Bragg degenerate direction, leaving a strip of grating vectors that have no x-components on the κ-sphere. The .75 mm in orthogonal shift is enough to move the grating vectors that have no x-components out of the field of view of the detector array.

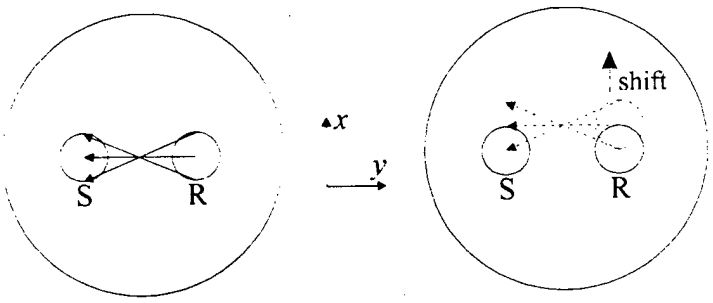

(a) (b)

Figure 1.41 : κ-sphere representation of shift multiplexing using a spherical reference beam in the shrinkage insensitive geometry. (a) Recording a hologram between a signal and reference beam with the same bandwidth. (b) Shifting in the degenerate direction by half the hologram height during reconstruction.

1.3.4 Experimental Setup

After figuring out how shift multiplexing works, we are now ready to construct a photopolymer based, holographic 3-D disk recorder/player system using shift multiplexing. Figure 1.42 shows the schematic diagram of a shift multiplexed holographic 3-D disk setup. It is very similar to the setup used in the previous experiment and many of the same components are used. An E-beam lithographed chrome plate is used as the input spatial-light-modulator (SLM). The center-to-center spacing of the pixels is 45 μm, and the fill factor is 100%. Nikon f/1.4, 3.9-cm-aperature camera lenses are used for imaging (the

chrome plate is pressed up against the Nikon lens to ensure that all the pixels within the lens aperture are captured). A total of 590,000 pixels fit in the apertures of the two Nikon lenses and a sharp image of the entire field is obtained at the detector plane. The recording material, DuPont's HRF-150 100 micron thick photopolymer, is laminated on the non anti-reflection coated side of a 1.2 mm thick transparent glass disk. The glass disks used in this experiment has the same physical dimensions as the compact disc. Figure 1.43 shows a picture of a photopolymer based holographic 3-D disk next to a cube of $LiNbO_3$. The glass disk laminated with the DuPont photopolymer is then attached to a microstepping-stepper motor. This particular stepper motor can be set to 125,000 steps per full revolution. This corresponds to a shift distance of approximately 3 microns per step at the outside radius of the disk. The entire glass disk and stepper motor assembly is mounted on a translation stage so the disk could be moved up or down to access different tracks on the disk. The spherical reference beam is formed by using a *f*/1.1 miniature projection lens. The holograms are recorded with the recording material slightly past the Fourier transform plane of the Nikon lenses. At that position, the diameter of the signal beam is 1.5 mm and its spatial uniformity is much better than at the exact Fourier plane. The spherical reference beam generated by the *f*/1.1 projection lens focuses behind the recording material in the shrinkage insensitive geometry discussed in Chapter 1.3.3.3. The center rays of the signal and reference beams each makes an angle of 30 degrees (outside) with respect to the disk's surface normal. The intensity of the signal and reference beams are 10 $\mu W/cm^2$ and 80 $\mu W/cm^2$ respectively, measured from the collimated planewaves before they become focused by the Nikon and projection lenses. At the detector plane, a

regular video rate CCD camera is used to read the reconstructed holograms. Figure 1.44 shows a picture of the setup.

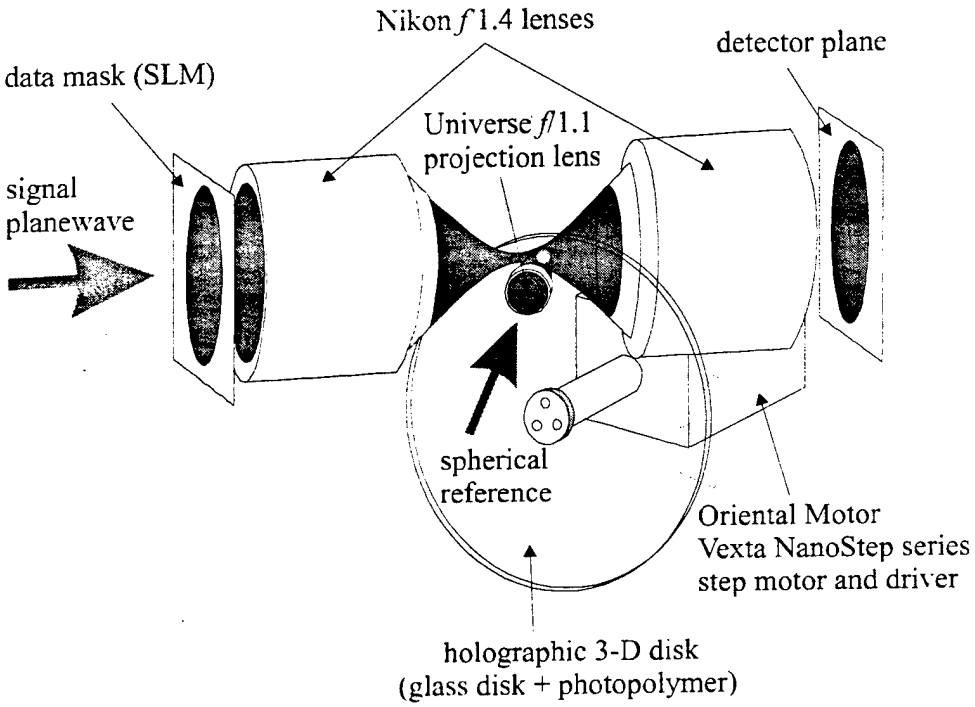

Figure 1.42 : Schematic diagram of a holographic 3-D disk setup using shift multiplexing.

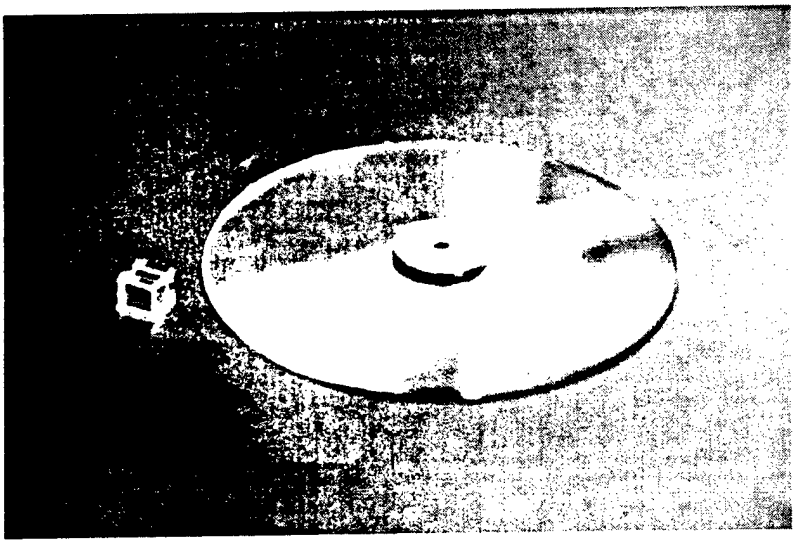

Figure 1.43 : A picture of a photopolymer based holographic 3-D disk next to a cube of $LiNbO_3$.

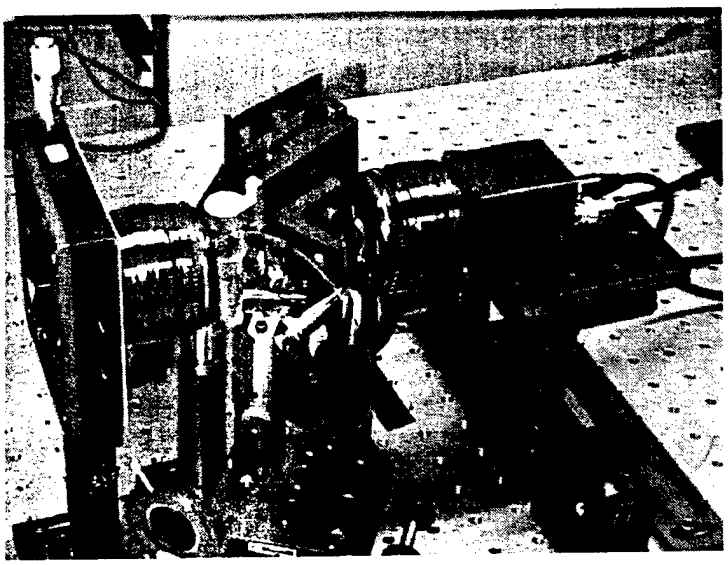

Figure 1.44 : A picture of the holographic 3-D disk setup using shift multiplexing.

We know from Chapter 1.2 that the 100 micron thick DuPont photopolymer can achieve a surface density of 10 bits/μm^2 with sufficient SNR. Therefore, we will tune the new setup to achieve it again. For the holographic 3-D disk, the in-track density is defined as the number of pixels in a hologram over the effective area of the hologram. Since the holograms are recorded in partially overlapping areas by using shift multiplexing (see Figure 1.45), the effective area can be computed as the height of the hologram times the shift distance required to separate the next hologram. It is similar to having a distinct hologram stored within each shift distance. To achieve the goal of 10 bits/μm^2 with the new setup, we will first start with an in-track surface density of 5 bits/μm^2. Then by overlapping the tracks, boost the surface density to the target 10 bits/μm^2. For this setup, we have again 590,000 pixels in each hologram over a hologram height of 1.5 mm. Therefore, to achieve an in-track surface density of 5 bits/μm^2, a maximum shift distance of 78 micron between holograms is allowed. To double the surface density to 10 bits/μm^2, we overlap the tracks by storing one track at half the hologram height above and another

track at half the hologram height below, with respect to the middle track. This in effect give us two completely overlapping tracks for a surface density of 10 bits/μm^2.

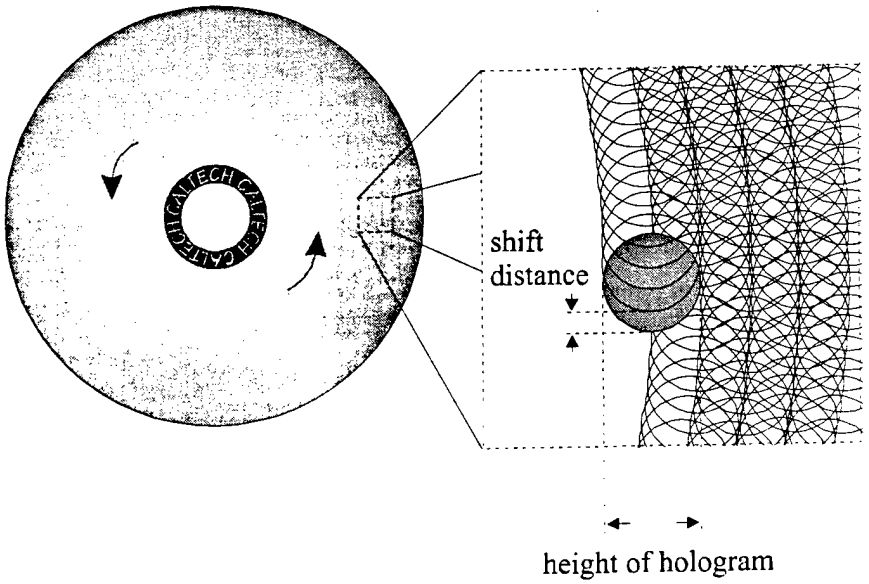

Figure 1.45 : The layout of overlapping holograms in tracks and overlapping tracks in the holographic 3-D disk.

1.3.5 Experimental results

So far, a surface density of 10 bits μm^2 has been achieved on paper by determining the shift distances required. From Figure 1.40 of Chapter 1.3.3.3, we know it is possible to pack in-track holograms as closely as 50 μm in separation and overlap additional tracks at half the hologram height above and below the current track. To demonstrate that we can actually store a hologram every 78 μm in in-track shift without too much cross-talk with the setup shown in Figure 1.44, we recorded one hologram and measured its diffraction efficiency as a function of shift distance (Figure 1.46). In Figure 1.46, the 78 μm in-track shift between holograms actually corresponds to approximately the fourth

null. Therefore very little cross-talk is expected (the next hologram would be recorded at position 688 and 532 micron). For track overlapping, we observed that by shifting the recording material radially by .75 mm (half the hologram height), is enough to deflect the reconstruction of the Bragg-matched strip completely off of the detector plane. Therefore, another track could be recorded at half the hologram height above and below the current track with essentially zero cross-talk.

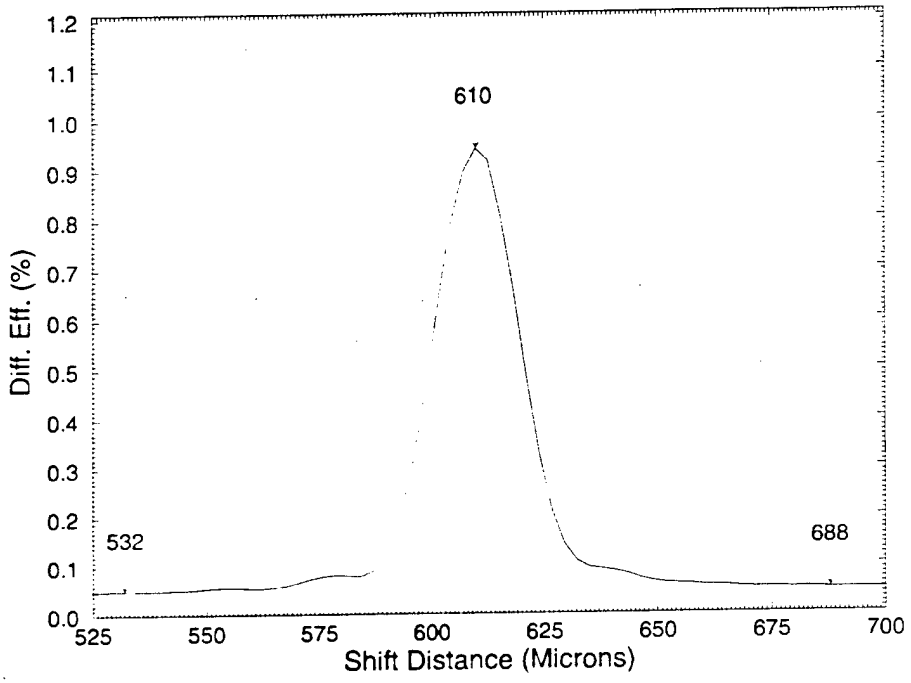

Figure 1.46 : Diffracted power as a function of shift distance for a high density hologram recorded with our shift multiplexed holographic 3-D disk setup.

To experimentally demonstrate 10 bits/μm^2, three overlapping tracks separated radially by .75 mm were stored. In each track, 100 holograms were recorded with an in-track separation of 78 μm (some initial holograms in the middle track were omitted so cross-talk noise could be characterized). Before recording, the photopolymer disk was uniformly sensitized in room light for 5 minutes. The holograms were then recorded with a constant 500 ms exposure per hologram and the middle track was recorded first, then

the upper and lower. The average diffraction efficiency of the holograms was approximately half of a percent. Figure 1.47 shows the comb function of the stored holograms (diffracted power as a function of shift distance). The strength of the holograms were very uniform by using the simple constant exposure schedule for the first track recorded (middle track). The holograms recorded later in the upper and lower tracks were slightly weaker due to the limited dynamic range of the material. To boost the strength of these holograms, they could have been recorded for longer durations.

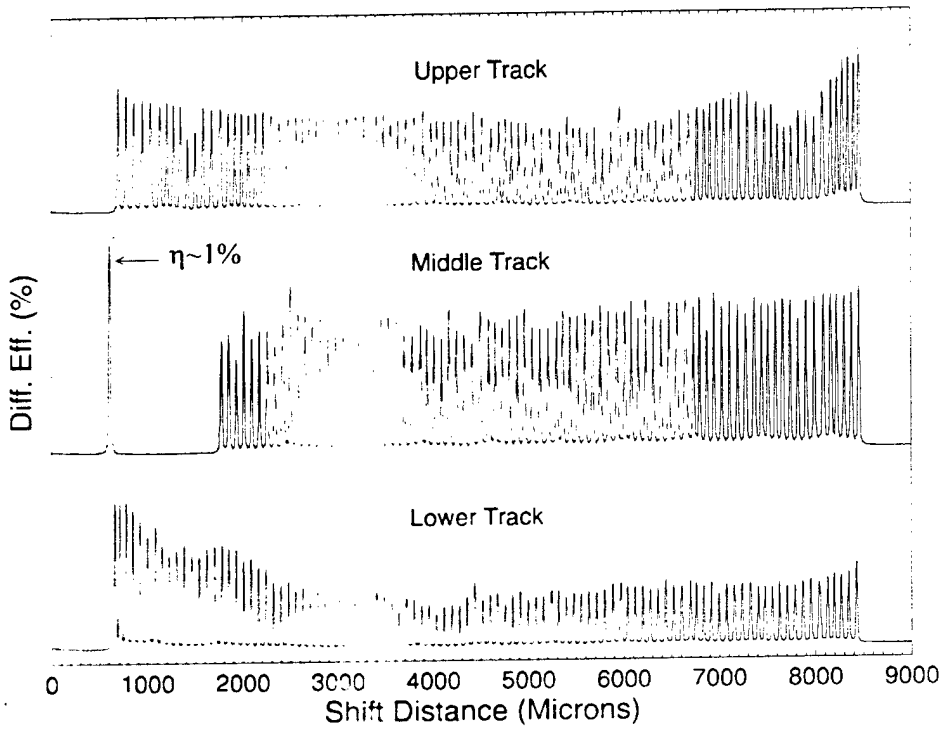

Figure 1.47 : Diffracted power as a function of shift distance for three overlapping track, each track containing approximately 100 holograms.

One of the reasons why the diffraction efficiency of the upper and lower tracks are less than the middle track is because of the "run-time" effect discussed in a previous experiment. From pre-exposure to recording to UV curing, the room light is kept on to maintain the sensitivity of the photopolymer. The amount of time spent on recording 100

holograms in a single track is around 100 seconds (500 ms exposure time + 500 ms delay to allow the stepper motor to stabilize for each hologram). This means by the time the lower track is started, the photopolymer has already been in the room light for about 8 minutes. During this time, the photosensitizing dye is slowing being depleted by the room light, causing the photopolymer to be less sensitive. We also tried other sensitizing techniques such as letting the larger reference spot pre-expose the next hologram area automatically during the recording process. This technique pre-exposes the minimum amount of photopolymer necessary for hologram formation. With the right combination of exposure time and incident intensity, we were able to get this method to work but not always consistently from disk to disk.

Figure 1.48 shows a reconstructed hologram from the middle of the middle track, where the cross-talk noises are most pronounce. Since the CCD array used was much smaller than the entire reconstruction, only a window of the reconstruction can be read out at a time. The three frames in Figure 1.48 correspond to the left, center and right sides of the reconstructed hologram. Visually, the quality of the reconstructed hologram is quite high and the reconstruction from the other holograms were all similar or better than this. To estimate the bit-error-rate of our system, we generated a histogram from the reconstructed hologram, using the same method as shown in Figure 1.10. The black area in Figure 1.49 represents the occurrences of the 'off' pixels while the shaded area represents the occurrences of the 'on' pixels, plotted against their intensity value. The two lobes are distinct, meaning that an intensity threshold could be selected to classify the pixels as originally 'on' or 'off' without errors. The estimated probability of error derived from fitting the 'on' pixel histogram to a first order χ^2 distribution is 2.4×10^{-5}.

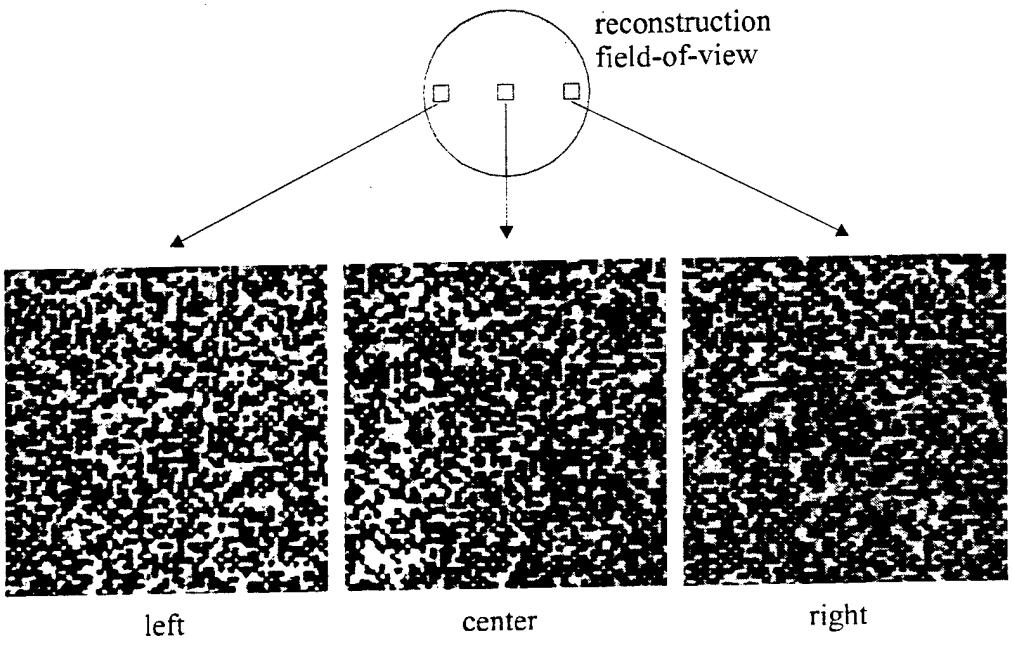

Figure 1.48 : The left, center, and right sides of a reconstructed hologram from the 10 bits/μm^2, photopolymer based holographic 3-D disk experiment.

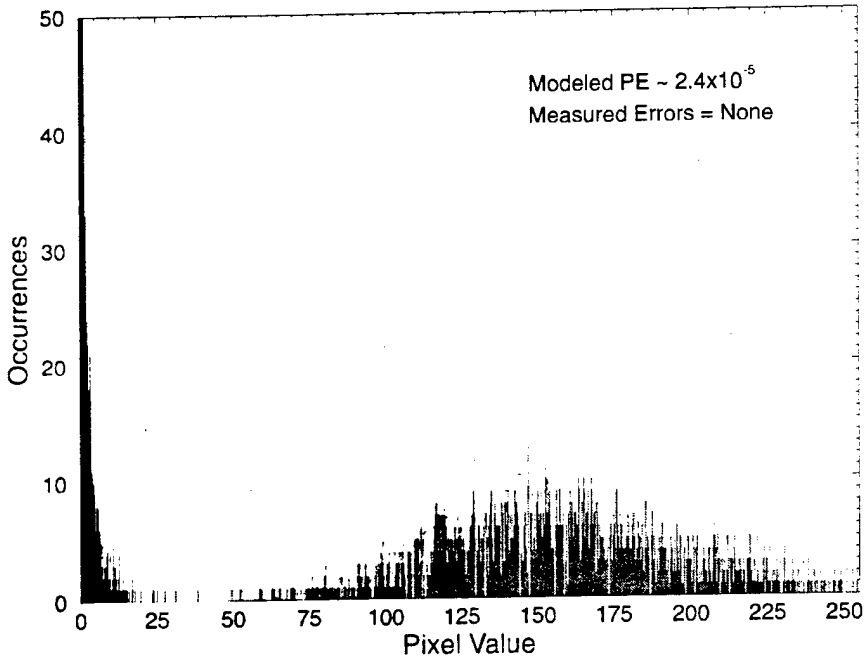

Figure 1.49 : Combined histogram obtained from three different sampled windows for the 10 bits/μm^2, photopolymer based holographic 3-D disk experiment.

We also measured the SNR of the system under various experimental conditions as shown in Figure 1.50. The SNR for both the shift multiplexed holographic 3-D disk

experiment and the previous angle+peristrophic multiplexed experiment are plotted for comparison. The first SNR measurement of the shift multiplexing holographic 3-D disk setup is 11.5, which is due to system noises only (lens aberrations, SLM imperfections, detector noise, scattering and multiple reflections from lenses and other optical components, laser non-uniformity and fluctuations, and SLM-to-CCD pixel misalignment). We obtained this by transmitting the signal beam through the system without any recording material. An improvement of 1.5 in SNR when compared with the angle+peristrophic multiplexing setup is due to the E-beam lithographed, chrome plated data mask used in the holographic 3-D disk setup. The optically lithographed data mask used in the previous setup did not have the uniformity nor the contrast of the E-beam lithographed mask. By placing the one side AR-coated 1.2 mm thick glass disk at the recording plane, the SNR drops to 10.9. This slight drop in SNR is mostly due to aberration and internal reflections caused by the disk substrate. However, the new setup has an additional SNR improvement of 0.4 over the old setup (when the SNR increase of 1.5 have already been taken into account). This small increase in SNR is due to the anti-reflection coating on the glass disk. In the old setup, regular 1 mm thick glass slides were used to support the photopolymer. We suspect that the SNR would have been even better had the glass disk been AR coated on both sides. However, this was not done since the photopolymer is laminated on one side of the disk and would have ruined the AR effect. When we introduced a piece of UV-cured photopolymer laminated on the disk substrate at the recording plane, the SNR dropped further to 8.8. The major cause of this drop in SNR is most likely due to internal reflections within the film and the glass substrate and scattering caused by the photopolymer film. Since the same type of photopolymer was

used in both experiments, the drop in SNR caused by the UV-cured photopolymer is the same for both setups.

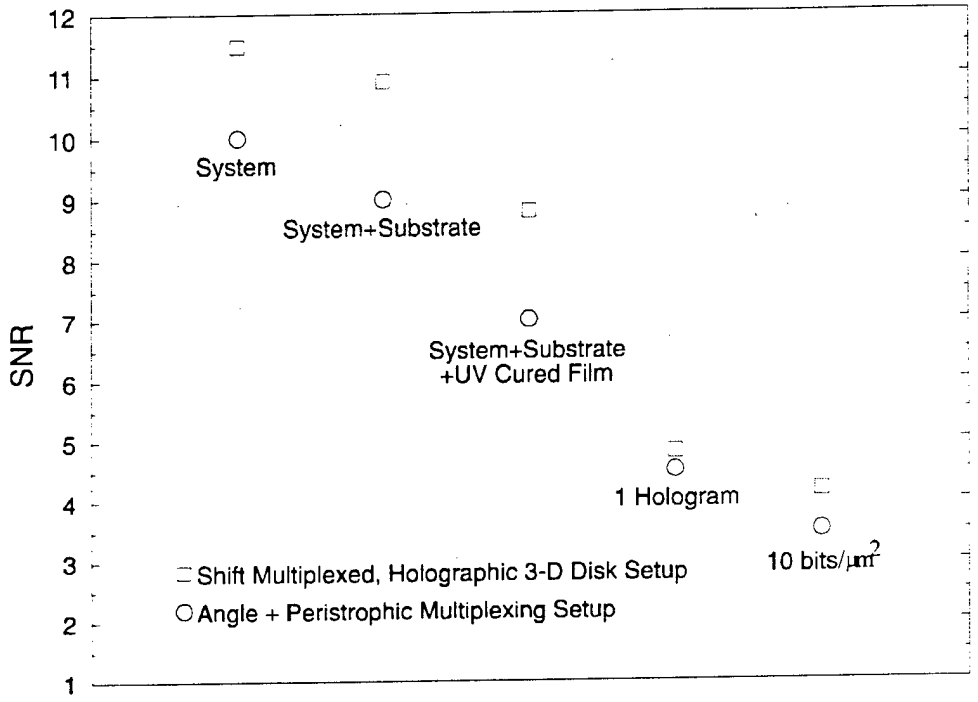

Figure 1.50 : SNR characterization for the shift multiplexed, photopolymer based holographic 3-D disk setup.

A SNR of approximately 4.8 was obtained when a single hologram was recorded on the disk and its reconstruction evaluated. No errors were observed in the reconstruction and the histogram of the 'on' and 'off' pixels were still clearly separated. However, when compared with the old setup, the lead in SNR enjoyed by the new setup has shrunk to only 0.3 (from a lead of 1.8 before). To a large extent, this significant drop in SNR (from 8.8 to 4.8) is due to internal reflections from the boundaries. Figure 1.51 shows a close-up diagram of the recording plane. The signal beam is a high bandwidth (f/1.4) spherical beam that focuses in front of the recording material and the reference beam is an even higher bandwidth (f/1.1) spherical beam that focuses in the back. Unlike the angle+peristrophic multiplexing setup where the reference beam was just a planewave

and internal reflections caused an interference pattern that was distributed across the entire hologram. The reflected spherical reference beam for the holographic 3-D disk setup re-focuses near the right side of the hologram. Therefore, the quality of a hologram stored in the geometry shown in Figure 1.51 will have poorer SNR on the right side when compared to the center or the left. For the one hologram experiment, the right side had an SNR of 4.2 while the left and the center had an SNR of 4.6 and 5.6, respectively, for an average SNR of 4.8. If there was a way to AR coat the photopolymer to reduce the back reflections, the SNR should improve significantly.

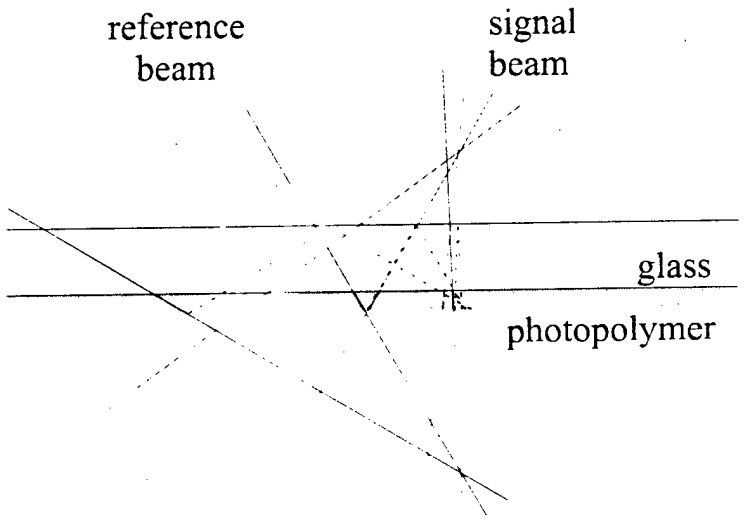

Figure 1.51 : Internal reflections within the holographic 3-D disk cause the right side of the stored hologram to have lower SNR.

For the final 10 bits/μm^2 surface density experiment with three overlapping tracks (100 holograms in each track), the measured SNR is 4.16. This is about 0.6 higher than the angle+peristrophic setup for the same surface density. Instead of maintaining a lead of 0.3 in SNR for one hologram, the SNR actually increased by another 0.3 for the 10 bits/μm^2 experiment using shift multiplexing. This is probably because for the shift multiplexed holographic 3-D disk setup, less cross-talk noise is introduced between the in-

track holograms when compared to the angle holograms of the angle+peristrophic setup. Furthermore, since the holograms are recorded in partially overlapping areas (instead of recording all the holograms at the same spot), the index modulation effect is probably less. The better SNR for the 10 bits/μm^2 shift multiplexed holographic 3-D disk experiment translates to a lower estimate bit-error-rate of 2.4×10^{-5}, more than 4 times lower than the angle+peristrophic experiment shown in Chapter 1.2.

1.4 100 bits/μm^2 High Density Experiment Using Shift Multiplexing and a 1 mm Thick $LiNbO_3$

1.4.1 Introduction

In Chapter 1.3, a surface density of 10 bits/μm^2 was achieved with a shift multiplexed holographic 3-D disk system, using a 100 micron thick photopolymer. The storage capacity of a 120 mm photopolymer based holographic 3-D disk would be around 10 Gbytes (at 10 bits/μm^2). That is about 10 times higher than the capacity of the current compact disk. However, the next generation compact disc due in early 1997, the Digital-Versatile-Disc (DVD), will have a capacity of ~6 Gbytes per layer, for a maximum planned capacity of ~20 Gbytes per double-sided disk with two layers on each side. That translates to a surface density of approximately 20 bits/μm^2 for the 4 layered DVD disk. Unless we can get a much higher surface density than 20 bits/μm^2 with the holographic 3-D disk system, there is no need to compete with the DVD for the same market with an inferior product.

So far the recording material we have used is only 100 micron in thickness. According to Eq. 1.15 and 1.20, the number of holograms you can pack in the same area is directly proportional to the thickness of the recording material. The thicker the recording material, the more holograms you can store in the same area and therefore, the higher the surface density. For example, if we were to use a 1 mm thick photopolymer based holographic 3-D disk, the surface density should increase by a factor of 10X to 100 bits/μm^2. Certainly a comfortable margin over the projected surface density of the DVD system. However, no 1 mm thick photopolymer exists at the current time so we will have to use another recording material as a substitute for now. A candidate that readily presents itself is $LiNbO_3$. Its photorefractive properties are well known and a 1 mm thick sample would be easy to obtain. $LiNbO_3$ can be polished to optical quality and AR coated on both sides to reduce reflections. However, some of its less desirable properties will force us to change our setup slightly. Due to the expense of acquiring large samples of $LiNbO_3$, we will not be able to make a $LiNbO_3$ based, holographic 3-D disk in the style shown in Figure 1.43. Instead, we will use a 2 cm by 2 cm piece of $LiNbO_3$ to demonstrate the system. For transmission geometry $LiNbO_3$, there is a preferred crystal axis for hologram formation. If the crystal is rotated like a disk during recording, the preferred axis will introduce a sinusoidal variation in the diffraction efficiency of the stored holograms [16]. Therefore we will not rotate the $LiNbO_3$ to achieve shift multiplexing. Instead, we will translate the crystal horizontally to record in-track holograms and vertically to overlap the tracks. Furthermore, since $LiNbO_3$ is not as sensitive in the green region (532 nm) where we have done the previous experiments, we will move the setup to a large frame Argon laser that produces nearly 1 Watt of power at 488 nm.

The spirit of the experiment remains unchanged: to demonstrate that a surface density of 100 bits/μm^2 is possible with a 1 mm thick recording material by using shift multiplexing. The results obtained from this experiment can be applied to a photopolymer based, shift multiplexed holographic 3-D disk system when a 1 mm thick photopolymer becomes available.

1.4.2 Experimental Setup

The setup for this experiment is pretty much the same as the shift multiplexed holographic 3-D disk system shown in Chapter 1.3.4. A pair of Nikon *f*/1.4, 3.9-cm-aperture camera lenses were used to image an E-beam lithographed chrome plated data mask to a CCD detector. A total of 590,000 pixels fit in the apertures of the two Nikon lenses, and a sharp image of the entire field was obtained at the detector plane. The center-to-center spacing of the pixels was 45 μm and the fill factor was 100%. The recording material, 2 cm × 2 cm × 1 mm iron doped $LiNbO_3$ was mounted on two translation stages for shift multiplexing. Horizontal displacement (parallel to the plane of interaction) was provided by a Klinger CC1.2 linear stage and controller. The resolution of the Klinger linear stage is .1 μm step and the scan time for 400 steps (40 μm) is about 8 seconds. Vertical displacement was provided by a manual translation stage. The spherical reference beam was formed by using a *f*/1.1 projection lens. The holograms were recorded with the $LiNbO_3$ slightly past the Fourier transform plane of the Nikon lenses. At that position, the diameter of the signal beam was 1.5 mm on the entrance side and its spatial uniformity was much better than at the exact Fourier plane. Figure 1.52 shows a schematic diagram of the setup and Figure 1.53 shows a picture of the setup.

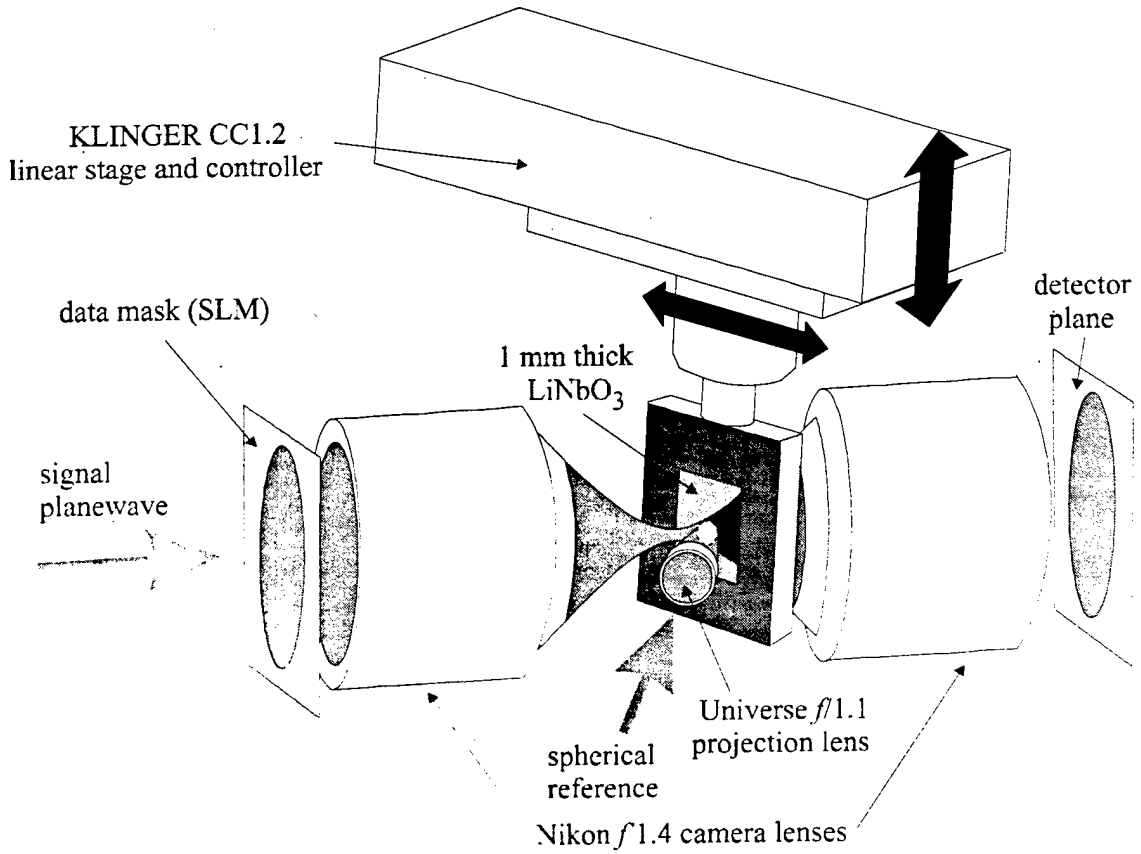

Figure 1.52 : Schematic diagram of a shift multiplexed high density setup using a 1 mm thick $LiNbO_3$.

One nice thing about $LiNbO_3$ is that it doesn't shrink when exposed to light. This frees us from the restrictive shrinkage insensitive geometry. For example, Figure 1.54 shows a recording geometry where both the signal and reference beams focus in front of the recording material. For this setup, the angle between the reference and signal rays for a localized grating remains relatively constant throughout the entire hologram. For the shrinkage insensitive geometry of Figure 1.34, the angle between the reference and signal rays is small on the right side and gets progressively bigger toward the left side of the hologram. Therefore, the Bragg selectivity of the entire hologram should be more uniform for the setup shown in Figure 1.54 when shifted parallel to the plane of interaction. We

tried this geometry with the center ray of the signal (reference) beam making an angle of 45° (35°) with respect to the recording material's surface normal.

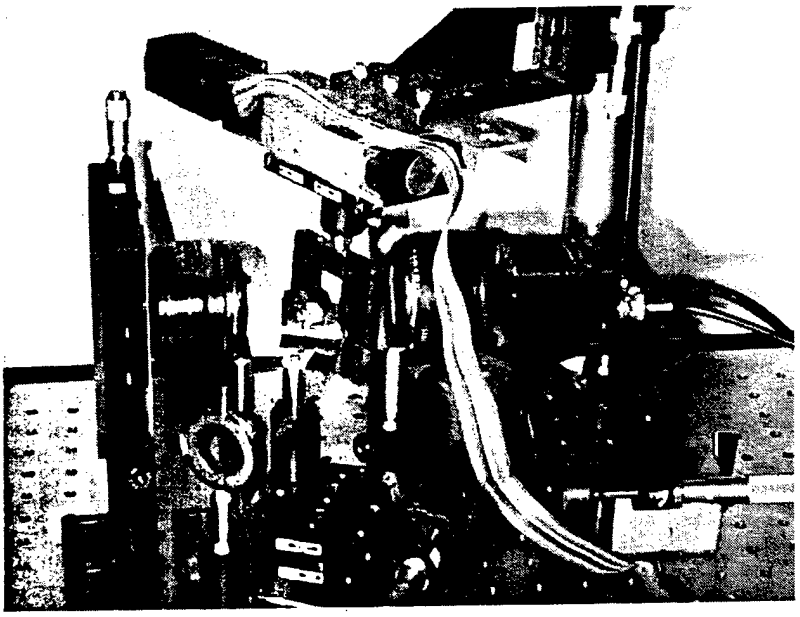

Figure 1.53 : A picture of the shift multiplexed high density setup using a 1 mm thick $LiNbO_3$.

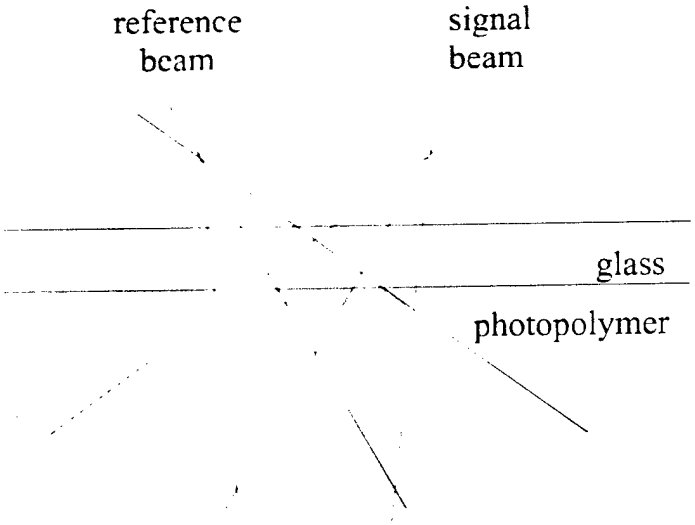

Figure 1.54 : A possible geometry for recording shift multiplexed holograms in $LiNbO_3$.

What we found was that the right side of the stored hologram Bragg-mismatched much more slowly than the left side, despite our effort to make the angle between the

reference and signal rays more uniform across the entire hologram. Upon further analysis, it became clear why this happened. In order to have good angular selectivity (Eq. 1.7), it is desirable to have a large θ_s. The gratings on the right side of the hologram have a smaller θ_s when compared to the left side. Therefore, the angular selectivity for the gratings on the right side of the hologram is poorer than the left. Furthermore, since the focal spot of the spherical reference is in front of the recording material, it is further away from the right side of the hologram. This causes the rate of change in the reference ray angle to occur more slowly for the right side when the recording material is shifted. These two effects combine to make the right side Bragg-mismatch noticeably slower than the left side. For the shrinkage insensitive geometry of Figure 1.34, θ_s on the right side is also smaller than the left. However, the focal point of the spherical reference beam is closer to the right side when it is focused behind the recording material. Therefore, these two effects cancel each other to some degree, producing a more uniformly Bragg-mismatch hologram when shifted parallel to the plane of interaction. Hence, even though $LiNbO_3$ does not shrink, we will still use the shrinkage insensitive geometry for this setup by focusing the spherical reference beam behind the recording material.

The angular selectivity equation when written explicitly for wavelength and angles measured from outside of the recording material is :

$$\Delta\theta = \sin^{-1}\left(n\sin\left(\frac{\lambda}{nL} \frac{\cos\left(\sin^{-1}\left(\frac{\sin\theta_s}{n}\right)\right)}{\sin\left(\sin^{-1}\left(\frac{\sin\theta_s}{n}\right)+\sin^{-1}\left(\frac{\sin\theta_r}{n}\right)\right)} + \sin^{-1}\left(\frac{\sin\theta_r}{n}\right)\right)\right) - \theta_r \qquad (1.21)$$

where n is the index refraction of the recording material, λ is the wavelength of the laser, L is the thickness of the recording material, and θ_s (θ_r) is the angle between the signal

(reference) ray and the surface normal of the recording material. For the photopolymer based, shift multiplexed holographic 3-D disk setup shown in Chapter 1.3, $n = 1.525$, $\lambda = 532$ nm, $L = 100$ μm, and the center ray of the signal and reference each made an angle of 30° with respect to the surface normal of the recording material. For the shift multiplexed, high density setup using $LiNbO_3$, the index of refraction of $LiNbO_3$ is 2.25 (2.35 for the ordinary axis), $\lambda = 488$ nm, and $L = 1$ mm. The shorter wavelength and higher index of refraction (compresses the wavelength inside the recording material) helps to sharpen the selectivity function. However, the higher index of refraction also decreases the angle of the signal and reference rays inside the recording material, which hurts the selectivity function. From Eq. 1.21, it is unclear if the overall effect of using a 488 nm laser and a recording material with an index of refraction of 2.25 increases or decreases the amount of $\Delta\theta$ required to reach the first null in Bragg condition. By using the parameters of the photopolymer based holographic 3-D disk, we get a $\Delta\theta$ of 0.5° from Eq. 1.21 for the grating recorded between the center rays. Using $\theta_r = \theta_s = 30°$, $n = 2.25$, $L = 1$ mm, and $\lambda = 488$ nm, we get a $\Delta\theta$ of 0.071° for the $LiNbO_3$ high density setup. This means that the higher index of refraction of the $LiNbO_3$ crystal hurts the selectivity function more than it helps since the 1 mm thick recording material did not reduce $\Delta\theta$ by a factor of 10X. Perhaps we can regain some selectivity by using larger incident angles for the reference and signal beams. According to Eq. 1.21, the best $\Delta\theta$ we could get with an index of refraction of 2.25 and a wavelength of 488 nm is 0.06° with $\theta_r = \theta_s = 45°$.

Experimentally, we were unable to record good quality holograms with such oblique angles. Through trial-and-error, we settled on a geometry where the center ray of

the signal and reference beams each made an angle of 35° with respect to the surface normal of the recording material. Theoretically, that gives a $\Delta\theta$ of 0.065° for the grating recorded between the center rays in the 1 mm thick $LiNbO_3$ crystal. This is roughly a 30% increase in the expected angular change required for Bragg-mismatching when compared to the results obtained for the 100 micron thick, photopolymer based holographic 3-D disk system.

To convert from $\Delta\theta$ to shift distance, we need to figure out where the focal point of the spherical reference beam is. For the photopolymer based holographic 3-D disk system, the focal point is placed just far enough from the backside of the disk so the reference illumination completely covers the signal beam spot on the photopolymer. For the 1 mm thick $LiNbO_3$ crystal, the entrance spot size is smaller than the exit spot size, since the signal beam expands inside the recording material. In order to cover the entire signal beam inside the recording material, the focal point of the spherical reference beam would have to be displaced further away from the recording material so the exit spot area is covered. However, that would significantly increase the amount of shift required to Bragg-mismatch a stored hologram. On the other hand, if the focal point of the spherical reference beam is placed so only the entrance spot is covered, then some of the signal illumination will not be recorded, leading to a weaker hologram. For this experiment we struck a compromise by covering all the entrance area and most of the exit area on the $LiNbO_3$. A decent hologram selectivity was maintained and the SNR of reconstructed holograms was sufficient for error free readout.

On a related topic, since the entrance spot size is different from the exit spot size, the intensity of the signal beam on the front face of the $LiNbO_3$ is different from the back

surface. In order to get a good index modulation, the signal intensity should be similar to the reference intensity in the recording material. The intensities we finally settled on were 7.9 mW/cm^2 for the reference beam and 500 μW/cm^2 for the signal beam (both measured in the planewaves before the lenses). The intensity of the reference beam was a little weaker than the signal beam at the front surface and a little stronger than the signal beam at the back surface. This seems to produce the best quality holograms possible.

Other than just worrying about the possibility of packing enough holograms in the same volume to achieve a surface density of 100 bits/μm^2, we also have to make sure that the reconstructed holograms have enough power to be read out by the detector array. With the photopolymer based holographic 3-D disk, we did not have to worry about the diffraction efficiency of each hologram since the *M*/# is so high and only a few holograms overlapped in the same area. As a matter of fact, we consistently under-utilized the dynamic range of the photopolymer in order to simplify the exposure schedule and to record better quality holograms. With $LiNbO_3$, the *M*/# is usually much lower than the photopolymer given the same thickness. For the 1 mm thick iron doped $LiNbO_3$ crystal we used in this experiment, the *M*/# is 0.34 for vertically polarized incident beams and approximately 1 for horizontally polarized beams (this agrees with theory pretty well since the R_{33} coefficient is about 3 times bigger than the R_{13} coefficient in the electro-optic tensor for LiNbO3 [17]). So for horizontally polarized holograms, we can expect a diffraction efficiency that is 9 times higher than for holograms recorded with vertically polarized beams (for the same exposure time). Therefore, we will use horizontally polarized reference and signal beams in this setup.

Even with a *M*/# of 1, the efficiency of the 1 mm thick $LiNbO_3$ still pales in comparison with DuPont's HRF-150-100 photopolymer. With $1/10^{th}$ the thickness, the *M*/# of the 100 micron thick photopolymer is around 6.5 times higher than the 1 mm thick $LiNbO_3$. In order to achieve a surface density of 100 bits/μm^2, we will need to store about 10 times more overlapping holograms in the same area than before. For a 1 mm thick photopolymer, this would not be a problem since the *M*/# would also increase by a factor of 10 due to the increased thickness. Therefore, the diffraction efficiency per hologram would remain about the same. However, for the 1 mm thick $LiNbO_3$, we will not have a *M*/# of 65 to play with. In terms of diffraction efficiency, each hologram recorded in the 1 mm thick $LiNbO_3$ will be 4,000 times less intense when compared to holograms recorded in a 1 mm thick photopolymer (if the full dynamic range of both materials were used). So for this experiment, we will really have to keep an eye on the SNR of the stored holograms to make sure the diffracted power is above the noise level. We will do this by monitoring the SNR as a function of surface density, from 1 hologram stored to 100 bits μm^2. If at anytime the SNR drops below the desired value, we will modify the setup to either reduce the noise level or to increase the signal level.

To achieve the goal of 100 bits μm^2 with the 1 mm thick $LiNbO_3$, we will first start with an in-track surface density of 50 bits/μm^2. This means the in-track holograms have to be separated by no more than 7.8 μm in horizontal shift. Then by overlapping one track at half the hologram height above and anther at half the hologram height below, boost the surface density to 100 bits/μm^2. It is kind of funny talking about the 'height' of a hologram since the hologram has two different 'heights', one at the front face of the crystal and a bigger one at the back surface. We can go back and think about the surface density in

terms of number of pixels in a hologram over the effective area of the hologram. For this experiment, we have again 590,000 pixels in each hologram over an effective hologram area of .75 mm (amount of vertical shift required to store another hologram) times 7.8 μm (amount of horizontal shift required to store the next in-track hologram), for a surface density of 100 bits/μm^2. Figure 1.55 shows the arrangement of holograms in the $LiNbO_3$ crystal.

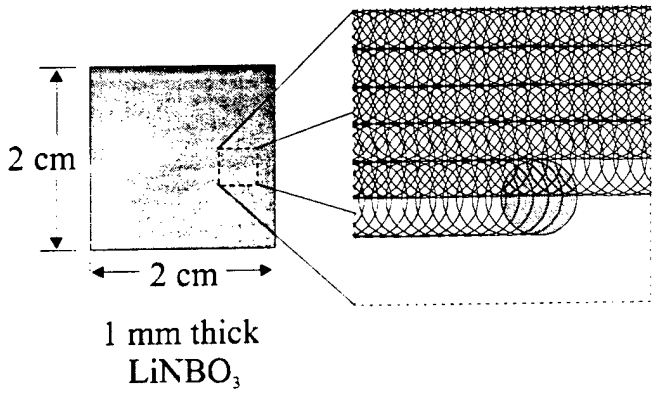

Figure 1.55 : The arrangement of holograms in the $LiNbO_3$ crystal.

1.4.3 Experimental Results

To determine if in-track holograms could be stored as closely as 7.8 μm in shift with the 1 mm thick $LiNbO_3$, we stored one hologram and measured its selectivity. Figure 1.56 shows the diffraction efficiency of the stored hologram as a function of shift distance. A 7.8 μm in-track shift between holograms corresponds to approximately the 2nd null for this setup. As explained previously in Chapter 1.4.2, the higher index of refraction and the extra thickness of the $LiNbO_3$ hurt the selectivity a little. Instead of storing in-track holograms at the 4th null like in the holographic 3-D disk experiment (Chapter 1.3.5), for

this experiment we will have to store additional in-track holograms at the 2nd null to get to 100 bits/μm^2. Therefore, more cross-talk noise is expected. For track overlapping, since the bandwidth of the signal and reference beams are roughly the same for the stored holograms, when the recording material is shifted radially by .75 mm, the reconstruction of the Bragg-matched strip is deflected completely off of the detector plane.

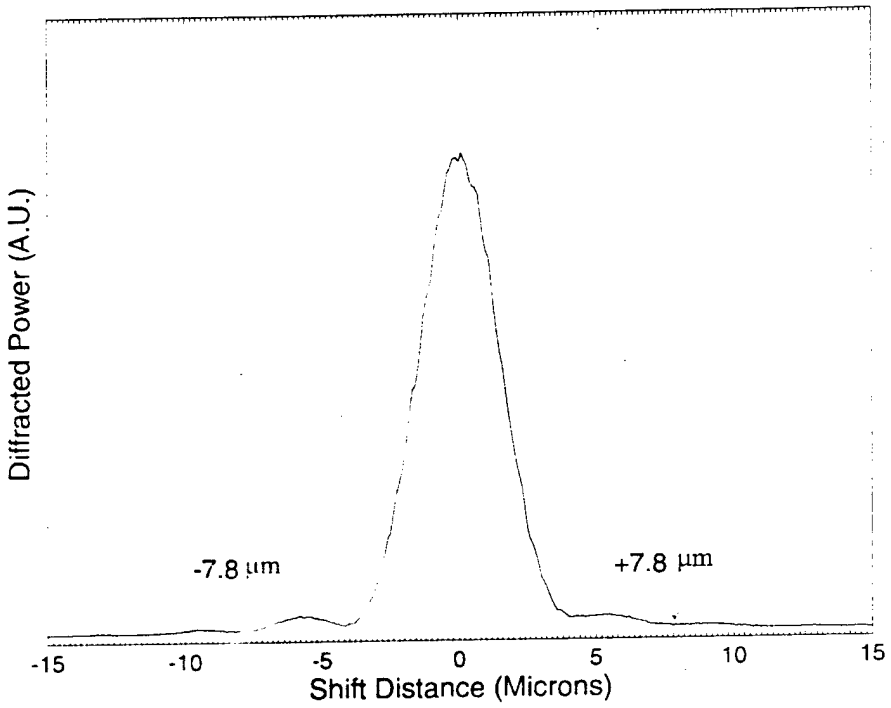

Figure 1.56 : Diffracted power as a function of shift distance for a high density hologram recorded with our shift multiplexing setup, using a 1 mm thick $LiNbO_3$.

We now know the setup can achieve a surface density of 100 bits/μm^2 as far as hologram selectivity is concerned. But before jumping directly to do the 100 bits/μm^2 experiment, we would like to take it step by step and solve possible difficulties along the way. Figure 1.57 shows the measured SNR of the system under various experimental conditions. A SNR of 9.5 was measured by imaging the E-beam lithographed data mask through the system without any recording material. Even though the imaging system for the $LiNbO_3$ setup is exactly the same as the holographic 3-D disk experiment of Chapter

1.3.5, the system SNR is lower here. I suspect the mode quality of the Argon laser is not quite as good as the DPSS laser used in the holographic 3-D disk experiment.

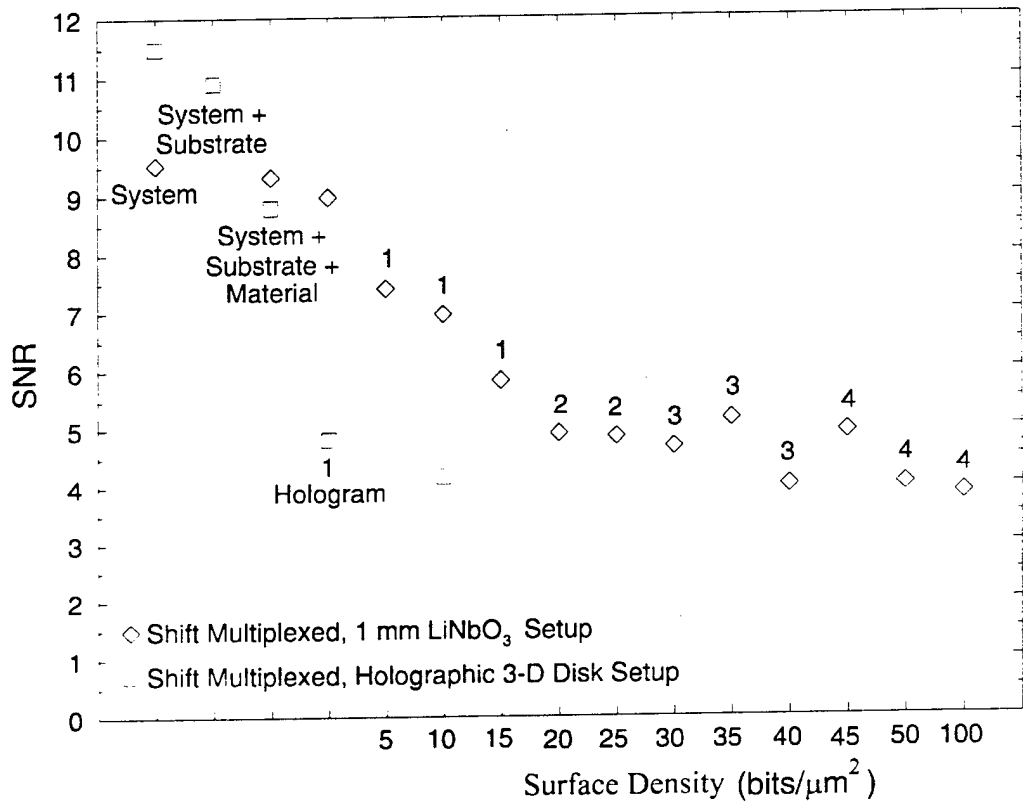

Figure 1.57 : SNR characterization for the shift multiplexed 1 mm $LiNbO_3$ setup.

When the AR coated 1 mm thick $LiNbO_3$ is placed at the recording plane, the SNR drops slightly to 9.3. However, due to $LiNbO_3$'s much better optical quality and AR coatings on both sides, the SNR of the $LiNbO_3$ setup becomes better than the photopolymer based holographic 3-D disk setup. The difference in SNR between the two setups is even larger for the case where the SNR of one hologram is analyzed. For the $LiNbO_3$ setup, a SNR of 9 was obtained as compared to a SNR of 4.8 for the photopolymer disk experiment. Again, the better optical quality and AR coatings really helped the $LiNbO_3$ setup in obtaining a higher SNR. To measure the effect of hologram multiplexing on the SNR, we stored shift multiplexed holograms in the $LiNbO_3$ at 5

bits/μm^2 in-track density increments, up to 50 bits/μm^2. For each experiment, the SNR of a reconstructed hologram near the middle of the track is measured. If the SNR is good and no errors are observed, then the in-track density for the next experiment is increased by 5 bits/μm^2 by decreasing the separation between adjacent holograms. However, if the SNR drops much below the SNR obtained for the 10 bits/μm^2 photopolymer based holographic 3-D disk experiment or if errors are observed, then parameters of the setup is modified to achieve a better SNR. For the final 100 bits/μm^2 experiment, the 50 bits/μm^2 in-track density experiment is repeated three times with a track separation of .75 mm. Table 1.1 shows a summary of the setup parameters and experimental results for the in-track density experiments with $LiNbO_3$.

For the 5, 10, and 15 bits/μm^2 in-track density experiments, the SNR measured were all well above 4.16 (the value measured for the 10 bits/μm^2 photopolymer based holographic 3-D disk experiment) and no errors were observed. Each hologram was recorded with a constant 20 seconds exposure and for the 5 bits/μm^2 experiment, the dynamic range of the $LiNbO_3$ was not yet fully utilized. Figure 1.58 shows the diffraction efficiency as a function of material shift for the 15 bits/μm^2 in-track density experiment. Notice the diffraction efficiency at the beginning and near the end is much higher than the middle (the power detector saturated for the last few holograms). This is caused by the erasure effect inherent in photorefractive materials such as $LiNbO_3$. Holograms multiplexed later in the sequence decay the strength of the already stored holograms. Since the holograms at the beginning and the end of the track have fewer adjacent holograms, they don't get erased as much (for the last hologram, it doesn't get erased at all).

In-track Density (bits/μm^2)	# of Holograms	Hologram Separation (μm)	Exposure Time (seconds)	Average Diffraction Efficiency (%)	SNR
5	75	78	20	0.06	7.4
10	150	39	20	0.04	7
15	230	26	20	0.017	5.8
20	track 1 : 155 track 2 : 155	track 1 : 39 (0) track 1 : 39 (+19.5)	track 1 : 20 track 2 : 9	0.01	4.9
25	track 1 : 192 track 2 : 192	track 1 : 31.2 (0) track 2 : 31.2 (+15.6)	track 1 : 20 track 2 : 7	0.004	4.8
30	track 1 : 155 track 2 : 155 track 3 : 155	track 1 : 39 (0) track 2 : 39 (+13) track 3 : 39 (+26)	track 1 : 20 track 2 : 10 track 3 : 5	0.0038	4.7
35	track 1 : 175 track 2 : 175 track 3 : 175	track 1 : 34.2 (0) track 2 : 34.2 (+11.4) track 3 : 34.2 (+22.8)	track 1 : 20 track 2 : 8 track 3 : 5	0.0063	5.2
40	track 1 : 205 track 2 : 205 track 3 : 205	track 1 : 29.4 (0) track 2 : 29.4 (+9.8) track 3 : 29.4 (+19.6)	track 1 : 20 track 2 : 7 track 3 : 4	0.004	4
45	track 1 : 172 track 2 : 172 track 3 : 172 track 4 : 172	track 1 : 34.8 (0) track 2 : 34.8 (+8.7) track 3 : 34.8 (+17.4) track 4 : 34.8 (+26.1)	track 1 : 20 track 2 : 7 track 3 : 4 track 4 : 3	0.0052	4.9
50	track 1 : 192 track 2 : 192 track 3 : 192 track 4 : 192	track 1 : 31.2 (0) track 2 : 31.2 (+7.8) track 3 : 31.2 (+15.6) track 4 : 31.2 (+23.4)	track 1 : 20 track 2 : 6 track 3 : 4 track 4 : 3	0.0015	4

Table 1.1 : A summary of setup parameters and experimental results for the in-track density experiments with $LiNbO_3$.

The erasure effect will also force us to change the way in which the holograms are stored. For the 20 bits/μm^2 in-track density experiment, when all 310 holograms were stored sequentially by using the constant 20 seconds exposure per hologram, a lot of errors were observed on the right side of the reconstructed holograms. The SNR for the left, center, and right sides of a reconstructed hologram were 5.5, 4.3, and 1.7, respectively. With a SNR of only 1.7 for the right side, the 'on' pixels were

indistinguishable from the 'off' pixels. The reason why the SNR on the right side is so poor has to do with non-uniform erasure introduced by shift multiplexing in $LiNbO_3$.

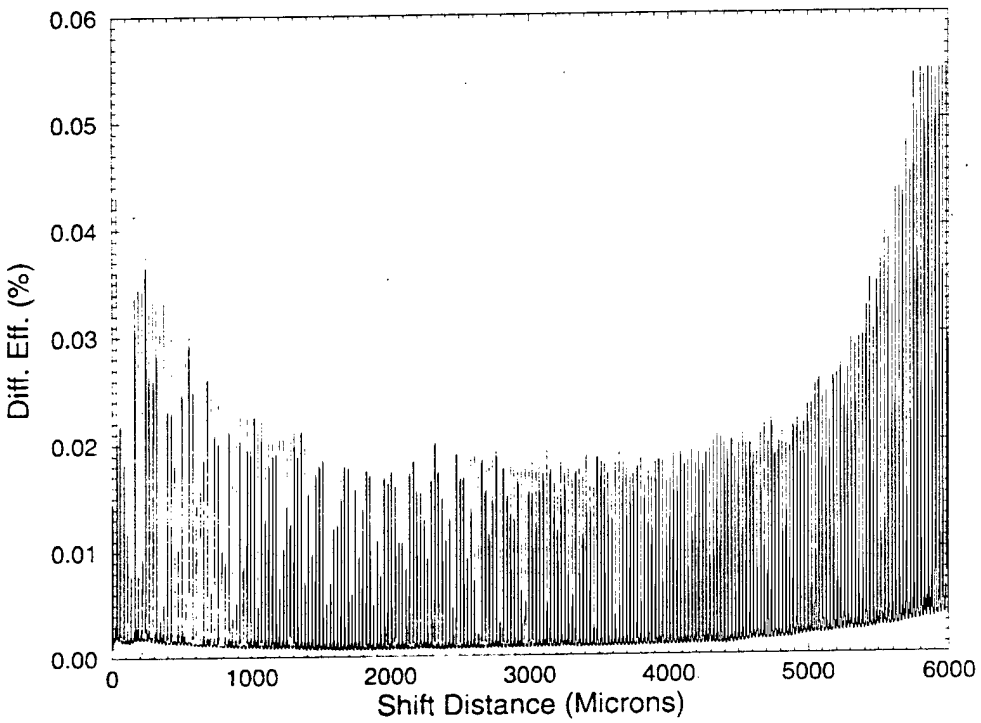

Figure 1.58 : Diffraction efficiency as a function of shift distance for the 15 bits/μm^2 in-track density experiment with $LiNbO_3$.

Figure 1.59 (a) shows a single track of holograms shift multiplexed sequentially from left to right and Figure 1.59 (b) shows the resulting diffraction efficiency. Once a hologram is stored, additional holograms are shift multiplexed to the right in partially overlapping areas. Therefore, the right side of a stored hologram becomes more erased, producing a reconstruction similar to the one shown in Figure 1.59 (a) (where the shaded black area represents lower intensity). This problem was also present in the 5, 10, and 15 bits/μm^2 in-track density experiments but it did not cause any errors until the 20 bits/μm^2 experiment (because more holograms are stored). We need to solve this non-uniform erasure problem before moving on to the next higher density experiment.

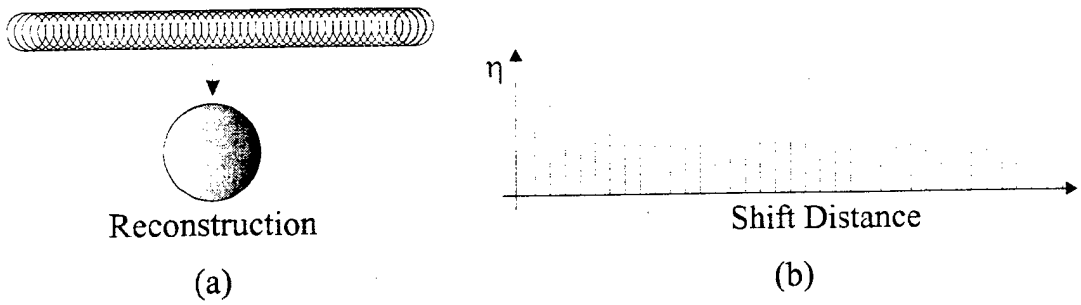

Figure 1.59 : Shift multiplexing in $LiNbO_3$ using a constant exposure schedule. (a) A single track shift multiplexed sequentially from the left to the right and a reconstruction from the middle of the track. (b) Diffraction efficiency of the stored holograms as a function of shift distance.

One method to solve the non-uniform erasure problem is to interleave the holograms during recording. Instead of storing all the holograms sequentially in a single pass, a track can be recorded by doing multiple passes as shown in Figure 1.60 (a). The starting point of each pass is shifted slightly so when all the holograms are recorded, the resulting track looks the same as Figure 1.59 (a). Since the holograms in each pass do not overlap, there is no non-uniform erasure. However, we do have to take into account the uniform erasure from multiple passes. The exposure schedule to achieve similar diffraction efficiency for multiple passes can be computed in the same matter as for angle multiplexed holograms [18]. Basically it involves recording the earlier passes stronger than the later passes, according to properties of the photorefractive recording material (Figure 1.60 (b)). Erasure from recording subsequent passes decays the strength of the earlier passes so they all have the same diffraction efficiency when the track is completed. With this method of recording in-track holograms, the intensity and the SNR of the reconstruction should be more uniform across the entire hologram.

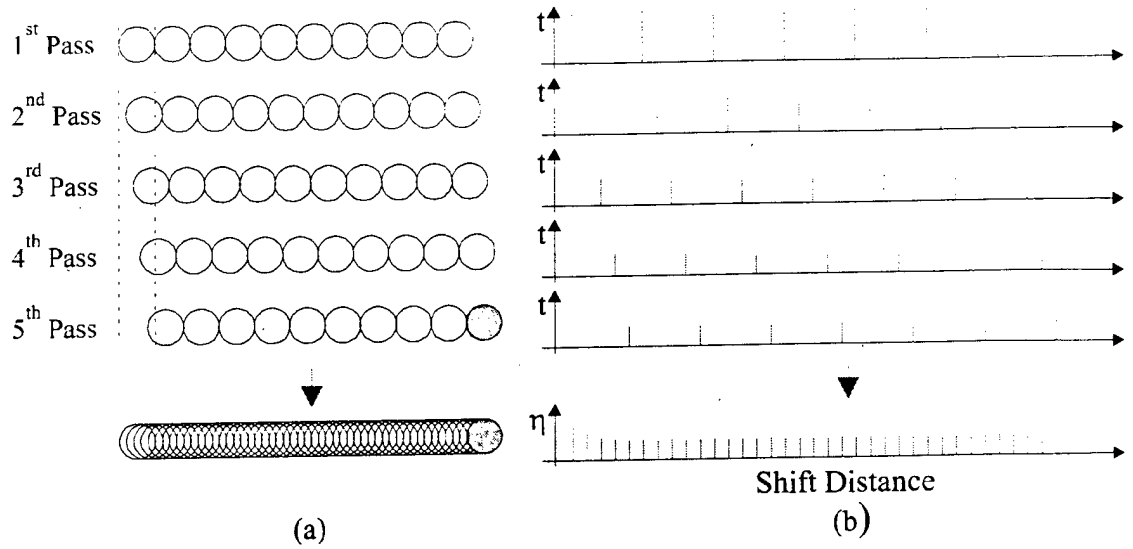

Figure 1.60 : Shift multiplexing in $LiNbO_3$ using multiple passes. (a) A single track shift multiplexed with multiple passes. (b) Exposure time for the different passes and the resulting diffraction efficiency of the stored track.

Unfortunately for our setup, it is not feasible to record completely non-overlapping holograms in each pass. The signal beam spot diameter on the entrance side of the $LiNbO_3$ is 1.5 mm. In order to separate the next hologram by 1.5 mm, we would have to wait approximately 5 minutes for the automated translation stage to move the recording material that far (we operated the KLINGER linear stage in the "slow" mode to obtain better repeatability). At that rate, the entire 20 bits/μm^2 in-track density experiment would take more than 24 hours. Instead, we compromised by recording multiple passes with partially overlapping holograms in each pass to save time. For example, the uniformity of the holograms in the 10 bits/μm^2 experiment was good enough to have zero errors. So for the 20 bits/μm^2 experiment, we recorded two 10 bits/μm^2 passes with the second pass displaced from the first by 19.5 μm. The holograms in the first and second passes were recorded for 20 and 9 seconds each, respectively. These exposure times were obtained

through trail-and-error to give the most uniform diffraction efficiency. The entire track took two hours to record and the resulting SNR was 4.9 with no errors observed.

For the 25 bits/μm^2 in-track density experiment, the track was recorded with two passes and the SNR was sufficient for error free reconstruction. However for the 30 bits/μm^2 experiment, the non-uniform erasure effect again caused errors and we had to go to three passes to record a single track without errors. To see if changing the modulation index would help improve the SNR, the reference and signal beam intensities were increased to 9.3 mW/cm^2 and 532 mW/cm^2, respectively (both measured from the planewaves before the lenses) for the next experiment. The SNR and the diffraction efficiency did improve slightly with the new modulation index for the 35 bits/μm^2 experiment. However for the 40 bits/μm^2 in-track density experiment, the SNR again dropped close to the error level due to non-uniform erasure. Figure 1.61 shows a portion of the diffraction efficiency as a function of material shift curve for the 40 bits/μm^2 experiment.

For the 45 bits/μm^2 experiment, the number of passes was increased to 4 and we began to notice significant cross-talk noise between adjacent holograms. A shift separation of 8.7 μm between holograms corresponds to a null spacing of approximately 2.2 according to Figure 1.56. The amount of cross-talk introduced was enough to cause some errors in the reconstruction. To decrease the inter-page cross-talk, we increased the selectivity of the setup by moving the focal point of the spherical reference beam closer to the recording material. Figure 1.62 shows the resulting selectivity curve for a hologram recorded with the refocused spherical reference beam.

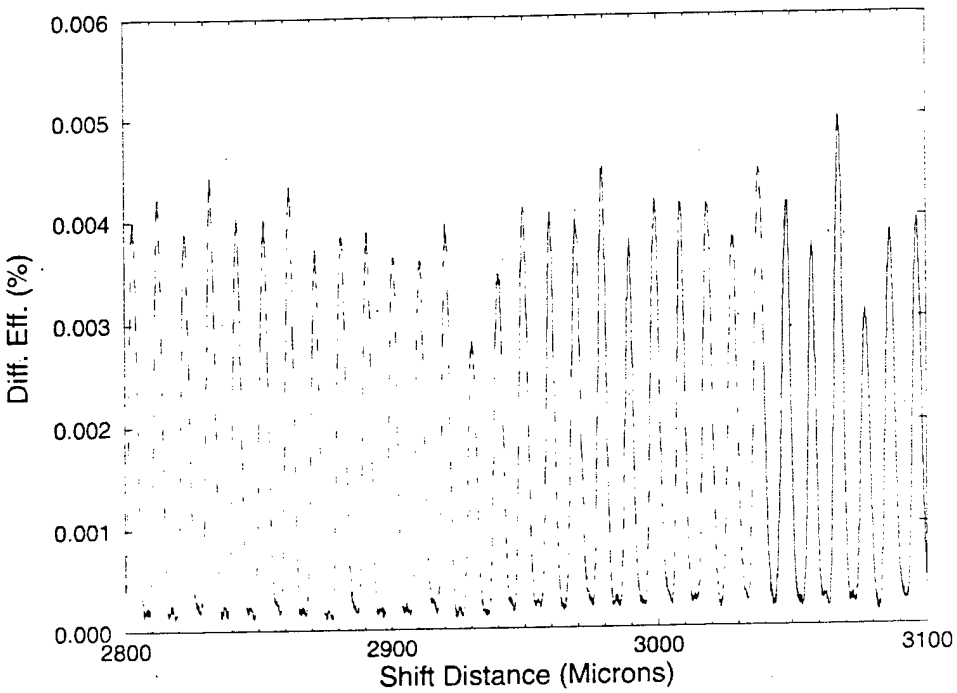

Figure 1.61 : A portion of the diffraction efficiency as a function of shift distance curve for the 40 bits/μm^2 in track density experiment with $LiNbO_3$.

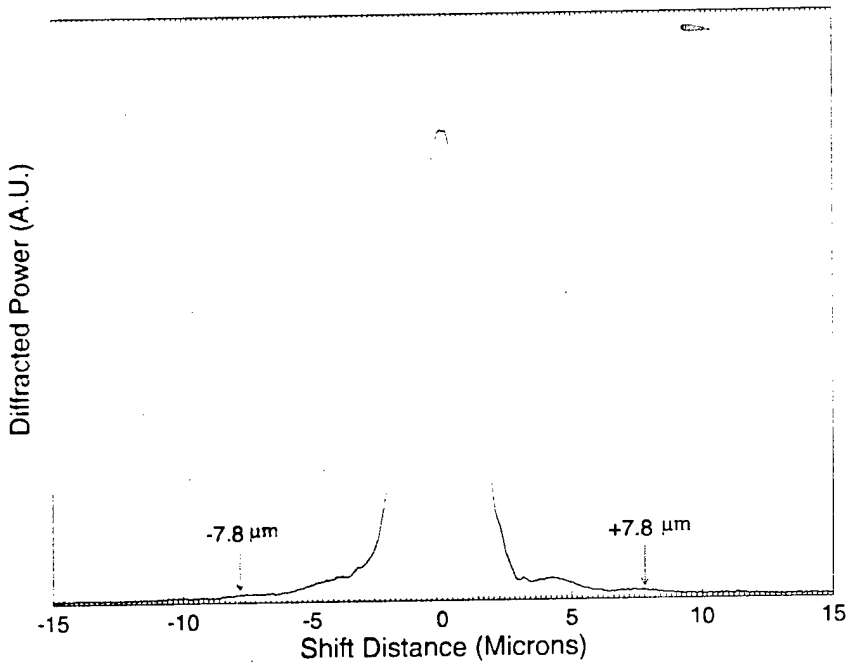

Figure 1.62 : Diffracted power as a function of shift distance for a high density hologram recorded with the refocused spherical reference beam.

With the refocused reference beam, a hologram separation of 8.7 μm now corresponds to a null spacing of 2.8 for the 45 bits/μm^2 experiment. Furthermore, for the 50 bits/μm^2 in-track density experiment, adjacent holograms can be stored at 2.5th null. The better selectivity should decrease inter-page cross-talk noise and increase the SNR of the stored holograms. However, by moving the focal point of the spherical reference beam closer to the recording material, less of the signal spot at the exit side of the $LiNbO_3$ is covered. This might decrease the hologram SNR. For the 45 bits/μm^2 experiment with 4 passes and refocused reference beam, the SNR obtained was 4.9 and no errors were observed. This shows that the gain in inter-page cross-talk noise suppression out-weighted the loss of SNR due to a smaller recording volume. The average diffraction efficiency also showed a slight improvement, possibly due to the increased reference beam intensity during recording.

The 50 bits/μm^2 in-track density experiment presented us with a new challenge. For the first trial with 4 passes, the resulting SNR for the left, center, and right sides were 3.5, 3.6, and 2.4, respectively. The average diffraction efficiency was 2.5×10^{-5} and there were some errors in the reconstruction. The chief cause of these errors was the scattering noise overpowering the reconstructed hologram. The diffraction efficiency of this experiment was dangerously close to the scattering diffraction efficiency of $\eta_{scat} \simeq 10^{-5}$. η_{scat} was determined by passing the reference beam through the 1 mm thick $LiNbO_3$, measure the total energy collected by the Nikon lens at the detector plane, and then normalize it by the reference beam power. For this setup, nearly all the scattering noise was generated by the reference beam lens since η_{scat} did not change appreciably with the $LiNbO_3$ removed. Reflections between the multiple optical elements in the Universal *f*/1.1

projection lens create a cone of scattered light with the intensity strongest in the direction of the reference beam. The Nikon lens captures some of the scattering and images it to the detector plane. Since the right side of the Nikon lens is closer to the reference beam, the right side of the detector plane has more scattering noise. This combined with weaker diffraction efficiency on the right sides of the stored holograms caused most of the errors in the 50 bits/μm^2 experiment.

There are two immediate solutions to the scattering problem : (1) increase the diffraction efficiency of the stored holograms; (2) reduce the scattering diffraction efficiency. Since we are already using the entire dynamic range of the $LiNbO_3$, it is not possible to raise the diffraction efficiency much higher than the current level. We could make the diffraction efficiency more uniform across the hologram by making more passes per track, but that would only be a temporary solution since the diffraction efficiency of each hologram will still be pretty low. Therefore, we have to reduce the scattering noise level through some type of filtering process in order to increase the SNR. Figure 1.63 shows the setup we used to filter the scattering noise for the 50 bits/μm^2 in-track density experiment. The new setup is exactly the same as the one shown in Figure 1.52, except for a second 4-f system in the signal arm. A spatial filter with an opening just big enough to pass the signal beam is placed at the Fourier plane of the second 4-f system. Since scattering originates from a different spatial position than the signal beam, most of it becomes blocked by the spatial filter. This is evident in the much lower scattering diffraction efficiency of $\eta_{scat} \simeq 3.4 \times 10^{-7}$ for the new setup. However, with more lenses in the signal beam, the system SNR might drop. We couldn't measure the system SNR directly since we only had three Nikon $f/1.4$ camera lenses, but we could measure the SNR

of a single hologram recorded with the new setup and it was 7.6. Compared with a SNR of 9 for a single hologram recorded with the setup shown in Figure 1.52, we lost 1.4 in SNR due to the extra pair of Nikon lenses in the signal beam. So the question now is: for low diffraction efficiency holograms, do we gain more SNR from the filtering process than we lose on the extra 4-*f* system? To find out, the same 50 bits/μm^2 in-track density experiment was repeated with the new setup and a SNR of 4 was obtained. This SNR is better than without filtering and no errors were observed in the sampled reconstruction. The measured diffraction efficiency of the stored holograms did go down to 1.5×10^{-5} since most of the scattering noise was blocked.

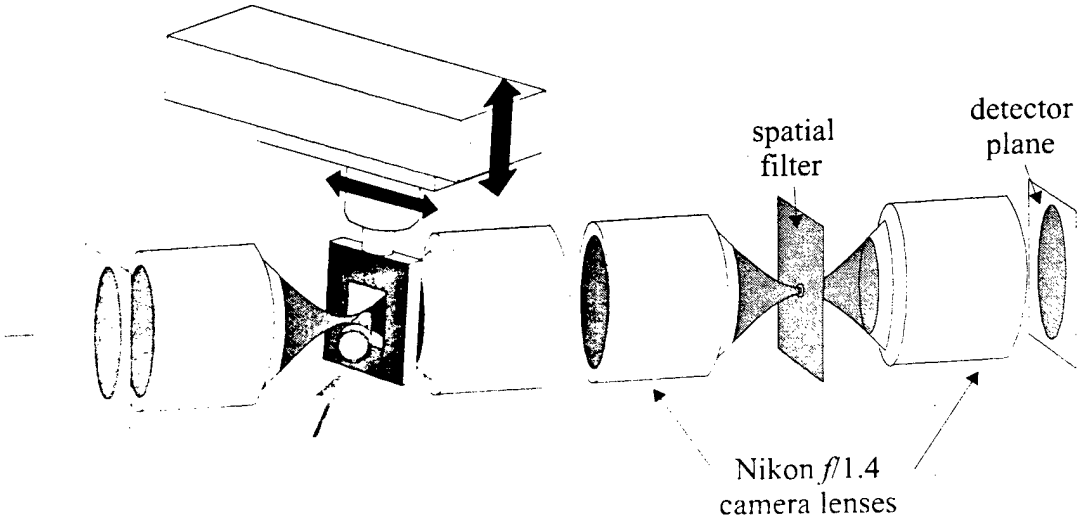

Figure 1.63 : Setup for the 50 and 100 bits/μm^2 high density experiments (with filtering).

A surface density of 100 bits/μm^2 was achieved by repeating the 50 bits/μm^2 in-track density experiment three times in partially overlapping tracks. Each track was separated by a vertical displacement of .75 mm and the in-track holograms were shifted horizontally by 7.8 μm. This gave an effective area per hologram of .75 mm $\times$ 7.8 μm = 5850 μm^2. Since each hologram contained 590,000 pixels, the surface density achieved

was 590,000 bits / 5850 μm^2 = 100 bits/μm^2. Figure 1.64 shows a portion of the diffraction efficiency as a function of shift distance curve for the middle track of the 100 bits/μm^2 experiment. The holograms were stored very close together so inter-page cross-talk was the source of most of the noise encountered. The tracks were recorded sequentially from top to bottom and the average diffraction efficiency of the holograms in the middle track was 0.00044%. This diffraction efficiency is much lower than the previous 50 bit/μm^2 in-track density experiment because the bottom track partially erases the middle track. Nevertheless it is about ten times higher than the scattering diffraction efficiency after filtering. The SNR achieved was 3.85 and no errors were observed in the sampled reconstruction when localized threshold values were used (since the intensity of the reconstructed hologram varied across the page due to the non-uniform erasure effect).

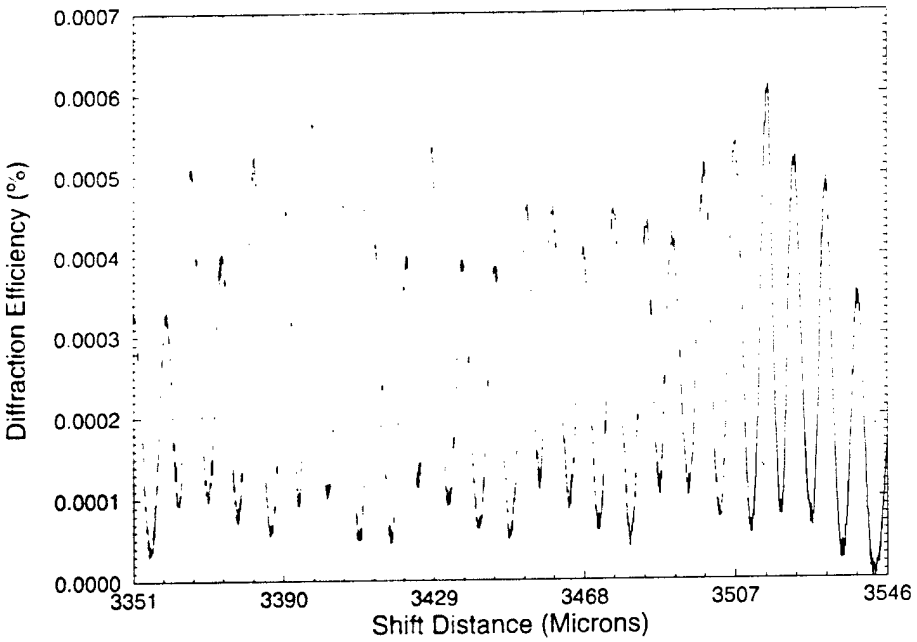

Figure 1.64 : A portion of the diffraction efficiency as a function of shift distance curve for the middle track of the 100 bits/μm^2 experiment with $LiNbO_3$.

Figure 1.65 shows a reconstructed hologram from the middle of the middle track. The three frames correspond to the left, center and right sides of the reconstructed hologram. The visual quality of these frames are slightly poorer than the images shown in Figure 1.48 for the 10 bits/μm^2 photopolymer based 3-D disk experiment. To estimate the bit-error-rate (BER) of 100 bits/μm^2 experiment, a histogram was generated from the reconstructed hologram and then fitted to a first order χ^2 distribution (as shown in Figure 1.66). The estimated BER obtained by integrating the tail areas of the χ^2 distribution for both the 'on' and 'off' pixels was approximately 9.5×10^{-5}. This BER is about the same as the original 10 bits/μm^2 surface density experiment using peristrophic and angle multiplexing.

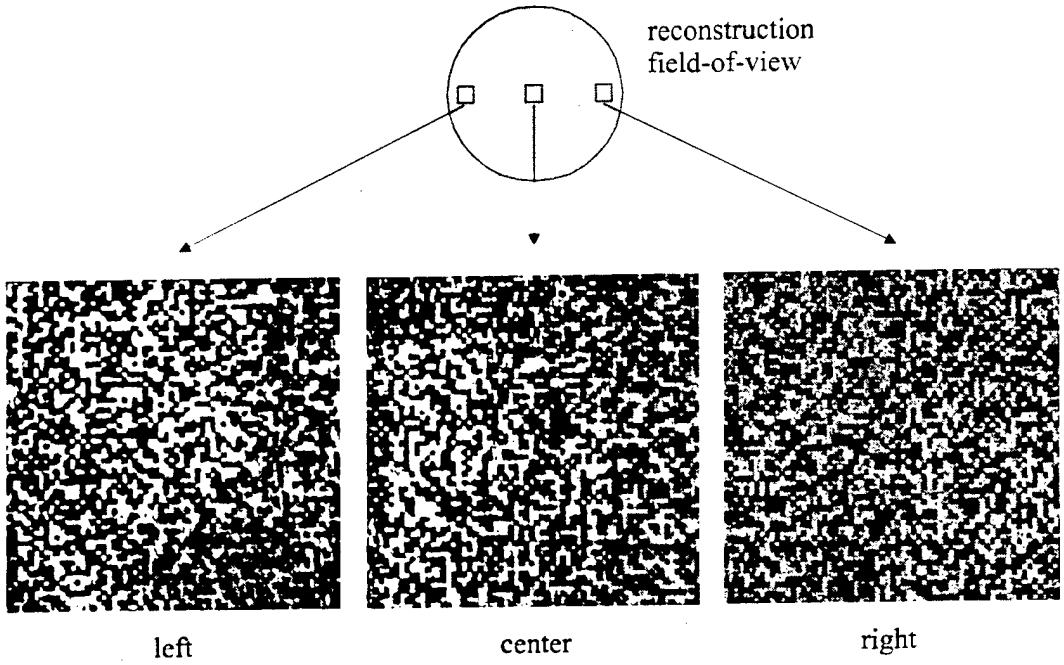

Figure 1.65 : The left, center, and right sides of a reconstructed hologram for the 100 bits/μm^2 experiment using $LiNbO_3$.

In Figure 1.66, the histograms for the 'on' and 'off' pixels actually cross-over. This means that a global intensity threshold value cannot be picked to classify all the pixels

correctly for the entire reconstruction. Due to the non-uniform erasure effect from shift multiplexing partially overlapping holograms in $LiNbO_3$, we need to use localized threshold values to classify the recalled pixels. When different threshold values were used to classify the left, center, and right sides, the reconstructed pixels from a sampled hologram were all classified correctly.

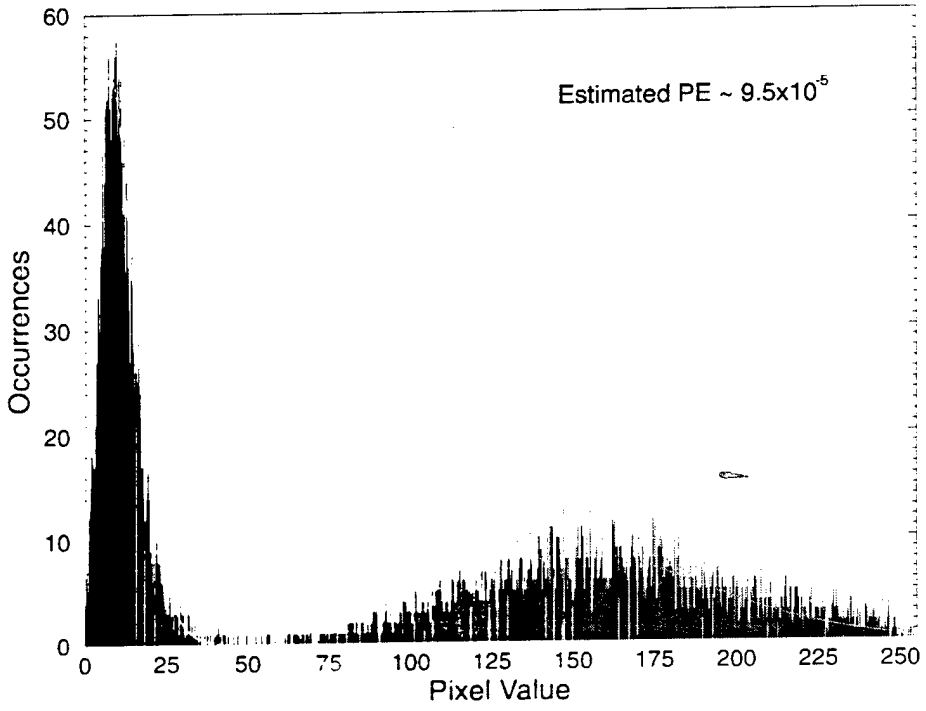

Figure 1.66 : Combined histogram obtained from three different sampled windows for the 100 bits μm^2 experiment using $LiNbO_3$.

1.5 Discussions and Conclusions

The market segment where we think a holographic data storage device can achieve acceptance, with currently available components, is mass distribution of pre-mastered information. This brings the holographic data storage device into direct competition with the widely popular compact disc. In order to succeed in a market where the compact disc

holds dominance, the holographic data storage device must offer better performance at a comparable price. In this chapter we have demonstrated that a surface density many times higher than the compact disc can be achieved holographically. One of the systems implemented used a photopolymer based holographic 3-D disk that has the same physical dimensions as the compact disc. The holograms were recorded sequentially in partially overlapping areas along a spiral track. A spherical reference beam was used to reconstruct the stored holograms while the rotational motion of the disk provided access to different holograms. This system was designed to be similar to the compact disc so many existing components could be used to reduce cost. Table 1.2 summarizes the experimental results we have obtained so far and the target values we need to make holographic 3-D disks competitive.

	100 μm Thick Photopolymer Based Holographic 3-D Disk System	1 mm Thick $LiNbO_3$ System	Target System
Surface Density	10 bits/μm^2	100 bits/μm^2	100 bits/μm^2
Capacity per 120 mm Disk	10 Gbytes	100 Gbytes	100 Gbytes
Recording Rate	1.1 Mbits/sec	70 Kbits/sec	as fast as possible
Readout Transfer Rate	.4 Mbits/sec	.4 Mbits/sec	> 100 Mbits/sec
Average Diffraction Efficiency	0.5%	0.00044%	as high as possible
Raw Bit-Error-Rate	2.4×10^{-5}	9.5×10^{-5}	$<10^{-6}$

Table 1.2 : Experimental results obtained so far and the target values.

For the 100 micron thick photopolymer based holographic 3-D disk system, we achieved a surface density of 10 bits/μm^2. The total data capacity per 120 mm disk at 10

bits/μm^2 is about 10 Gbytes, roughly ten times higher than the conventional compact disc. However, the projected surface density of the next generation compact disc, the Digital-Versatile-Disk (DVD), is around 6 bits/μm^2 per layer. The single layered DVD will be introduced in the first quarter of 1997 and the dual layered disks sometime shortly after. The maximum number of layers planned so far is 4, which brings the total surface density of the most advanced DVD up to approximately 20 bits/μm^2. In order for holographic 3-D disks to be competitive, we need to have a surface density that is much higher than the maximum projected density of DVD. A simple way to increase the surface density of holographic 3-D disks is to use a thicker recording material. To reach the target surface density of 100 bits/μm^2, we would need a 1 mm thick photopolymer. However, a 1 mm thick photopolymer is not currently available so we used a 1 mm thick $LiNbO_3$ to achieve 100 bits/μm^2. For a 1 mm thick holographic 3-D disk with a surface density of 100 bits/μm^2, the capacity per 120 mm disk is around 100 Gbytes, roughly 5 times higher than the projected capacity of the most advanced DVD.

One major performance issue we have neglected completely in the high density experiments is data transfer rate. For a read only holographic 3-D disk system, the recording rate is probably not a big issue. Nevertheless the recording material should be sensitive enough so the disks can be replicated quickly. The readout transfer rate on the other hand is a key measure of system performance. Holographic data storage devices have the potential for very fast data readout rate due to the page format of the stored holograms. For both the photopolymer disk and $LiNbO_3$ experiments, the CCD array used was much smaller than the aperture of the Nikon lens. Approximately 140 × 100 data mask pixels were captured within the CCD array aperture at a frame transfer rate of

30 Hz. This gives a data readout rate of only .4 Mbits/s as compared to the projected DVD channel bit rate of about 25 Mbits/s. If we had a CCD array large enough to capture all 590,000 reconstructed pixels within 33 ms (30 Hz), then the data readout rate would be 17 Mbits/s, which is still slower than DVD. In order to achieve the target value of >100 Mbits/s data readout rate, we need an imager that can transfer 590,000 pixels at a frame rate of ~180 frames/s. Not an impossible task considering Kodak's EktaPro Model 4540 CCD [19] camera can achieve a maximum transfer rate of 4,500 frames a second. At 256 × 256 pixels per frame, that is about 280 Mbits/s data transfer rate. However, at such a high frame rate, the diffraction efficiency of the stored holograms becomes an issue. For a signal-to-detector noise-ratio of greater than 40:1 with most CCD detector arrays, it is necessary to collect approximately 1,000 photons per pixel. The amount of time it takes to accumulate P photons per pixel can be expressed as:

$$\tau = \frac{PhcN_p}{\eta I_{inc}\lambda} \tag{1.22}$$

where h is the Planck's constant, c is the speed of light, N_p is the total number of pixels, η is the diffraction efficiency, I_{inc} is the incident power of the reference beam, and λ is the wavelength. For example, if we chose the values from the 10 bits/μm^2 photopolymer disk experiment (N_p = 590,000, η = 0.5%, λ = 532 nm, and a reference power of I_{inc} = 20 mW to read the stored holograms), then the required integration time per pixel, τ, is equal to ~ 2 μs, much less than the frame integration time of 200 μs at 4,500 frames/s. So with the photopolymer as the recording material, we probably don't have to worry too much about collecting enough photons per pixel to achieve good signal-to-detector noise-ratio.

Another important measure of system performance is the raw bit-error-rate. For the high density experiments shown in this chapter, the estimated raw BER were in the range of 10^{-4} to 10^{-5}, similar to the raw BER of compact discs. Using error correction codes with similar overheads as the compact discs, the BER of the holographic systems can be made to be less than 10^{-12}. We can achieve the target raw BER of 10^{-6} by eliminating more noise sources such as multiple reflections and reference beam scattering through AR coating.

What we ultimately want to construct is a holographic 3-D disk storage device similar to the one shown in Figure 1.67. The system consists of two major components : the read/write head and the holographic 3-D disk. The read/write head is mounted on a mechanical slide so the spherical reference beam can access different tracks on the disk while the spinning motion of the disk continuously reconstructs the in-track holograms. The spherical reference beam reconstructs a page of data at a time and the data is readout with a 2-dimensional detector array. For a system with recording capability, the data is presented on the SLM and then recorded on the disk by mixing it with the spherical reference beam. For a read-only drive, the signal beam is not required and the system becomes very similar to compact disk drives. Notice there are no moving parts inside the read write head and only about ten components are required. Some standard components from compact disc drives, such as the objective lens assembly, can be used in this setup to generate the spherical reference beam and to provide focus and tracking control. The holographic 3-D disk setup shown in Figure 1.67 offers both the simple compact disc-like architecture and high speed page access/high surface density of a holographic device.

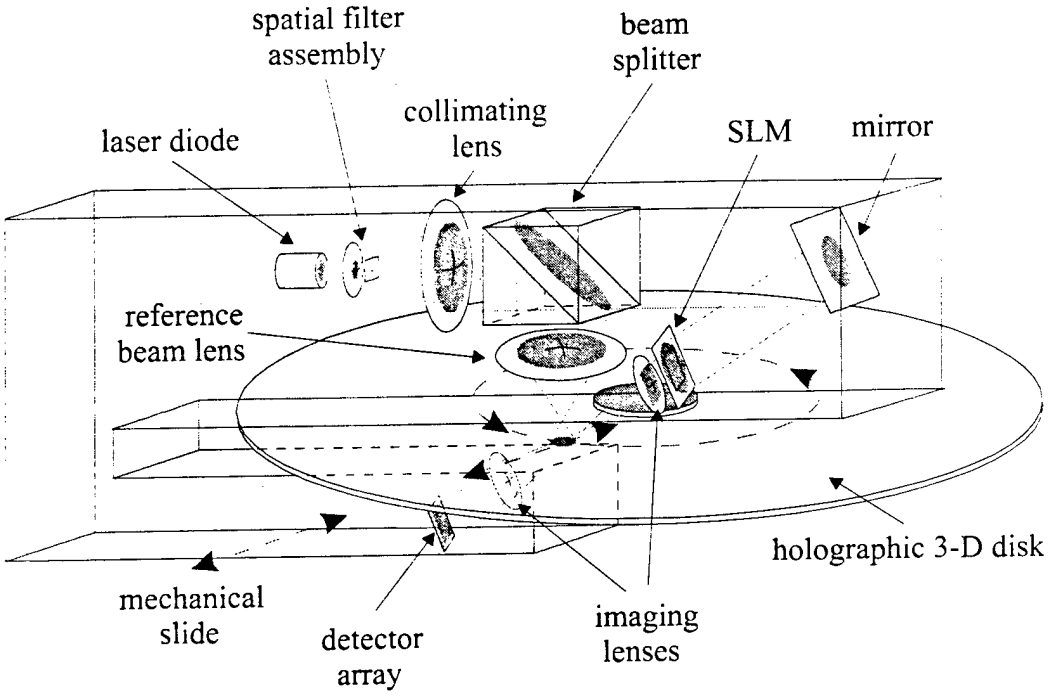

Figure 1.67 : A possible compact implementation of a photopolymer based holographic 3-D disk system.

We are still a fair distance away from making a holographic 3-D disk system that can be marketed as a commercial product. The biggest roadblock is the recording material. Currently, the most promising material for the type of application we have in mind is DuPont's photopolymer. However, in order to achieve the target surface density of 100 bits μm^2, a recording material around 1 mm thick is required. So far, no 1 mm thick photopolymer is commercially available. Furthermore, similar to a compact disc drive, a fully operational holographic 3-D disk device has to provide focusing and tracking error signals. For the system shown in Figure 1.67, the spherical reference beam is on-axis with respect to the disk. Therefore, the same differential detection method used in compact disc drives can be applied here. However, if we want to use the shrinkage insensitive recording geometry with the reference beam off-axis, then perhaps special markers could be embedded in the holograms to provide the error signals. Maybe a

completely new method can be invented for holographic 3-D disk devices that exploits some aspect of holography. Further research and development is required to deal with the disk's axial and radial run-out problems.

To achieve the target readout transfer rate of greater than 100 Mbits/s, we could use fast CCD detectors such as Kodak's EktaPro cameras. However, the cost of these cameras exceeds $100,000 per unit and therefore would not be practical for our application. What is needed are CMOS detectors custom designed for holographic data storage. The CMOS detectors can be designed with multiple outputs for fast frame transfer and smart electronics to classify the reconstructed pixels on the fly. Mass production of these detectors should bring the cost down to be compatible with consumer electronics.

For the compact disc, a lot of research has been done in the area of data structure, modulation, and error-correction-codes to optimize the performance. With holographic 3-D disks, the data is stored as discrete 2-dimensional pages. The extra dimension might offer designers more flexibility (or headaches) in the selection of optimal codes. Some researchers are beginning to address these issues for holographic data storage [20-22] and a standard might emerge in the near future.

One of the reasons why the compact disc has been so successful is the ease of disk replication. A compact disc can be made in less than a minute for less than 50 cents. This has allowed the music industry to rake in huge profits in recent years. Fortunately, holographic 3-D disks can also be replicated quickly and cheaply. One possible process involves copying the entire master disk through a single exposures [23]. This technique

has been demonstrated for conventionally multiplexed holograms (angle, peristrophic, etc.) but further development is needed for shift multiplexed holograms.

In this chapter, a new multiplexing method that is especially well suited for the holographic 3-D disk application is shown. In its current implementation, a spherical lens in placed in the reference beam to generate a spherical reference beam for shift multiplexing. This technique works fine but perhaps the optimal shift multiplexing configuration is still undiscovered. It may be possible to obtain better shift selectivity and/or less inter-page cross-talk by making simple modifications to the reference beam. For example, Figure 1.68 shows the shift multiplexing selectivity curves for three different configurations. The solid black line is the same curve as Figure 1.38 while the two dotted curves were obtained by placing random phase plates of different resolutions in front of the spherical lens in the reference arm. By decreasing the pixel size of the random phase plate, the rays in the reference beam become more distorted and therefore the selectivity improves (at the expense of increased background noise level). It might also be possible to shape the intensity profile of the reference beam to reduce inter-page cross-talk noise [24].

It is hard to predict the future of holographic data storage base on current stage of development. Some have estimated its chances at 50/50 and I believe that is overly optimistic. We have presented most of the technical roadblocks but perhaps the biggest one of all is politics. Even if holographic 3-D disks can produce the target performance numbers, why should the compact disc industry abandon their proven technology? Luckily, within a few years we will be able to tell if holographic data storage is a boom or bust.

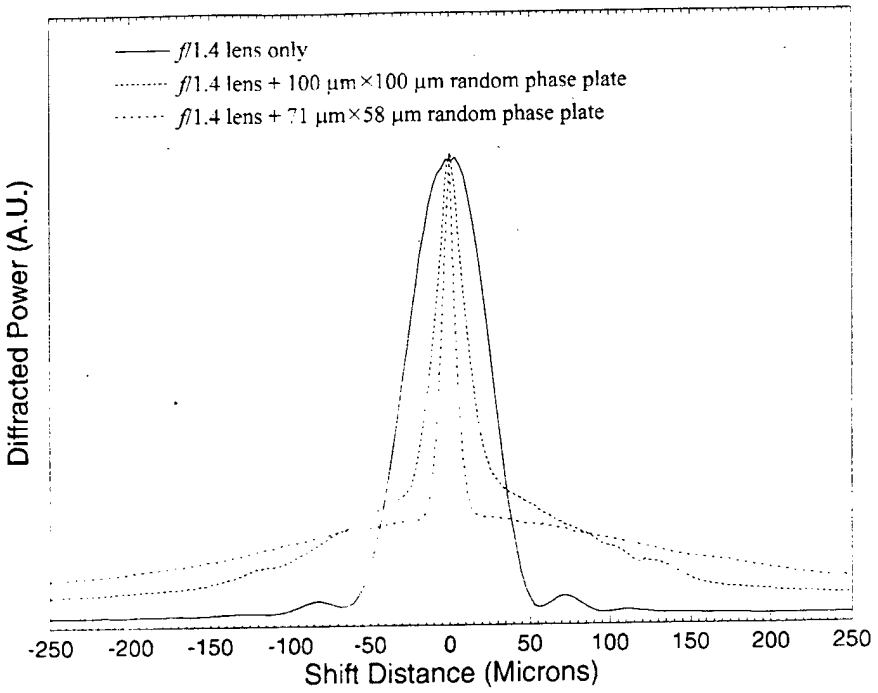

Figure 1.68 : Shift selectivity curves for three different configurations.

References

[1] D. L. Staebler, J. J. Amodei, and W. Philips. "Multiple storage of thick holograms in $LiNbO_3$." *VII International Quantum Electronics Conference*, Montreal, Canada (1972).

[2] F. H. Mok, M. C. Tackitt, and H. M. Stoll. "Storage of 500 high-resolution holograms in a $LiNbO_3$ crystal," *Optics Letters*, 16(8):605-607, 1991.

[3] S. Yin, H. Zhou, F. Zhao, M. Wen, Y. Zang, J. Zang, and F. T. S. Yu. "Wavelength-multiplexed holographic storage in a sensitive photorefractive crystal using a visible-light," *Optics Communications*, 101(5-6):171-176, 1991.

[4] G. A. Rakuljic, V. Levya, and A. Yariv. "Optical data storage by using orthogonal wavelength-multiplexed volume holograms," *Optics Letters*, 17(2):1471-1473, 1992.

[5] C. Denz, G. Pauliat, and F. Rosen. "Volume hologram multiplexing using a deterministic phase encoding method," *Optics Communications*, 85:171-176, 1991.

[6] Y. Taketomi, J. E. Ford, H. Sasaki, J. Ma, Y. Fainman, and S. H. Lee. "Incremental recording for photorefractive hologram multiplexing," *Optics Letters*, 16(22):1774-1776, 1991.

[7] D. Psaltis, D. Brady, X. G. Gu, and S. Lin. "Holography in artificial neural networks," *Nature*, 343(6256):325-330, 1990.

[8] F. H. Mok. "Angle-multiplexed storage of 5000 holograms in lithium niobate," *Optics Letters*, 18(11):915-917, 1993.

[9] K. Curtis, A. Pu, and D. Psaltis. "Method for holographic storage using peristrophic multiplexing," *Optics Letters*, 19(13):993-994, 1994.

[10] D. Psaltis, M. Levene, A. Pu, G. Barbastathis, and K. Curtis, "Holographic storage using shift multiplexing," *Optics Letters*, 20(7):782-784, 1995.

[11] *Toshiba SD (Super Density).* Format technical specifications. (Toshiba, Japan, 1995).

[12] H. Y. S. Li and D. Psaltis. "Three-dimensional holographic disk," *Applied Optics*, 33(17):3764-3774, 1994.

[13] C. B. Burckhardt. "Use of a random phase mask for the recording of Fourier transform holograms of data masks," *Applied Optics*, 9(3):695-700, 1970.

[14] Y. Takeda, Y. Oshida, and Y. Miyamura. "Random phase shifter for Fourier transformed holograms," *Applied Optics*, 11(4):818-822, 1972.

[15] A. Iwamoto. "Artificial diffuser for Fourier transform hologram recording," *Applied Optics*, 19(2):215-221, 1980.

[16] H. -Y. S. Li. *Photorefractive 3-D disks for optical data storage and artificial neural networks*. Ph.D. thesis, California Institute of Technology, 1994.

[17] A. Yariv. *Optical Electronics*, (Saunders College Publishing, Florida, 1991), Fourth Edition.

[18] D. Psaltis, D. Brady, and K. Wagner. "Adaptive optical networks using photorefractive crystals," *Applied Optics*, 27(9):1752-1759, 1988.

[19] *Kodak EktaPro HS Motion Analyzer, Model 4540*, Technical specifications. (Kodak, San Diego, 1995).

[20] J. F. Heanue, K. Gurkan, L. Hesselink. "Signal-detection for page access optical memories with intersymbol interference," *Applied Optics*, 35(14):2431-2438, 1996.

[21] W. F. Hau and A. A. Sawchuk. "Performance analysis of smart pixel interfaces for optical page-oriented memories," OSA annual meeting, MKK3, Rochester, New York. Oct 1996.

[22] M. A. Neifeld and J. D. Hayes. "Error-correction schemes for volume optical memories," *Applied Optics*, 34(35):8183-8191, 1995.

[23] F. Mok, G. Zhou, A. Chugh. "Read-only data storage system," OSA annual meeting, MAAA8, Rochester, New York. Oct 1996.

[24] M. A. Neifeld and M. McDonald. "Technique for controlling cross-talk noise in volume holography," *Optics Letters*, 21(16):1298-1300, 1996.